Ministry of National Infrastructures
Energy and Water Resources
Geological Survey of Israel

Tectono-Sedimentary Processes in the deep Levant Basin

Yael Sagy

This thesis was submitted for the degree "Doctor of Philosophy" to the senate of Tel-Aviv University, Israel.

The study was carried out under the supervision of:
Prof. Zohar Gvirtzman, Geological Survey of Israel
Prof. Moshe Reshef, Department of Geosciences, Tel-Aviv University, Israel

Report GSI/24/2016 Jerusalem, July 2016

Acknowledgement

My deepest gratitude goes to my main advisor Prof. Zohar Gvirtzman, his enthusiasm and passion for geology have been a constant source of inspiration, as well as his optimistic attitude, everlasting encouragement to seek beyond the obstacles and expand one's horizons.

My deepest thanks go to my second advisor Prof. Moshe Reshef that encouraged me to undertake this long journey, opened his door and taught me with devotion and patient the foundations of geophysics and seismic imaging.

I would like to thank Dr. Yizhaq Makovsky for sharing his knowledge in seismic imaging and collaborating along parts of the research.

I had a great opportunity to work with Pinchas Trachtman and Lenid Sobolevsky and to learn from their vast experience and expertise in seismic data processing.

My gratitude goes to Prof. Zvi Garfunkel who taught me the deep aspect of geology and whose door was always opened for advices and discussions. I would like to thank Prof. Zeev Reches for his deliberate advices in structural geology along the way. Also thanks to Prof. Uri Ten Brink for his advices in gravity and magnetic modeling.

To my many friends who each set a hand somewhere along the path: Dr. Benny Medvedev, Yaniv Marig, Oz Dror, Adi Yourman, Itai Rochlin, Anastasya Yankelzon, Hila Weiss, Roee Zisholz, Michal Rofee, Pavel Sinitzin, Dr. Josh Steinberg, Igor Goldberg and many others, thank you.

Thank you to Dr. Uri Freislander (former GII CEO) and Dr. Yuval Ben-Gai (former head of the GII's Geophysical division) for encouraging me to take this journey in the framework of GII. Many thanks to Eldad Levi (head of the GII's Geophysical Department) for enabling me to pursue my studies while being part of the GII staff. I am grateful to Dana Birenbaum of ParadigmLtd., and to Jean Steinberg (former GII's IT manager) for their devoted technical support.

I would like to acknowledge Dr. Miki Gardosh and Dr. Avi Honigstein from the Israeli Ministry of National Infrastructures, Energy and Water Resources for their financial support and permission to use the seismic data.

I am deeply grateful to my mother who raised me with her infinite love and taught me to dream, and to my father who inculcated me willpower and perseverance.

This is indeed the longest run I have ever made which wouldn't have been achieved without the love and the unconditional support of my husband Amir, his knowledge and hours of discussions have changed my perception of research. Most of all, thank you for being there for me in the bad and in the good, in the better and the worst, along with our beloved and very patient children Harel and Tamar.

Contents

List of figures

Abstract

Recent giant gas discoveries within deeply buried structural highs in the middle of the Levant basin have attracted the attention of the industrial and academic communities striving to understand the origin of these structures, their relations with the tectonic history of the basin, and their evolution through time. The location of the Levant basin, at the conjunction of two plate boundaries separating the African Plate from Eurasia in the north and from Arabia in the east, further questions the relationship between the basin's deformation and the regional plate tectonic processes. In particular, several fundamental questions are addressed here: what is the origin of the deeply buried structures in the basin? Are they related to the Early Mesozoic rifting or to the Late Mesozoic – Early Tertiary Africa-Eurasia convergent phase? How are the structures in the basin related to the closure of the Tethys Ocean, to the onshore Syrian Arc fold belt (~1000 km – long fold belt extending from northern Egypt through Israel to Syria), and the Dead Sea transform? How far west did the Syrian Arc deformation extend, and how it varies in the deep basin? How many deformation episodes occurred, how long was each episode active and are they related to onshore activity?

In order to answer these questions a basin-wide seismic analysis of ~500 2D time-migrated seismic reflection lines with accumulated length of ~27,000 km was carried out. In addition, five regional lines were selected and reprocessed using the Pre-Stack Depth Migration procedure (PSDM) that yields a depth section, correct for geometric distortions, and improves the imaging of the deep part of the sections.

Based on this huge database, horsts were distinguished from folds; geometric relations such as onlap over preexisting structure were identified; thickness variations

related to syn-tectonic deposition were examined; and distinct episodes of folding activity were identified. This analysis leads to several new understanding of the basins structure and development that were further tested by gravity and magnetic modeling. In what follows the main findings of this study are described.

Seismic interpretation conducted in this study encompasses the sedimentary section deposited since ~160 Ma, which approximately coincides with the post-rift stage of the basin. Structural maps reveal three regional basement block separated by two structural steps. The continental block is vertically separated from the continental margin block by the 1-2 km high coastal plain step. Farther west (~60 km), the continental margin block is separated from the deep basin block by > 2km high and ~10 km wide Continental Margin Fault Zone (CMFZ).

Superimposed on the regional 3-block structure, the basin hosts a variety of shorter wave structures which are the focus of this study. Interpretation and mapping of 72 folds throughout the basin demonstrated that most of them are asymmetric elongated structures, varying in length from less than 1 km to ~50 km and trending to the NNE with an average azimuth of 36^0. Few of them are associated with deep reverse faults. Timing of folding activity was identified by examining the geometry of the reflectors approaching each fold and by analyzing thickness variation along them. Combining this analysis with a set of nine isopach maps enabled to determine the temporal and spatial evolution of the folds in the entire Levant basin.

Results show that the main folding activity started during the Santonian mostly along the continental margin block and the CMFZ (more or less the nowadays continental shelf and slope), and also in the deep basin. Then, during the Late-Eocene and Oligocene, folding in the deep basin ceased, while intensive activity continued in

the eastern part of the basin (continental margin block and CMFZ). Extensive folding in the deep basin renewed in the Early Miocene and continued during the Middle Miocene. Since the Late Miocene folding activity in the entire basin declined. In the Early Pliocene only few folds were active and only in the eastern part of the basin (the nowadays shelf area), and since the Late Pliocene no folding activity was detected anywhere in the basin

Overall, the structural and the chronological similarity between offshore and onshore (Syrian Arc) folding reveals the existence of a wide deformation zone extending more than 100 km landwards of the present shoreline into Syria, Lebanon, Israel Sinai and western Egypt, and more than 200 km offshore towards the Eratosthenes seamount. This deformation zone started its activity in the Santonian (~85 Ma) and continued till the Early Pliocene (~4 Ma).

In a larger scale deformation in the Levant area lines up with a series of compressional structures observed from Morocco to Syria along the northern margins of the African plate. Hence it is suggested here that the north-east African plate margin which shaped during Early Mesozoic rifting, played an essential boundary condition for the following tectonic evolution. The subsequent Late Mesozoic – Cenozoic compression zone therefore reflect the scissor like closure of the Tethys Ocean, when Africa-Arabia had experienced a counterclockwise rotational northward drift and the thin weak crust of the plate margins deformed accordingly. The interplay of plate kinematics and pre-existing continental weakness zones dictated the deformation orientation in the Levant basin for more than 80 m.y.

Cessation of folding activity in the western part of the basin during Late Eocene – Oligocene is interpreted in this study as a result of the intensive shearing and folding

along the CMFZ, which absorbed much of the deformation at that time and "protected" the NW part of the basin. Similarly, declining of folding in the entire basin since the Late Miocene and its final cessation in the Late Pliocene is interpreted as a result of the formation of new plate boundaries near Cyprus and along the Dead Sea Transform, which absorbed much of the deformation.

In addition to the many folds described above, two major high structures were examined, Leviathan and Jonah. The Leviathan high, while seems to be at least partially congruent with the folding activity described above, differ in its dimensions and structure from the majority of the folds in the basin. It portrays a triangular wide shape in contrast to the elongated monocline or anticlines typical to Syrian Arc structures. The analysis presented here agrees with previous studies suggesting that it might be an early Mesozoic large horst, that was reactivated during the contractional phase of the basin and distinct monoclines were formed at its boundaries.

However, unlike the Leviathan high, this study suggests that the Jonah high is an ancient horst that was not reactivated. The Jonah high is particularly enigmatic as it is associated with one of the largest magnetic anomalies in the basin, though no significant gravity anomaly is observed. Previous studies raised several possibilities explaining its origin: an ancient horst related to the early stage of basin formation (Late Paleozoic or early Mesozoic); a Syrian Arc fold (Late Cretaceous to Neogene); a giant volcanic seamount; and an intrusive magmatic body.

This study suggests that the Jonah high is a horst bounded by grabens, most probably formed during continental breakup related to the Neo-Tethys formation. However, unlike other extensional structures that were reactivated and inverted during the Syrian Arc deformation, the Jonah high was never reactivated. Rather, it formed a

prominent seamount that persisted for 120-140 million years until the Early Miocene, when it was finally buried. This conclusion was further examined by gravity and magnetic modeling showing that a basement high (horst) can explain the observations without the need to add magmatic intrusions or extrusions.

1. Introduction

1.1 Motivation

The closure of the Tethys Ocean along with the northward drift of the African-Arabian continent toward Eurasia in the past ~90 M.Y has shaped significant parts of southern Europe, Northern Africa and the Middle East area (Sengor, 1979; Dercour et al., 1986; Savostin et al., 1986; Ricou et al., 1994; Stampfli et al., 2001; Frizon de Lamotte et al., 2011). While most of the Tethys Ocean does not exist today, a small relic of this immense ocean remained in the Eastern Mediterranean offshore the Levant coasts (Garfunkel, 1998; Robertson, 1998; Ben Avraham et al., 2002; Garfunkel, 2004). Moreover, since the Levant basin remained outside the main belt of Alpine deformation, it has preserved an exceptionally thick (>15 km) sedimentary section that record more than 250 M.Y. of tectonic and sedimentary history (Gardosh et al., 2008; Steinberg et al., 2011).

Large gas fields such as Tamar, Dalit and Leviathan, were discovered during the last few years within this thick sedimentary section. These new discoveries attract the attention of the industry, the academy, and the general community to subsurface geological structures that may lead to additional reservoirs. Indications for possible oil reservoirs below the Leviathan gas field (http://www.offshore-technology.com/news/newsnoble-energy-gas-leviathan-prospect-offshore-israel) further increase the importance of geological and geophysical investigations in this area. Information about the composition of the rocks and their burial history is essential for estimation of the economic potential of the area. In addition, the geometry of these structures, their age and evolution are crucial for understanding the basin's development as part of the regional plate tectonic.

Recent advances in drilling technology in the beginning of this century enabled exploring the deep water subsurface. Drilling data provide direct information of the rock column up to ~7 km, though it is one-dimensional information. Seismic imaging provide additional information down to much deeper targets (few tens of km) and on a broader scale: either as a 2D cross-section or as a 3D volume representing the subsurface. Therefore, seismic imaging is the most significant method for subsurface investigation and it constitutes the foundation for any basin analysis. In the late 80's innovation in seismic imaging had burst with the development of the pre-stack depth migration (PSDM) algorithms, which enabled a better representation of the subsurface in the depth domain (Reshef and Kosloff, 1986; Mc Mechan, 1989; Reshef, 1991). However, due to computational expenses and time consume, the PSDM procedure remains inherent to oil companies and is seldom available to the scientific community (compare to the time domain sections which are much more abundant). Recent increase in computational performances and in algorithm's efficiency facilitated the operation of this procedure.

The wealth of seismic data collected offshore Israel in the last four decades, new seismic interpretations of the Tertiary section in the basin (Steinberg et al., 2011), combined with leading edge processing technology and knowledge that were available to the present study provided significant tools to the research. The results of the PSDM enabled to perform structural and geometric analysis of subsurface structures and thus resolve geological questions that could not have been answered otherwise. The research offers an opportunity to investigate tectonic processes which might have wider implications in regard to regional folding episodes and to the evolution of the Tethys Ocean's margins.

The presence of structural highs in the Levant basin raises several fundamental questions: what is their origin? Are they related to the Early Mesozoic rifting? Did rupturing of the lithosphere occurred and hence whether thinned continental crust or oceanic crust underlain the thick sedimentary section in the basin? How the deformation in the basin relates or not to the regional plate tectonics? How far compressional field stresses originating from the North Africa – Eurasia collision are transmitted through the crust bordering these plates? These questions combined with the available tools provided the main motivation for this study. Consequently, investigation of the tectono-sedimentary processes recorded in the continuous sedimentary section constitutes the core of this research.

This research presents basin-wide interpretation of 10 horizons and processing raw data of five selected seismic lines using the PSDM procedure. It utilizes thickness variation of sedimentary units as a main observation for analyzing structure evolution through time and space.

1.2 Objectives

The thick (>15 km) sedimentary cover in the Levant basin, easternmost corner of the Mediterranean Sea (Fig. 1.1) hides several structures not expressed in the present-day bathymetry. A series of narrow and elongated anticlines and monoclines are prominent in the shallow part of the basin. These folds are quite similar in their geometry to the well-known Syrian Arc folds, ~1000 km-long fold belt extending from Sinai through Israel to Syria, originally defined by Krenkel (1924). The deeper part of the basin hosts fewer structures (Fig. 1.1). Some of them, such as the Tamar and Dalit gas bearing anticlines, are narrow and long, resembling the folds in the

shallow part of the basin. Others, such as the Leviathan and Jonah highs, are larger and different in their geometry and extent.

A previous interpretation of folds in the Levant basin by Gardosh et al. (2008) and in offshore Sinai by Yousef et al. (2010) suggested that the majority of the basin's structures were active or reactivated during Syrian Arc folding. This raises fundamental questions about the origin of the structures in the Levant basin. Are the structures in the basin related to the onshore Syrian Arc fold belt? If yes, how far west did this deformation extent? Was it coeval with onshore folding? Does it include reactivation of faults (Druckman et al., 1995)? For how long did the deformation occur? How did fold's direction vary with time and space? On the other hand, if offshore deformation is not related to the Syrian Arc system, what caused the deformation offshore?

A particularly interesting structure is the Jonah high, which is one of the largest structures in the basin whose geometry, dimensions and location compared to nearby structures is enigmatic. It is buried under more than 3 km of Late Tertiary sediments, and is associated with one of the largest magnetic anomalies in the basin, though no significant gravity anomaly is observed. Previous studies raised several possibilities explaining its origin: Late Paleozoic or early Mesozoic horst related to the early stage of basin formation; a Syrian Arc fold (Late Cretaceous to Neogene); a giant volcanic seamount; and an intrusive magmatic body.

This range of possibilities touches fundamental questions. Assuming that the Jonah high is an ancient horst bounded by deep grabens may solve basic questions related to crustal structure and the amount of extension during Late Paleozoic and Early Mesozoic rifting. If the Jonah high is a magmatic body, it is interesting to know its age, and is it related to the magmatism associated with rifting (Garfunkel, 1998;

Robertson, 1998); to Early Cretaceous intra-plate magmatic activity previously identified in the hinterland (Garfunkel, 1989); or to Cenozoic magmatism related to the Arabia-Africa breakup? Lastly, if the Jonah high is a Syrian Arc fold, why its structure is different from other Syrian Arc folds?

To solve these opened questions the following specific aims were defined:

(1) Creating depth sections by processing raw data and performing PSDM in order to obtain the best representation of the subsurface structure. Particularly, revealing the shape of reflectors inside the Jonah high that are hardly seen in presently available time sections or alternatively, determine that they are seismic artifacts. Also improving the imaging of the lateral boundaries of the Jonah high.

(2) Computing interval velocity maps extending to the entire study area for each horizon. Theses maps will enable to convert time structural maps to depth.

(3) Constraining the timing of deformation in the Levant basin and its spatial extent. Mainly by mapping the various structures in the basin and determining their timing of generation and evolution episodes by analyzing thickness variation along each structure.

(4) Reconstruct the evolution of the Jonah high. Exploring whether internal folded layers or extrusive structures exist within it. Analyzing the geometric relationship between the structure and the reflectors bordering it, specifically to check whether they are truncated, syn-tectonic or post-tectonic. Further analyzing its deeper boundaries in order to define its bordering faults.

(5) Test the consistency of the geological model of Jonah high with gravity and magnetic data.

1.3 Thesis layout

A brief description of the Levant basin's tectonic setting and plate configuration is presented below (section 1.4). The data available for this study and the specific methods used are described in chapter 2. This chapter comprises a profound technical description on the seismic data processing and interpretation. The results of this study are subdivided to three chapters each focusing on their own topic: Chapter 3 presents the results of the seismic data processing. The interval velocities derived from the PSDM procedure are the basis for the time to depth conversion of structural maps, whereas the depth sections presented in this chapter are the foundation for the stratigraphic analysis and the mapping of Jonah high. Chapter 4 presents the evolution through time and space of more than 70 folds, detected in the shallow and deep Levant basin (Sagy et al., in preparation). The hypothesis that the folds in the basin are associated with the onshore Syrian Arc fold belt is tested. The timing of post rift deformation is examined in light of plate re-organization, followed by a discussion of the spatial distribution of the Syrian Arc folds in the Levant basin. The origin and tectonic evolution of the Jonah high is analyzed in chapter 5 (findings of this chapter were published (Sagy et al., 2015). A further discussion on the early Mesozoic extension that shaped the Levant basin is presented. The conclusions are provided in chapter 6.

1.4 Geological background

1.4.1 Tectonic setting of the Levant basin

The eastern Mediterranean Levant basin, located at the conjunction of the African-Arabian-Eurasian plates (Fig. 1.1), formed by Permian, Triassic and Early Jurassic pulses of rifting that shaped the continental margin (Freund et al., 1975;

Garfunkel and Derin, 1984; Robertson and Dixon, 1984; Ricou, 1994; Hirsch et al., 1995; Garfunkel, 1998; Robertson 1998; Gardosh et al., 2010; Hardy et al., 2010). Concurrently, oceanic crust formed further west in the Herodotus Basin as a part of the neo-Tethys opening (Garfunkel, 1998; Robertson 1998; Stampfli et al., 1991 Ziegler et al., 2001; Guiraud, 1998). Following the last extension phase, since the Mid-Late Jurassic (165-160 Ma) passive margin conditions were established with prolonged post-rift subsidence (Bein and Gvirtzman, 1977; Garfunkel and Derin, 1984; Gvirtzman and Garfunkel, 1998; Bar et al., 2013; Hawie et al., 2013).

In the Late Triassic and Liassic times alongside with the Tethyan rifting, up to 2.5 km of olivine basalts (Asher Volcanics) accumulated in northern Israel (Derin and Gerry, 1979; Bonen, 1980; Derin et al., 1982; Gvirtzman and Steinitz, 1983; Dvorkin and Kohn 1989). However, there is no agreement whether the Tethyan rifting in the Levant basin reached lithospheric tearing and oceanic spreading. Several wide-angle refraction surveys reveal crustal thinning from 35-33 km onshore to 30 km along the coastline, and to ~20 km in the deep basin (Makris et al., 1983; Ginzburg and Ben-Avraham, 1987, Ben-Avraham et al., 2002; Netzeband et al., 2006), where a 10 km thick crystalline crust is suggested to be covered by more than 10 km of sedimentary rocks (Ginzburg and Gvirtzman, 1979; Hirsch et al., 1995; Gardosh and Druckman, 2006; Steinberg et al., 2011). Interestingly, the 6.7 km/s, seismic velocity constraint for the crystalline basement in the deep Levant basin was interpreted as representing both an oceanic crust (Makris et al., 1983; Dercourt et al., 1986; Ginzburg and Ben-Avraham, 1987; Ben-Avraham et al., 2002, Segev et al., 2006; Schattner and Ben-Avraham, 2007) as well as a thin (lower) continental crust (Woodside, 1977; Hirsch et al., 1995; Ginzburg et al., 1994; Netzeband et al., 2006; Gardosh et al., 2010).

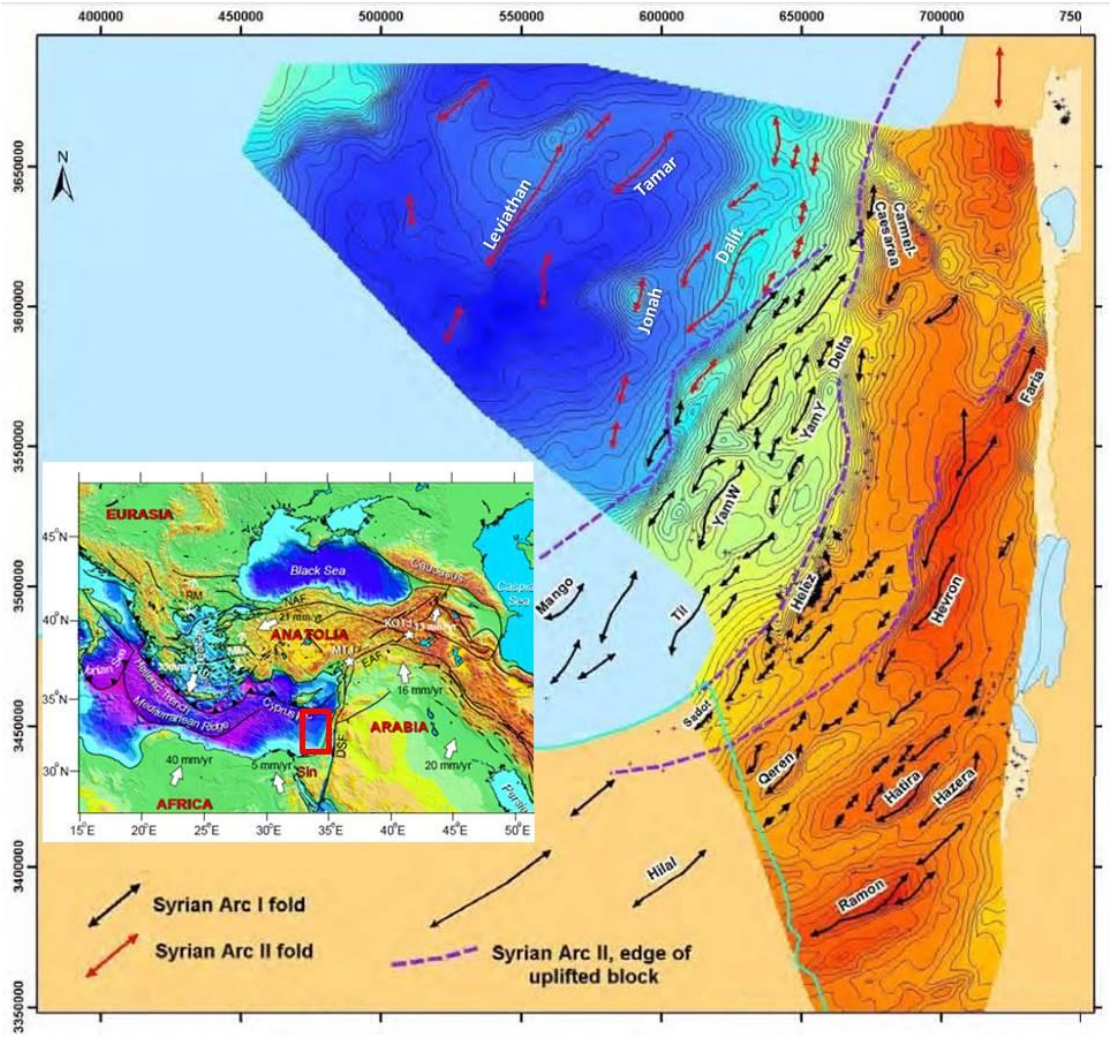

Figure 1.1: Middle Cretaceous offshore map modified from Gardosh et al. (2008), onshore top Judea (top Turonian) map after Fleisher and Gafsou (2003). Gardosh et al. (2008) divide the folds according to Walley (1998) to Phase I (Late Cretaceous) and Phase II (Eocene) Syrian Arc tectonism for the shelf and deep Levant basin respectively. This study adds much information to this preliminary mapping by distinguishing between horsts that were and were not reactivated and by identifying distinct folding events (Figs. 4.2, 4.3, 4.7). Inset: tectonic map of Eurasia-Africa-Arabia collision zone modified after Tectonic Crossroad Conference (2010) (http://www.geosociety.org/meetings/2010turkey/CollisionZoneMap.pdf). White arrow denotes plate convergence in mm per year, study area - red box.

In the Late Cretaceous (90-80 Ma), when the African–Arabian Plate started to collide with the Euro-Asian Plate, the regional stress field was reversed and the entire region was subjected to compression that resulted in the formation of extensive anticline and synclines throughout the Levant region, known as the Syrian Arc fold

belt, described in section 1.4.2 bellow (Krenkel, 1924; Hensen 1951; De Sitter, 1962; Freund et al., 1975; Eyal and Reches, 1983; Chaimov et al., 1992; Eyal, 1996; Walley, 1998; Bosworth et al., 1999; Moustafa, 2013).

A major uplift of Arabia-Africa in the Oligocene formed three structural steps along the eastern Levant basin and margin (Bar, 2009; Steinberg et al., 2011). In the south, the Red Sea rifting started while subduction in the Zagros area (north) took place (Fig. 1.1). Towards the end of the Oligocene and Early Miocene reactivation of the Levant passive margins as a result of the Africa-Arabia breakoff took place (Gvirtzman et al., 2008). The continental margin fault zone (CMFZ), which accentuated pre-existing folds 20-30 km offshore was further interpreted by Gvirtzman and Steinberg (2012) as an incipient plate boundary formed at the early stage of Africa-Arabia breakoff. Alongside with the breakup between Africa and Arabia, and coeval with the widespread magmatism that accompanied the Afar plum in East Africa and the Red Sea opening, magmatic activity migrated northwards, producing large volcanic fields and regional uplifting through western and northern Arabia (Ebinger and Sleep, 1998; Krienitz et al., 2009). Expression of this Cenozoic magmatism was identified along the Israeli coastline (The National Park Basalt, Gvirtzman, 1970) but not farther offshore.

Some major changes in plate configuration occurred during the Miocene. The establishment of the African plate subduction beneath Eurasia took place south of Cyprus, and the Dead Sea Transform, separating African plate from the northward moving Arabian plate, evolved (Quennell, 1958; Freund et al., 1970; Ben-Avraham, 1978; Bartov et al., 1980; Garfunkel, 1981; Garfunkel, 1998; Robertson, 1998a,b; Schattner, 2010). Toward the Late Early Miocene a second regional uplift of the Eastern Levant took place and was accompanied by cut-of rivers from their eastern

drainage area (Bar, 2009). Final suturing of northern Arabia and Eurasia in the Late Miocene resulted in basin inversion of the Palmyrides fold belt and Euphrates fault system (Brew et al., 2003; Chaimov et al., 1992). The ongoing left lateral displacement along the Dead Sea transform promoted N-S extensional faults in the Galilee (Israel) and activity along the Carmel fault took place (Steinberg et al., 2010; Schattner et al., 2006; Gvirtzman et al., 2011).

The end of the Miocene in the Levant basin was pronounced by the Messinian Salinity Crises, which deposited more than 2 km of evaporates throughout the Mediterranean basin (Hsu et al., 1973; Ryan and Cita, 1978; Mart and Ben-Gai, 1982). The Early Pliocene transgression that followed the Messinian regression, in the east Mediterranean, was marked by the establishment of the Nile cone in the southern of the Levant basin (Macgregor, 2011). During the Late Pliocene, concurrently with the ongoing Nile cone build up in the south, filling of the Jaffa basin, in the east, along the Israeli coastline took place and 2500 m of sediments accumulated building the nowadays Israeli shelf area (Gvirtzman et al., 2008; Steinberg et al., 2011). In the north of the Levant basin, accelerated subduction of the African plate underneath Cyprus has enhanced Eratosthenes subsidence and the deepening (>2 km) of the sea-floor towards the Cyprus arc (Robertson, 1998b).

Throughout a large time span of the Levant basin history, a unique deformation took place in the form of elongated folds that peppered the northern Africa through parts of Arabia. This phenomenon termed the Syrian Arc Fold system is described below (section 1.4.2).

1.4.2 The Syrian Arc Fold Belt

Compression during the closure of the Tethys Ocean resulted in the formation of extensive anticlines and synclines throughout the Levant region, known as the Syrian Arc fold belt (Krenkel, 1924; De Sitter, 1962; Freund et al., 1975; Eyal and Reches, 1983; Chaimov et al., 1992; Eyal, 1996; Walley, 1998; Bosworth et al., 1999; Moustafa, 2013). The trends of the Syrian Arc folds vary systematically from WSW-ENE direction in northern Sinai, to an almost N-S direction in central Israel, and to NE-SW in the Palmyra Mountains in Syria, forming an S shaped 1000 km long feature (Fig. 1.1). In Israel the folds are exposed inland (Bartov et al., 1980; Bruner, 1991; Beker, 1994) and are buried by younger sediments in the coastal plain and continental shelf (Druckman et al., 1995; Gardosh and Druckman, 2006). The fold amplitudes range from a few hundred meters to almost 1 km. It is commonly accepted that slip that occurred along reverse faults at depth led to the development of monoclines or folds in the upper part of the stratigraphic column (Reches et al., 1981; Eyal and Reches, 1983; Bruner, 1991). Some of the folds are associated with reactivation of Early Mesozoic normal faults in a reverse motion (Freund et al., 1975; Cohen et al., 1990; Bruner, 1991; Druckman et al., 1995; Brew et al., 2003; Moustafa, 2010; Yousef et al., 2010).

Studies from western Egypt, northern Sinai, Israel, Lebanon and Syria dated the onset of activity of the Syrian Arc folding to Turonian (Flexer et al., 1970; Honigstein et al. 1988; Eyal 1996), Coniacian (Bartov et al., 1980), and Santonian (Guiraud and Bosworth, 1997; Bosworth et al., 1999; Walley, 1998). Subsequently folding activity is observed in northern Sinai during the Campanian (Moustafa, 2010) and during the Maastrichtian in southern Israel (Hardy et al., 2010). In addition, a Late Eocene folding phase was identified in Israel (Bar, 2009; Bar, 2013; Steinberg et al., 2011)

and in Lebanon (Walley, 1998). Walley (1998) termed this activity as Syrian Arc Phase II and Gardosh et al., (2008) adopted this terminology to describe folds in the deep Levant basin.

Evidence for younger folding in Israel and Sinai are quite rare, because since the Late Eocene the inland region was gradually exposed (Adams et al., 1983; Buchbinder, 1996; Buchbinder and Zilberman, 1997; Ziegler et al., 2001; Gvirtzman et al., 2008; Gvirtzman et al., 2011; Bar et al., 2013), therefore much of the stratigraphic record is missing (due to erosion or non-deposition). Nonetheless, some indication for Oligocene folding was reported by Gvirtzman (1970) from the subsurface of Israel's coastal plain.

In the Palmyra mountains, Syria, middle Miocene folding pulses are apparent (El-Motaal and Kusky, 2003; Brew et al., 2003). Post Neogene activity was reported from the Fari'a anticline (Mimran, 1984) and young Pliocene phase of folding in central and north Israel was reported by Eyal (1996), which argued that Syrian Arc compatible deformation (not only folding) occurred, intermittently, from the late Turonian to the Recent due to remote and long term stress field.

Altogether these studies indicate a long history of folding, but a coherent depiction about how folding developed in time and space is still lacking. We take advantage of the relatively continuous section that was preserved in the Levant basin, and will show in chapter 4, for the first time, a continuous picture in time and space of the folding activity. The results portray a long-lived episodic activity extending, at least, till the Early Pliocene, with varying intensity and complex spatial pattern that is inconsistent with the simplified classification suggested by Gardosh et al. (2008) of Phase I in the Late Cretaceous and Phase II in the Oligocene.

2. Data and Methods:

The seismic method plays a prominent role in the research of subsurface structures, basin analysis, and for hydrocarbon exploration in particular. Conventional processing of seismic reflection data yields an earth image presented by a seismic section which is displayed in time units. In the presence of strong to severe lateral velocity variations, seismic imaging of the subsurface must be done using depth imaging techniques so as to properly account for lateral velocity variations, and the result is displayed in depth units (Yilmaz, 2001). Then, the depth migrated section can be considered as a close representation of the structural cross section of the subsurface. Improving the accuracy of the imaging by resolving detailed velocity variation, associated with both structural and stratigraphic targets, is one of the main goals undertaken in this study. It then enables to perform a complete synthesis of the interpretation and the imaging it relies on.

This chapter is composed of four parts. The data sets available for the project are first presented (Sec. 2.1), then the theoretical framework for seismic data processing and imaging is briefly described (Sec.2.2), followed by the interpretation methodology (Sec. 2.3), and at last the basic concepts of gravity and magnetic (Sec. 2.4).

2.1 The Database

The database for this study comprises mainly of 2D seismic reflection lines, oil exploration boreholes, gravity and magnetic data, and previously interpreted horizons (Steinberg, 2011), which were subsequently modified.

The seismic data set used in this research includes more than 20 2D seismic reflections surveys (~27,000 km long), extending from the coastal plain of Israel

through the continental shelf area to the eastern flank of the Eratosthenes sea-mount (Fig. 2.1). These surveys were acquired in the framework of hydrocarbon exploration activity in the past 40 years. The imaging and interpretation of the deep basin is based mostly on surveys that were acquired during the years 2000 and 2001. Their relatively long (>7 km) cable and long recording time (9 and 12 seconds for the 2001 survey of TGS-Nopec Geophysical Company L.P. and the 2000 Spectrum Energy and Information Technology, Ltd., respectively), enable to gain a better imaging at depth >7km in compare to older surveys (that used a shorter cable length and shorter recording time). The resulting time sections of these surveys (processed by the surveying companies) were used for the interpretation, whereas raw data (not-processed) of five selected lines were used for re-processing in order to improve the deep subsurface imaging. Some of the time sections were missing coordinates in their segy headers. Therefore a matching between the shot coordinates and the CMPS (Common Mid Point – representing the location of traces in the time section) was performed using the acquisition geometry. This process enabled to properly locate the seismic sections in a coordinate system (the UTM Zone 36 N was used). Altogether, the seismic data provide a vast coverage of the Levant Basin, with interpretable imaging down to a depth of at least 10 km and at places even deeper.

The boreholes data comprises of 30 wells located on the shelf area and onshore (Fig. 2.1). Detailed stratigraphic subdivisions of these wells used in this study are based on Fleischer and Varshavsky (2002). Formation tops were used to calibrate the interpreted horizons where velocity data and time-converted wire-line logs were available. Noteworthy, the recent deep water wells drilled in the Levant Basin are not deeper than ~6.3 km and due to commercial confidentiality restrictions these well's data were not available for the current research. However, few deep water wells (for

example: the Tamar-1 and the Leviathan-1 wells drilled in 2009 and in 2010, located 90 and 130 km offshore Israel, respectively, Fig. 1.1) provided insight into the architecture Levant basin and settled the debate between three very different stratigraphic interpretations. The presence of Early Miocene sediments at a depth > 3 km below the seafloor is consistent with the interpretation of a thick Oligocene-Miocene section below the Messinian evaporates (Gardosh et al., 2008; Gvirtzman et al., 2008) and challenges other interpretations that predicted Senonian-Eocene (Gardosh and Druckman, 2006; Roberts an Peace, 2007) or even Cretaceous strata (Peck, 2008) at depth where Miocene rocks were penetrated (Steinberg et al., 2011). This study adopted Steinberg et al. (2011) interpretation (which is consistent with Gardosh et al., 2008 and Gvirtzman et al., 2008) and enlarged the interpretation towards the NE part of the basin and onshore (the Zebulun plane NE Haifa bay), to the northern and western part of the basin using parts of the seismic lines that were not available during previous studies.

This work presents newly basin wide interpretation of the base Late Pliocene, base Late Miocene, base Santonian and base Late Jurassic horizons (Fig. 2.2). Moreover, six previously interpreted horizons (Steinberg, 2011) were modified and incorporated to the present database. The modifications made here are mostly local (north of the Carmel area, in the southern and northern and western part of the study area), whereas refinement of the interpretation of the Miocene and Pliocene sections in the shelf area was performed based on a revised biostratigraphy of several wells (Bar, 2009).

Gravity and magnetic data were collected as part of a reconnaissance survey for oil exploration (by TGS-Nopec Geophysical Company L.P) in 2001 (Fig. 2.1). A total of 320,000 stations were measured along the seismic lines at intervals of ~20 m. The

accuracy of the data (estimated on the crossing locations) is about a few nanoTesla for magnetic measurements and 0.1mGal for the gravity measurements. The free air gravity and the magnetic data are used here to test a geological model of Jonah high (Sec. 5.6).

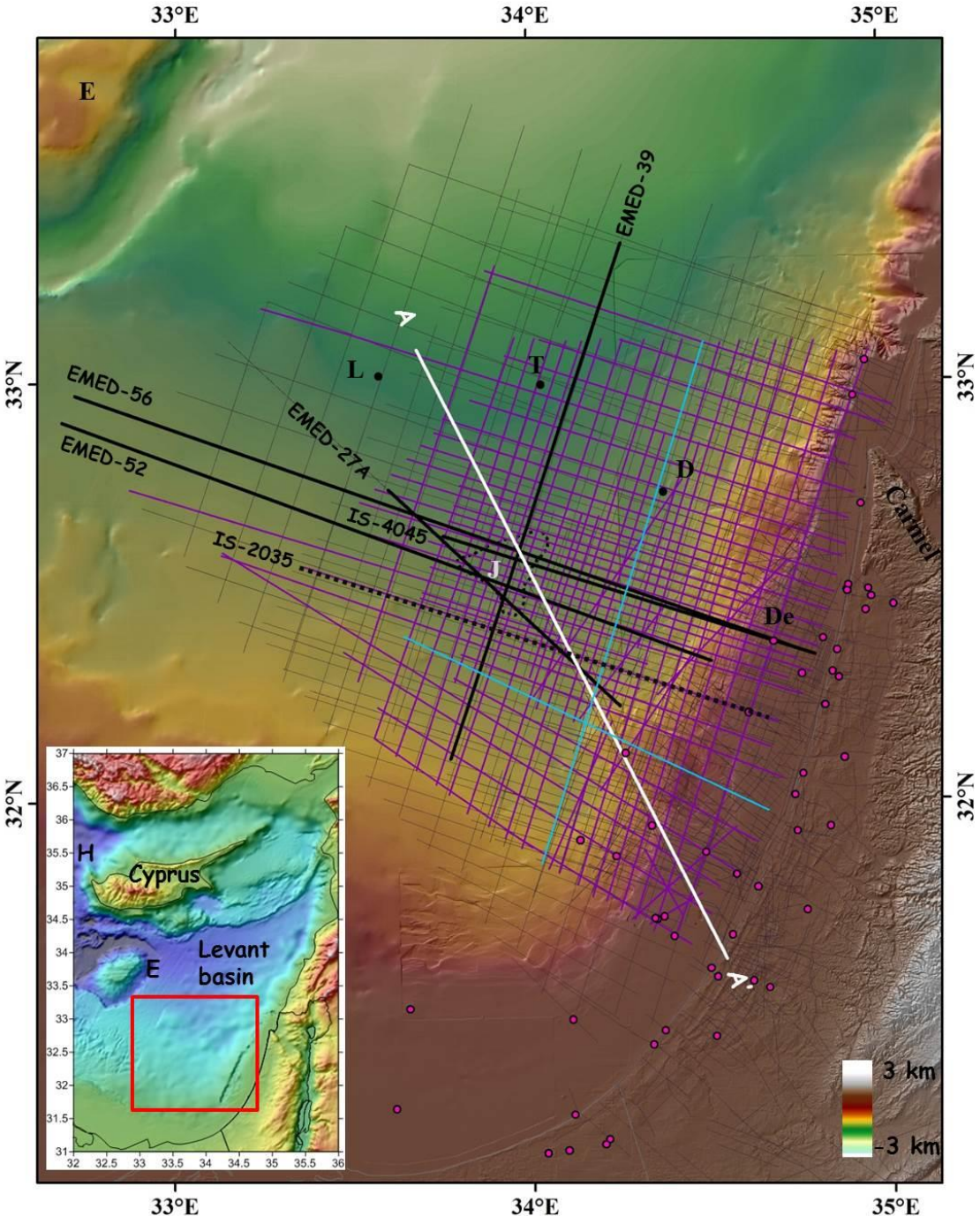

Figure 2.1: Location map. The bathymetry in the colored map is from Hall (1993). Dashed black polygon denotes the part of the Jonah high (J) where the lower Saqiye Gr. (Late Eocene-Oligocene) is missing. Regional bathymetry map (inset) is taken from ETOPO 11 (Amante and Eakins, 2009). Black

lines are the re-processed seismic lines in this study. Light blue lines were re-processed by Marig (2015). Black dotted line - interpreted time migrated line (Fig. 4.1). Fine purple mesh represents the 2001 TGS-Nopec seismic reflection survey that also collected gravity and magnetic data. Fine gray mesh represents all seismic lines used for interpretation. AA' is a regional section used for gravity and magnetic modeling (Fig. 5.8). Dots are wells used for correlation. Abbreviation: L-Leviathan, T-Tamar, D-Dalit, De-Delta-1, E-Eratosthenes seamount, H-Herodotus Basin.

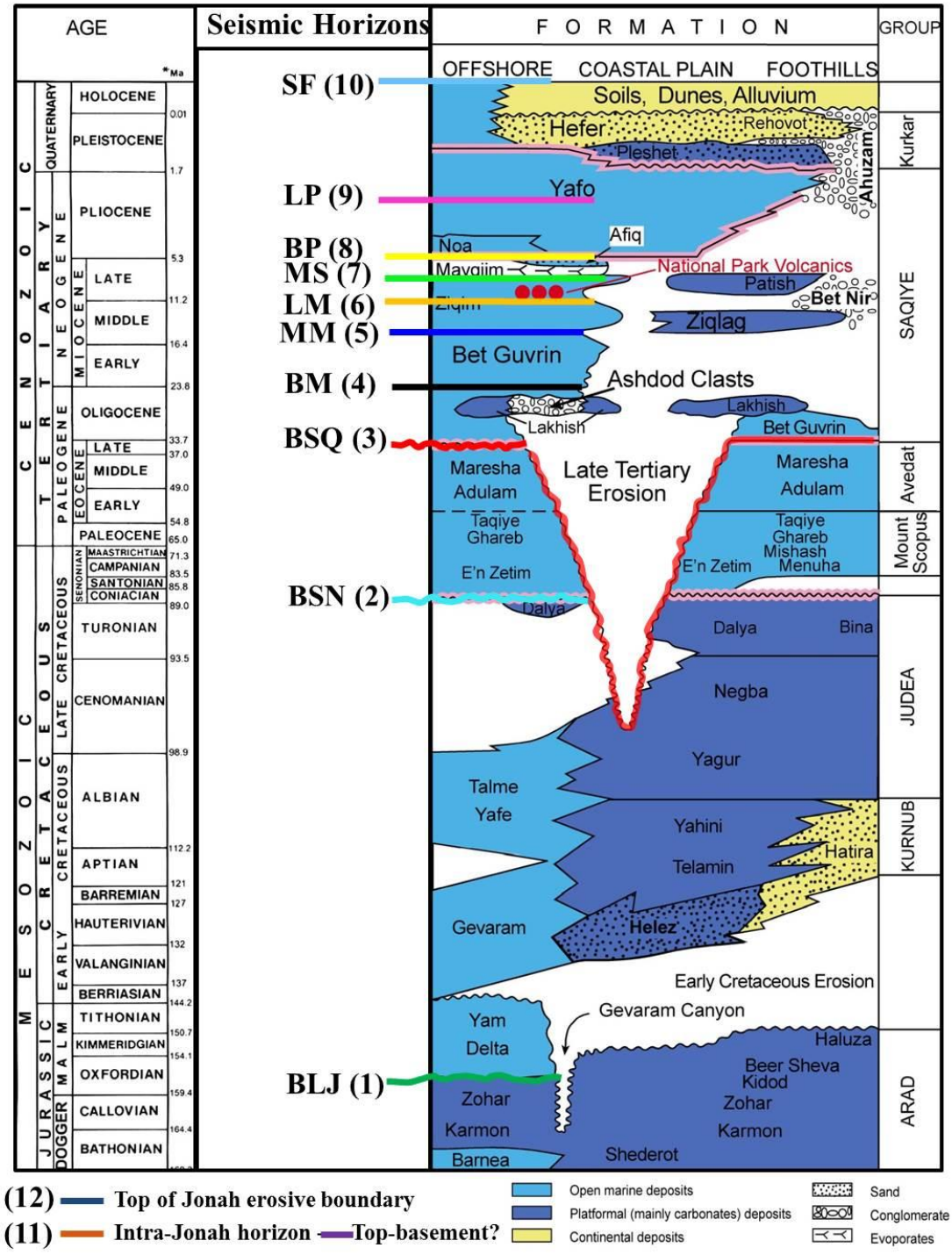

Fig. 2.2 Chronostratigraphic table modified from Gvirtzman (2004) Gvirtzman et al. (2008). Seismic horizons which have been interpreted are numbered and marked according to their position in the stratigraphic column: BLJ – Base Late Jurassic, BSN – Base Santonian, BSQ – Base Saqiye, BM – Base Miocene, MM – Base Middle Miocene, LM – Base Late Miocene, MS – Base Messinian, BP – Base Pliocene, LP – Base Late Pliocene, SF – Sea Floor.

2.2 Seismic Data Processing

The seismic processing procedure used in this study is presented in this section. The description is focused on methods and procedures applied to the specific seismic lines processed in this study. The section is mainly technical and is written based on the assumption that the reader is familiar with seismic processing. Mathematical principles of the seismic methods, as well as basic technical processing procedures are not described or discussed in details here.

2.2.1 General description

The seismic methods utilize the propagation of sound energy waves through the Earth where the different layers within the Earth's crust reflect back this energy. Reflected seismic waves are recorded by using hydrophone (in water) or geophones (on land). The reflected signals, their time of arrival and amplitudes are collected onto a storage medium, and then they are processed to produce seismic sections. Results of conventional processing of seismic data often are displayed in the form of CMP (Common Mid-Point)-stacked section, with the time as the vertical axis (e.g. Gardner, 1985; Yilmaz, 2001; Zhou, 2014). There is a well-established sequence for standard seismic data processing comprising: pre-stack processing, stacking, and post-stack processing making up the foundation of routine processing (Yilmaz, 2001). The processing sequence performed in this study included four stages: 1) pre-stack time processing, 2) building an interval velocity model in depth, 3) pre-stack depth

migration and 4) post-stack processing (Fig. 2.3). Migration is a process that moves dipping events to their supposedly true subsurface location and collapses diffraction (Scales, 1995). It can be performed either on CMP gathers prior stacking (pre-stack time migration) or on stacked data (post-stack time migration). As long as there are no lateral velocity variations, seismic imaging of the subsurface can be achieved using time migration techniques and the result can be displayed in time domain. However, in the presence of strong to severe lateral velocity variations, time migration is no longer valid. Instead, seismic imaging of the subsurface must be done using depth imaging techniques to properly account for lateral velocity variations, and the result must be displayed in depth domain (Yilmaz, 2001). Moreover, even without strong lateral velocities variations, converting a time migrated section to depth domain might also introduce errors. This occurs especially when there is a decrease in velocities with depth for example below a salt layer (such as the Messinian salt layer in the Mediterranean), as average velocities cannot account for such a velocity inversion, the use of interval velocities is essential in order to avoid inaccurate scaling of the time migrated section to depth. The depth migrated section can be considered as close representation of the structural cross-section of the subsurface only if the velocity-depth model is sufficiently accurate (Yilmaz, 2001; Scales, 1995). For example, part of the present research focuses on the Jonah high (Ch. 4) and the reflectors bordering it. Improving the imaging of this structure is aimed at answering several questions about this structure: are there any reflectors inside? Is it a faulted structure? What is its overall geometry? What is the geometry of the reflectors bordering it? How flat they are and how they terminate towards it? Answering these questions requires a detailed imaging in depth is required to properly solve reflector's geometry and

bounding issues that arises from this complex structure (lateral and vertical velocities variation).

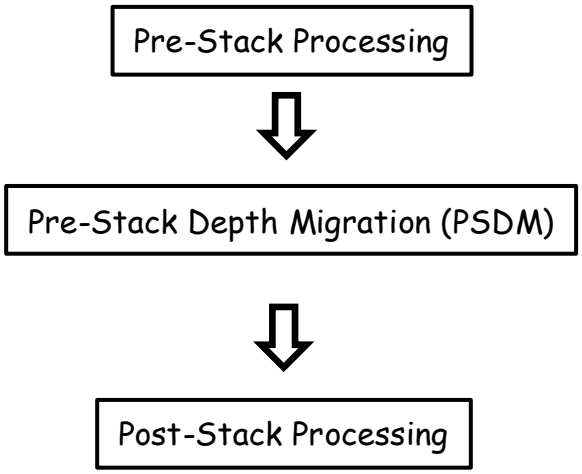

Figure 2.3: The major processing stages performed in this study. Special care was given for obtaining the Interval velocity model in depth (using the coherency procedure for obtaining an initial velocity model followed by several iterations of residual velocity analysis to obtain the final velocity model), which is part of the PSDM process.

In the present seismic analysis the following considerations were applied: 1) selecting a proper sequence of processing steps appropriate for the field data under consideration, 2) selecting an appropriate set of parameters for each processing step, and 3) evaluating the resulting output from each processing step, then diagnosing any problems caused by improper parameter selection. Some of the processes and the evaluation of the resulting output of each processing step are mainly sharped-eye decision based. Thus, processing results may vary from different analyst. Therefore, I present here the details of the processing sequence performed on the selected processed lines, the various tests that were performed for selecting optimal parameters for each module and the selection of specific modules. Decision making, throughout the processing stages, was not only eye-based, but combined with a geological

understanding of the subsurface, and geophysical understanding of the processing algorithms.

2.2.2 Pre-stack processing

Five seismic lines crossing the Jonah high having an overall length of 682 km were selected for reprocessing and for depth migration (Fig. 2.1). The lines were selected according to their spatial locations and the data quality. Acquisition parameters are described in table 2.1, and cable configuration for each survey is presented in appendix (A). The various processing stages were in part iterative processes and were accompanied by geological interpretation. For example, the depth migration procedure requires a well constrained interval velocity model. Therefore, during the refinement stage of the interval velocity model, several runs of PSDM (Pre-Stack Depth Migration) were performed in order to test the quality of the model. Most of the processing was performed using the Echos software from Paradigm®, while multiple attenuation was performed in the Promax software from Landmark.

Line name	Number of Channels	Group Interval (m)	Shot Interval (m)	Sample Rate (msec)	Streamer Length (m)	Record Length (sec.)	Processed Length (km)
EMED-27A	576	12.5	25	2	7200	12.288	86
EMED-39	576	12.5	25	2	7200	12.288	116
EMED-52	576	12.5	25	2	7200	12.288	171
EMED-56	576	12.5	25	2	7200	12.288	206
IS-4045	576	12.5	25	2	7200	9.216	103

Table 2.1: Acquisition parameters of the re-processed seismic lines

The purpose of the pre-stack processing is to clean the data from noise, multiples and improve the signal to noise ratio without deteriorating the data. The data were recorded with a sampling rate of 2 msec and channel spacing of 6.25 m. For a line length of ~100 km the raw data can reach more than 10 GB. The files sizes were reduced in order to enable a faster processing and an easier storage of the various

intermediate data sets, by down sampling to 4 msec and to 25 m for group interval (summing two nearby channels to result in one channel and thus having 25 m between consecutive channels). The down sampling might cause spatial aliasing. Therefore, I first performed a whole sequence of processing of line EMED-27 without down sampling, and then compared the resultant time stacked section with the same line processed with the down sampling. As no differences could be observed either on the stacked data or on the time gathers, I down sampled the other processed lines. Prior down sampling the channels, a K-filter was designed based on the spectral analysis of the data and applied in order to avoid any spatial aliasing. Then 2D geometry was assigned according to coordinates stored in the P190 files. A preliminary velocity analysis was performed and stacking the data yielded the brut stack. The first step of the processing is summarized in figure 2.4. Upon stack examination, regions of interest were identified, and the CDP (Common Depth Point) range (above the Jonah high) where the various tests were conducted was set.

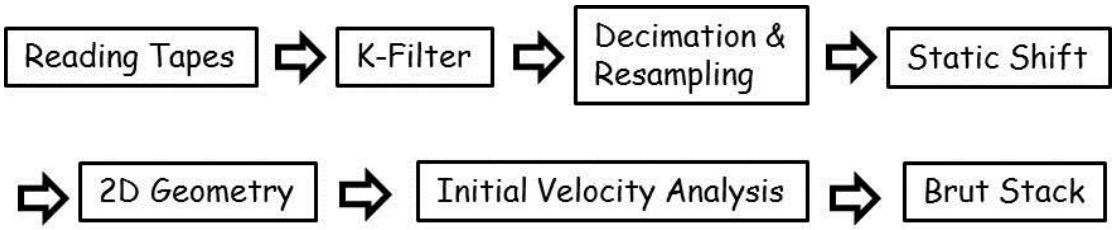

Figure 2.4: Pre-stack processing - first step. K-filter is a spatial filter (operating on the wavelength), decimation refer to the summing of two traces and hence reduce the number of traces by half, static shift refer to time corrections made to each trace.

The next step of the processing involved several tests for deconvolution, filtering, multiple attenuation etc., and is displayed in figure 2.5. These tests were combined with several iteration of velocity analysis to yield the best stacking velocity and the most enhanced signal to noise ratio data. The various parameters were all applied to

the pre-stack data but the results were observed either on the pre-stack data (CMP gathers) and or on stacked data.

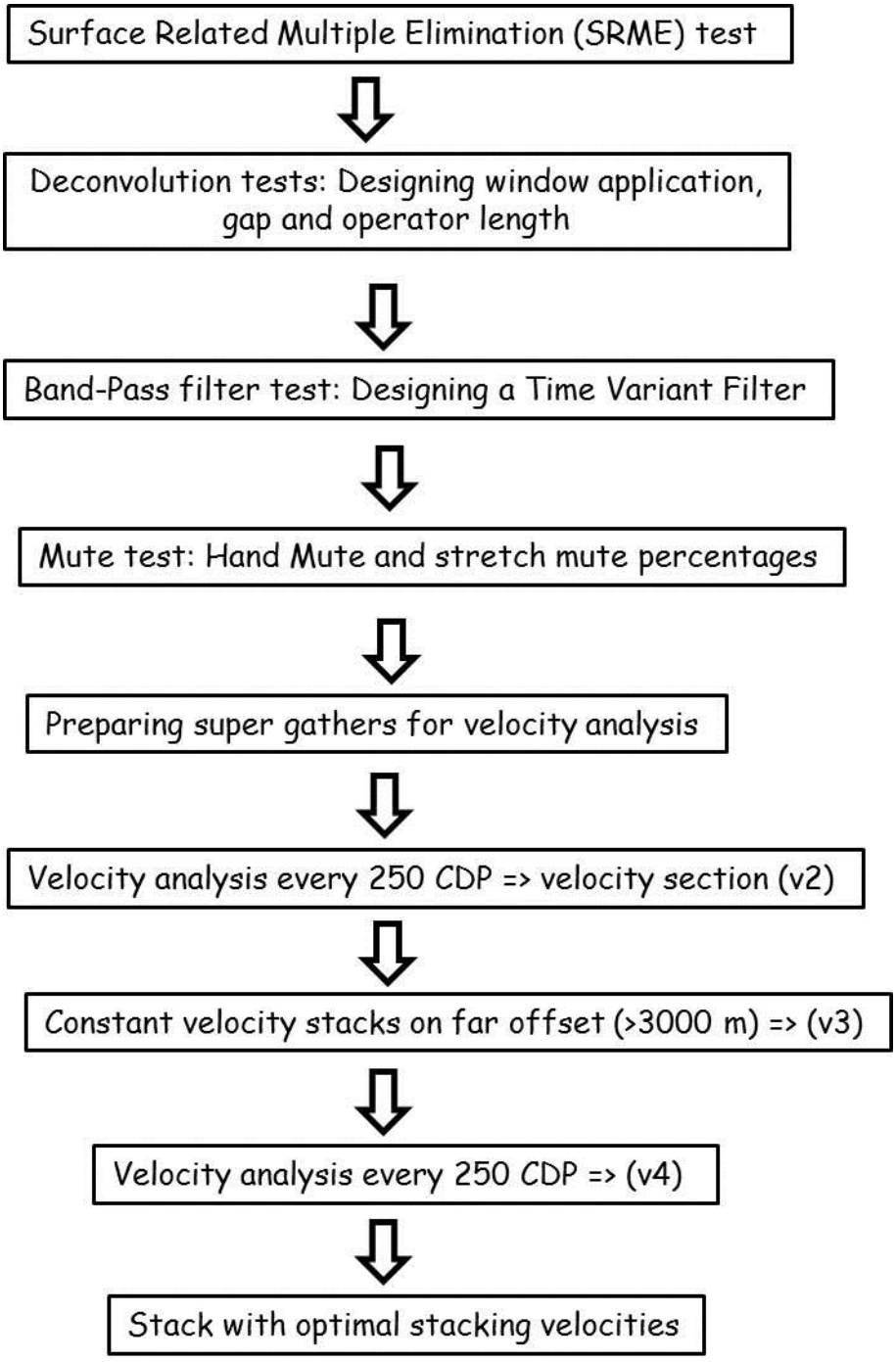

Figure 2.5: Pre-stack processing – second step: tests and velocity analysis.

At this stage of the processing a time section was obtained using optimal stacking velocity. This time section however revealed numerous multiple events from the seafloor, and mostly from the Messinian salt layer, which tends to confine the seismic wave creating intra-bed multiples. These multiples obscure part of the section below the base of the Messinian layer and may interfere with the top of Jonah structure (Fig. 2.6). Unfortunately the SRME (Surface Related Multiples Elimination) module performed in the pre-stack processing (Fig. 2.5) did not reduce those multiples (Fig. 2.6). Therefore a special care was given in order to reduce as much as possible various multiple events.

Multiples can be more easily detected on the τ-P ("Tau-P" time-slowness) domain and suppressed from the primaries (Gardner, 1991). The main radon filters are based on converting the data from the T-X domain to the τ-P domain and then selecting part of the data to be converted back to the T-X domain. In this procedure only the relevant data (the primaries) are mapped back to the T-X domain.

Other tests were performed in order to enhance the signal to noise ratio such as the trace mix, dip filter and far offset stacks using various offset ranges. Also post-stack time migration was performed to enable horizons interpretation on a time migrated section. These interpreted horizons are the basis for computing the initial interval velocity model (as described in the next section).

The pre-stack processing stage ends with optimal un-migrated CMP gathers, stacking velocities and post-stack time migrated section. The next step is to build an interval velocity model.

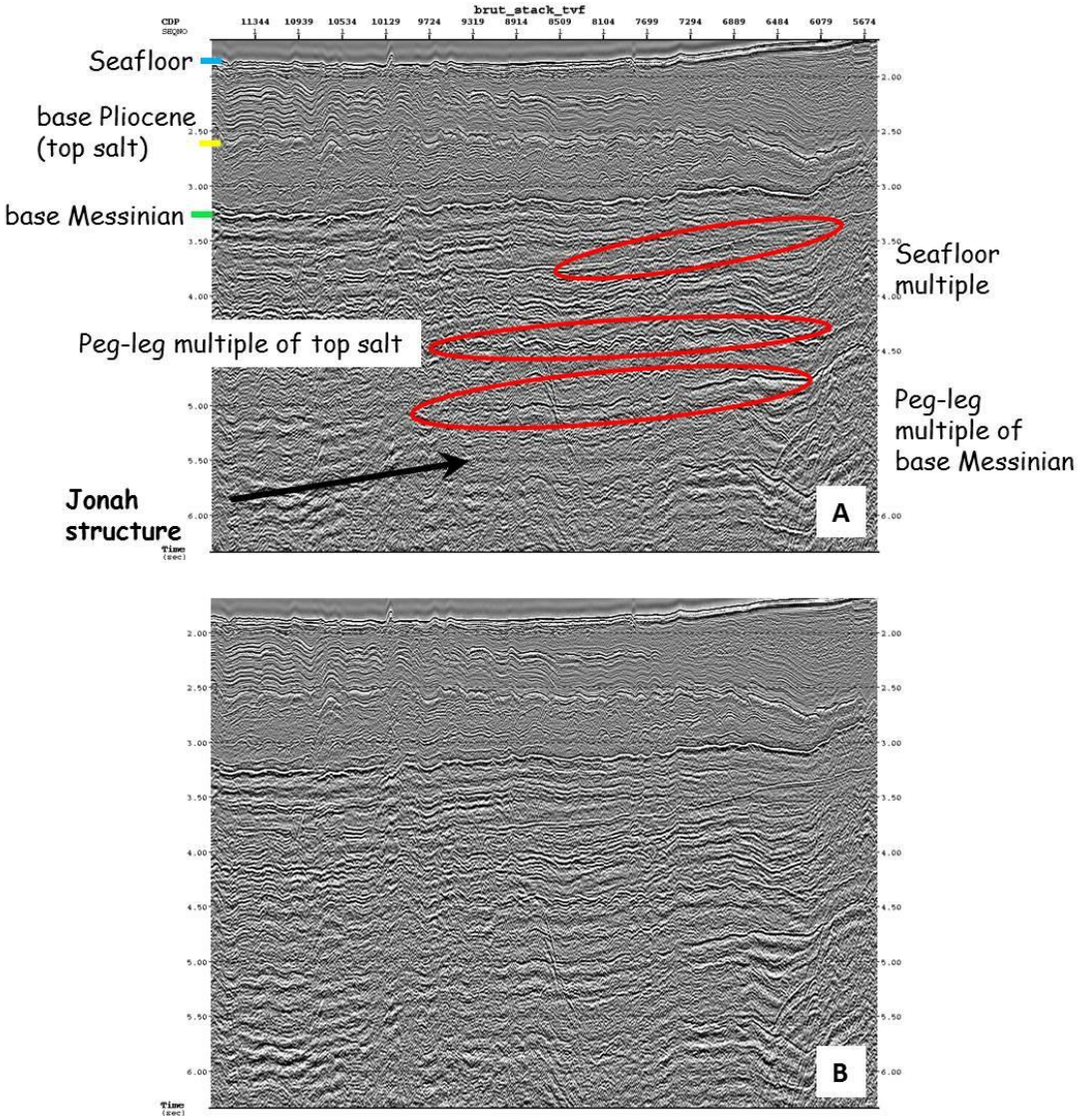

Figure 2.6: Time stack line EMED-52 a) Examples of various multiples affecting time stacked data of line EMED-52. b) After applying the SRME algorithm, multiples are still present in the data.

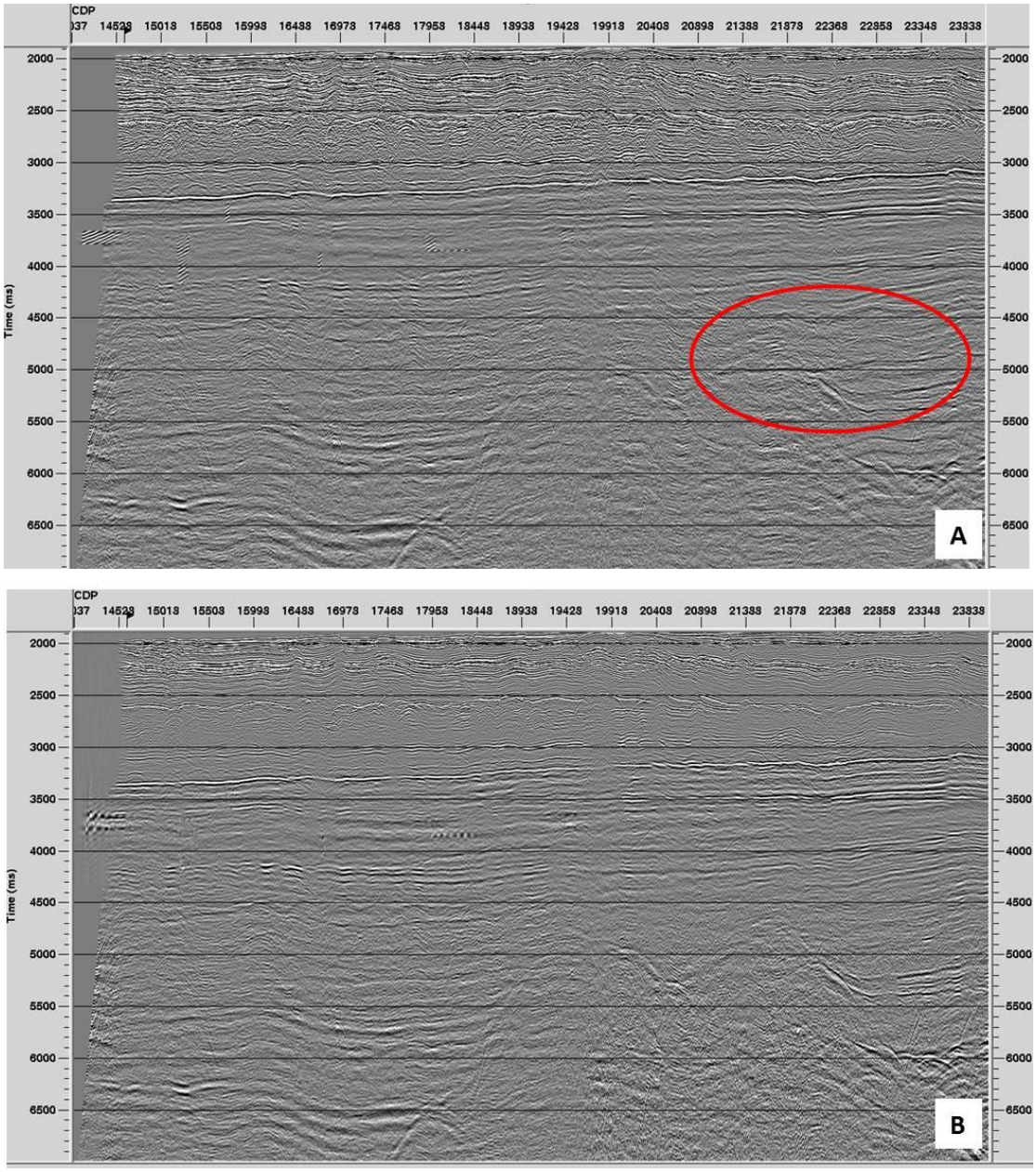

Figure 2.7: line EMED-27A, a) without Radon filter, multiples obscure the flanks and the top part of Jonah high. b) After application of Radon Filter, the multiples are attenuated, improving the imaging of Jonah high.

2.2.3 Interval Velocity Model

An earth model in depth usually is described by two sets of parameters: layer velocities and reflector geometries. Defining the optimal interval velocity model along each seismic line is one of the corner stone in seismic data processing. Building

the interval velocity model is usually performed iteratively as part of the PSDM procedure.

In this study the Coherency Inversion process (Landa et al., 1991) was used in order to build an initial interval velocity model in depth. This procedure is inherently a layer stripping process as expressed in figure 2.8. After obtaining an initial interval velocity model, tomography and subsequent residual moveout corrections were performed for further flattening the gathers.

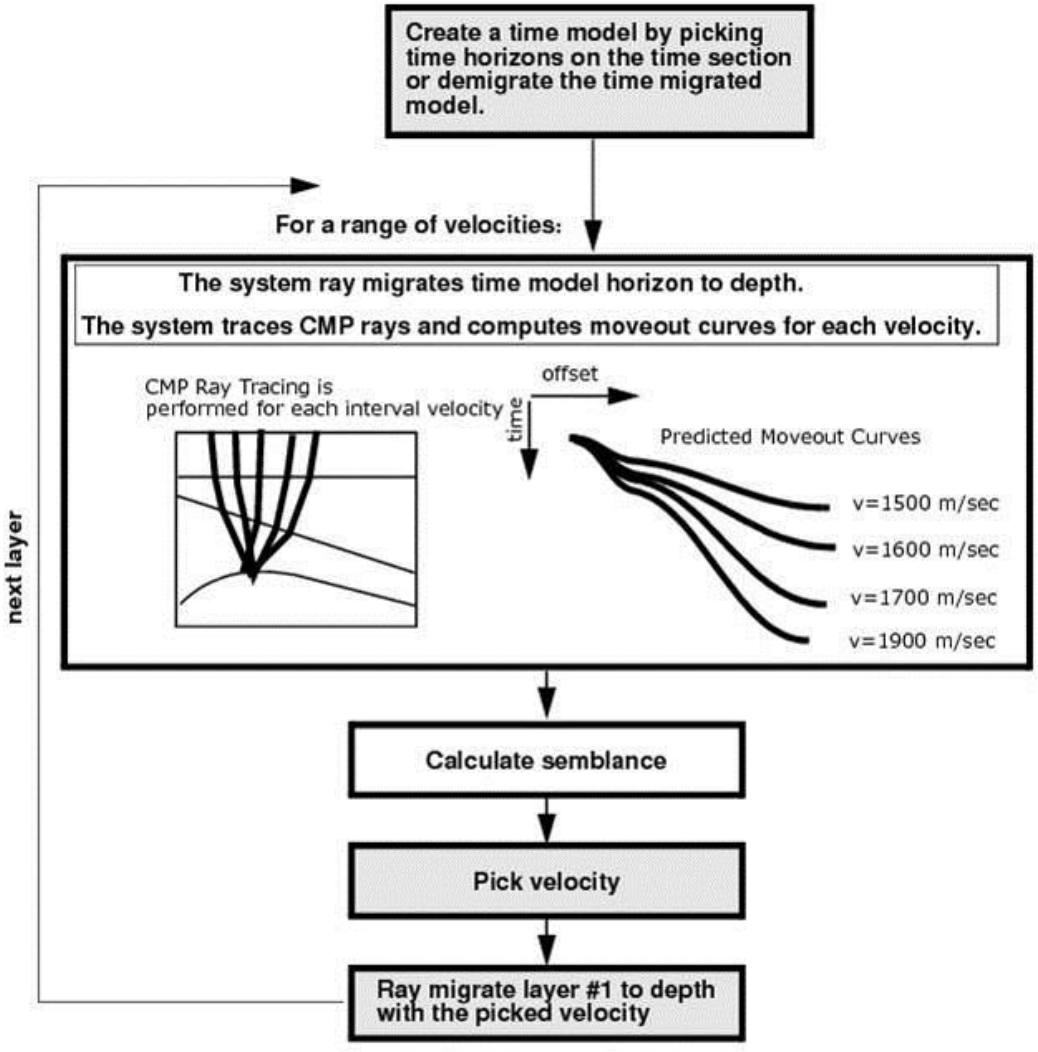

Figure 2.8: Model-based approach for interval velocity analysis (stripping process). For each horizon interval velocities are directly estimated using ray tracing. Non-hyperbolic moveout curves are computed for a number of different velocities. Modified after Paradigm® help.

Application of Paradigm®'s Tomography modules (Kosloff et al., 1996) were performed in a layer stripping method such that whenever the gathers were flat (from top to bottom of the section) the velocity model was kept fixed and updates were performed on the layer or layers underneath. Paradigm®'s Horizon Based Tomography was applied (hence long wavelength updates) and also the Grid Tomography module which uses an auto-picker (test for optimal segment length of auto-picker were performed), yielding intra-layer updates in velocities. The process of velocity refinement is repeated until flat gathers are obtained.

Due to inability to perceive reflections inside Jonah structure and due to the fact the depth gathers displayed flat reflectors at least down to the base-Saqiye horizon, constant velocity test was performed in the following manner: down to the Mid-Miocene horizon the most updated velocity section was used, bellow the Mid-Miocene horizon a constant interval velocity was used for the PSDM. The range of velocities that was tested: 3100 to 5500 m/s by step of 200. A final interval velocity section was selected and the pre-stack time gathers were migrated using the Kirchhoff PSDM algorithm to produce a final depth section. Radon test and dip-filter test were also performed directly on depth gathers and on scaled to time domain depth gathers. However, neither process was successful in improving the imaging below Jonah structure.

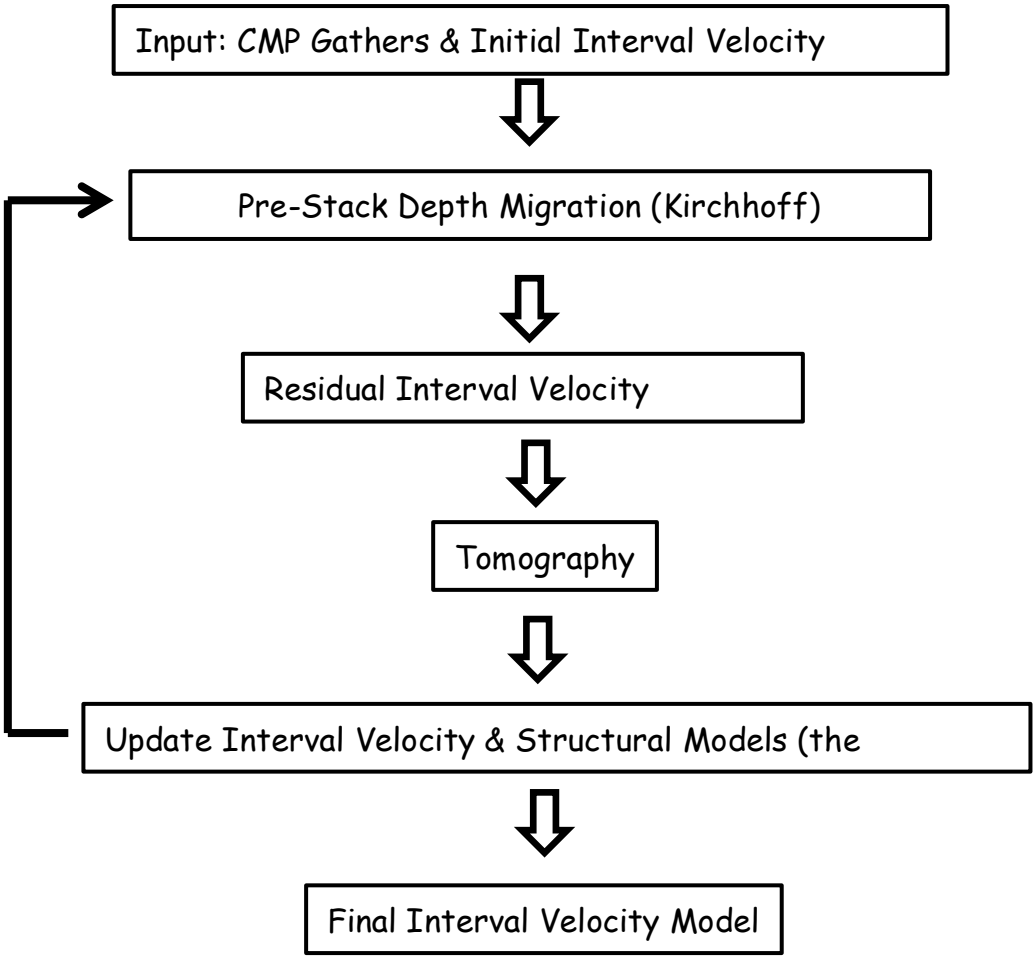

Figure 2.9: Workflow for refinement of the interval velocity model.

2.2.4 Final PSDM and post-stack processing

Using the final interval velocity model the Kirchhoff pre-stack depth migration was applied to the CMP gathers which were subsequently stacked to result in a depth section. Post stack processing was done in the time domain (the depth sections were scaled to time). It included an F-K filter and a time variant band-pass filter. At last, the time sections were scaled back to depth resulting in the final depth sections. Noteworthy, the interval velocities computed along each seismic line were gridded and smoothed in order to provide interval velocity maps for the entire study area. These interval velocity maps were used for the time to depth conversion of the structural maps as described below in Sec. 2.3.3.

2.2.5 Constrains and limitations

There is a fundamental problem with inversion applied to earth modeling in depth: velocity-depth ambiguity. This means that an error in depth is indistinguishable from an error velocity (Landa et al., 1988; Yilmaz, 2001). Therefore, an output from inversion is an estimated velocity-depth model with a measure of uncertainty in layer velocities and reflector geometries. As a result there may be additional velocity models that fit the measured data.

Cable length is an important limitation factor on the ability to resolve rock velocity. When offset is small in compare to reflector's depth, a large range of velocities will flatten the gather. Usually (depending on the data's quality) the loss of resolution occurs when the reflectors are at depth of 1 to 1.5 times the cable length (which is ~7 km for the processed data). This leads to uncertainty in the depths of the interpreted horizons where it may attain 10-15 % at the deeper part of the section (>14

km). For example, the reflector of the base Santonian horizon was found at depth of ~7 km with a +/- 300 m shift between preliminary depth migrated section and the final depth migrated section. These errors results from cumulative errors in the velocity model. Lack of well data further prevents minimizing the errors in the final horizon's positioning. Altogether, errors are expected at the deeper part of the section due to the decrease of signal quality with depth.

2.3 Interpretation

2.3.1 Horizon interpretation

Interpretation is basically aimed to gain geological understanding of the subsurface. It is primarily based on picking travel-times that are coincident with geological layer boundaries, and on manipulation of seismic amplitudes to enhance subtle features associated with depositional environment and sedimentology (Tearpock and Bischke, 2002).

An overall interpretation of 12 horizons is presented in this study (Fig. 2.2). Regional interpretation of four horizons (base Late Jurassic, base Santonian, base Late Miocene and Base Late Pliocene) was carried out on over more than 500 2D time-migrated seismic reflection lines. This interpretation completes six previously interpreted horizons by Steinberg et al. (2011) that were modified. In addition to the regional mapping, two local horizons were interpreted: the irregular top of Jonah high (denoted as the blue horizon) and an intra-Jonah reflector (denoted as the orange horizon). The horizons are: (1) BLJ – base Late Jurassic, (2) BSN – base-Santonian, (3) BSQ – the base of the Saqiye Group (which is an unconformity surface changing laterally from the base of the Late Eocene in the deep basin to the base of the Pleistocene section onshore, (Gvirtzman and Buchbinder, 1978) modified from

Steinberg et al. (2011), (4) BM – base Miocene (modified from Steinberg et al., 2011), (5) MM – base Middle Miocene (modified from Steinberg et al., 2011), (6) LM – base Late Miocene, (7) MS – base Messinian (modified from Steinberg et al., 2011), (8) BP – base Pliocene modified from Steinberg et al., 2011); (9) LP – base Late Pliocene; (10) SF – the seafloor (modified from Gvirtzman et al., 2014); (11) Intra-Jonah reflector; (12) top of Jonah.

A detailed interpretation of the depth migrated sections was performed in order to constrain the relationship between the Jonah structure and the reflectors around. In particular, we focused on faulting, truncation, on-lapping and thickness variations around the Jonah structure, and its internal reflectivity. This detailed analysis is presented in chapter 5.

This research uses thickness variation identified in seismic reflection data as a main observation for understanding syn-sedimentary tectonism. This rational arises from the assumption that if post- and pre-depositional effects can be identified and corrected for, observed thickness variations can be interpreted as a measure for syn-tectonic processes. In general, thickness variations of the sedimentary section are dictated by: processes that precede deposition, processes that operate during deposition and processes that post-date deposition. For example, the initial relief of a basin floor dictates the initial accommodation space (Fig. 2.10 A, B). On the other hand, thickness variations can be influenced by syn-depositional tectonic movements that uplift or lower the basin floor (Fig. 2.10 C, D), as well as the proximity to large sediment supply (such as major river outlets) (Fig. 2.10 E). Commonly observed thickness variations are not original, but may result from later erosion (Fig. 2.10 F), denudation, fluvial incision, underwater landslides, under-water incision, and more.

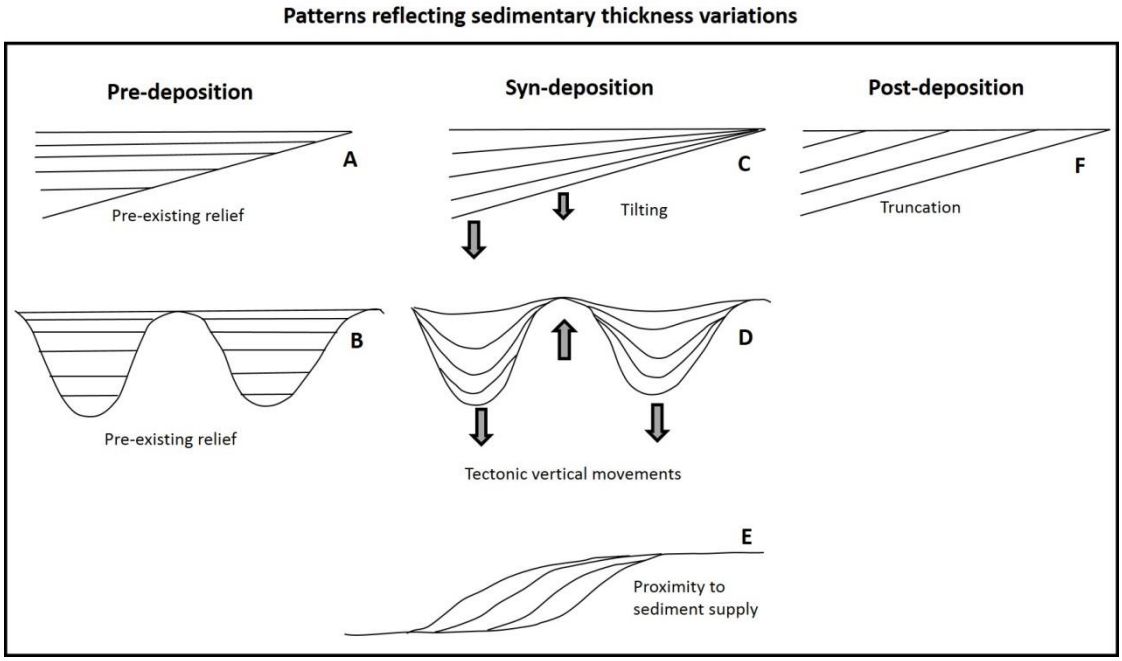

Figure 2.10: Schematic illustration of internal bedding geometries reflecting layer's thickness variations that arise from pre, syn and post deposition factors. When thickness variations occur due to pre-existing relief (A, B), the thickness of the internal layers remains constant. C) Wedging of internal reflector indicates syn-depositional tilting. D) Gradual thinning and thickening is due to syn-sedimentary vertical tectonic movements. E) Proximity to sediment supply (such as large river mouth or large alluvial fan) may dictate thickness variation of the sedimentary section as a whole and also of its internal bedding. F) Post-depositional erosion or truncation (either aerial or sub-aqueous) is responsible for the thickness variation however thickness of the internal layers remain constant.

Previous studies by Steinberg et al. (2011) described the rapid Tertiary filling of the Levant basin by more than 6 km in less than 37 m.y. Pelagic to hemi-pelagic sediments that were penetrated in the shelf area comprises the Late Mesozoic and early Cenozoic section (Fig. 2.2), hint for prevalence of intermediate to deep water depth that persisted during that time. These observations enable us to assume that accommodation space was practically unlimited and did not prevent sedimentation anywhere in the basin and also, that sediment supply was not influenced by proximity to fluvial sources at least until the Pliocene (where the Nile Delta cone provided major

proximal sediment supply and the nowadays shelf built up along the Israeli coastline). These assumptions enable us to deduce vertical tectonic movements from thickness variations as expressed by the gradual thinning of internal layers observed in seismic sections (Fig. 2.10 D).

2.3.2 Folds interpretation

In addition to horizons interpretation, fold's axes were mapped and interpreted across adjacent 2D seismic lines. The accuracy of the axes, their spatial orientation and lengths depends on the density and coverage of seismic lines. Therefore, the orientation of a fold whose length is smaller than 5 km is usually less accurate, whereas folds which were crossed by only one seismic line were not mapped. A careful examination of the reflectors in the vicinity of the folds was carried in order to define whether gradual thinning, on-lap, or abrupt termination, dictate the thickness variation along the fold. Further assessing the timing of activity of each fold was performed by consecutive flattening of horizons which shows the gradual folding of the underlying (not flattened) horizons. This detailed analysis is presented in chapter 4.

2.3.3 Structural analysis

Basin wide interpretation of the horizons resulted in structural maps in the time domain. In the absence of acute dips, the structural maps in time were converted to depth using the basin wide interval velocity maps (presented in Ch. 3) resulting from the pre-stack depth migration process. Conversion was performed in a "layer cake method"; each horizon (structural map in time) was converted using the interval velocity map of the layer above it (bounded at the top by the previous horizon and

bounded at the bottom by the current horizon), and the result was added to the previous horizon (the structural map in depth). However, structural maps record all the tectonic activity that occurred since the horizon was deposited. This amalgamation of events prevents distinguishing specific episodes of tectonic activity such as pulses of folding. Therefore, isopach maps were computed and fold axis of active folds during each period were digitized from the structural maps and copied on each isopach. Then, the mean azimuth of each fold axis was calculated (using the GIS software), and rose diagrams were prepared with the GeoOritent software (http://georient.software.informer.com). This enabled the analysis and assessment of folds orientation in each time period represented by the isopach (Ch. 4).

2.4 Gravity and magnetic anomalies

Anomalies in the Earth's gravity and magnetic fields primarily reflect lateral variations in density and magnetization from predicted simplified Earth models. Topography causes a positive gravity anomaly because of the elevated rock mass relative the oblate spheroid. However, the fact that the continents do not have positive gravity anomaly suggests that the influence of topography is compensated by a deep crustal root (Watts, 2001; Allen and Allen, 2013). Crustal roots cause negative gravity anomalies because of the presence of a density deficit at depth. At large wavelength, if the topography and root are perfectly balanced in hydrostatic equilibrium, there is zero surface gravity anomaly (Watts, 2001; Allen and Allen, 2013).

Similar to gravity anomaly, a magnetic anomaly originates in the magnetization contrast between rocks with different magnetic properties. However, the shape of the anomaly depends not only on the shape and depth of the source object but also on its orientation relative to the acquisition profile and to the inducing magnetic field, which

itself varies in intensity and direction with geographical location (Lowrie, 2007). Gravity and magnetic anomalies can be interpreted qualitatively to infer the general spatial distribution of rock types in the subsurface, and quantitatively, through computer-based modeling, to determine the geometries and specific locations of concealed rock bodies with specific different density or magnetization. Such interpretations are non-unique, because many different distributions of density and magnetization do not uniquely define a specific rock type. Combining the gravity and magnetic data with geologic, geochemical and other geophysical data is crucial in limiting the number of acceptable interpretations (Griscom and Jachens, 1989).

Gravity and Magnetic data were acquired during the TGS-Nopec 2001 survey (Fig. 2.1). The Geosoft software was used to model gravity and magnetic data extracted along a profile perpendicular to the Jonah high, in order to test the geological model deduced from the seismic interpretation. In particular, we strove to understand why the magnetic anomaly generated by the Jonah high is strong whereas its gravity anomaly is relatively weak. A variety of possible combinations of densities and susceptibility values of conventional rock types (as published in the literature) was examined, and were compared with the measured ones. Though gravity and magnetic models are not unique, the chosen model is consistent with the seismic and geological interpretation presented in chapter 5.

3. Depth-migrated section and velocity maps

This chapter presents cross-sections and maps which are the final products of depth migration, interval velocities and the associated interpretation. These maps are primary elements for further analysis of the basin tectonic and sedimentary evolution, such as presented in chapters 4-5. At first, sensitivity of the velocity models is analyzed in selected depth migrated gathers (section 3.1). Only if the velocity model is sufficiently accurate, the depth migrated section can be considered to represent the subsurface. The pre-stack depth migrated sections and the interval velocity model (in depth domain) for each line (Fig. 2.1) are presented in section 3.2. Subsequently, section 3.3 contain integration of the interval velocity model issued from the current study, with modified interval velocities of two other lines (Marig, 2015) resulting in interval velocity maps for the entire study area.

3.1 Sensitivity of the velocity models

Defining the optimal interval velocity model is essential in order to achieve a correct imaging of the subsurface. Pre-stack depth migration with an optimal velocity model should result in CIGs (Common Image Gathers) with flat reflectors. Figure 3.1 display examples of CIG along line EMED-39 and EMED-56. Figure 3.1 A and C show flattened reflectors down to ~12 km outside of the Jonah high implying that velocity models represent the velocity of the rocks at those depths. Figure 3.1 B and D display CIG above the Jonah high. Flat reflectors are observed down to ~9 km, however multiples having lower velocities are not flattened and obscure the primaries. The presence of multiples in the CIG demonstrates that in this case multiple removals were not sufficient. However a complete removal of multiple is never achieved, at

least without deteriorating the primaries. Therefore horizon velocity analysis at the deeper part of the section (>8 km) across Jonah high was not possible due to low S/N. Thus, in order to at least estimate the velocities at such depth, pre-stack depth migration was performed using a series of constant velocities bellow the Mid. Miocene horizon (no. 5 in Fig. 2.2). The accuracy of the velocity model inside the Jonah high and at the deeper part of the section is examined in Fig. 3.2, which display CIG above Jonah high migrated with various constant velocities. Optimal flat reflectors at depth of 9.5 km are obtained using an interval velocity of 5500 m/s (Fig. 3.2B).

Altogether, the CIGs display relatively flat reflectors outside the Jonah high and flat reflectors for the intra-Jonah horizon (at depth of ~9 km). This indicates that the velocity models presented bellow in section 3.2 (Figs. 3.3B-3.7B) matches the rock velocities throughout the sedimentary column.

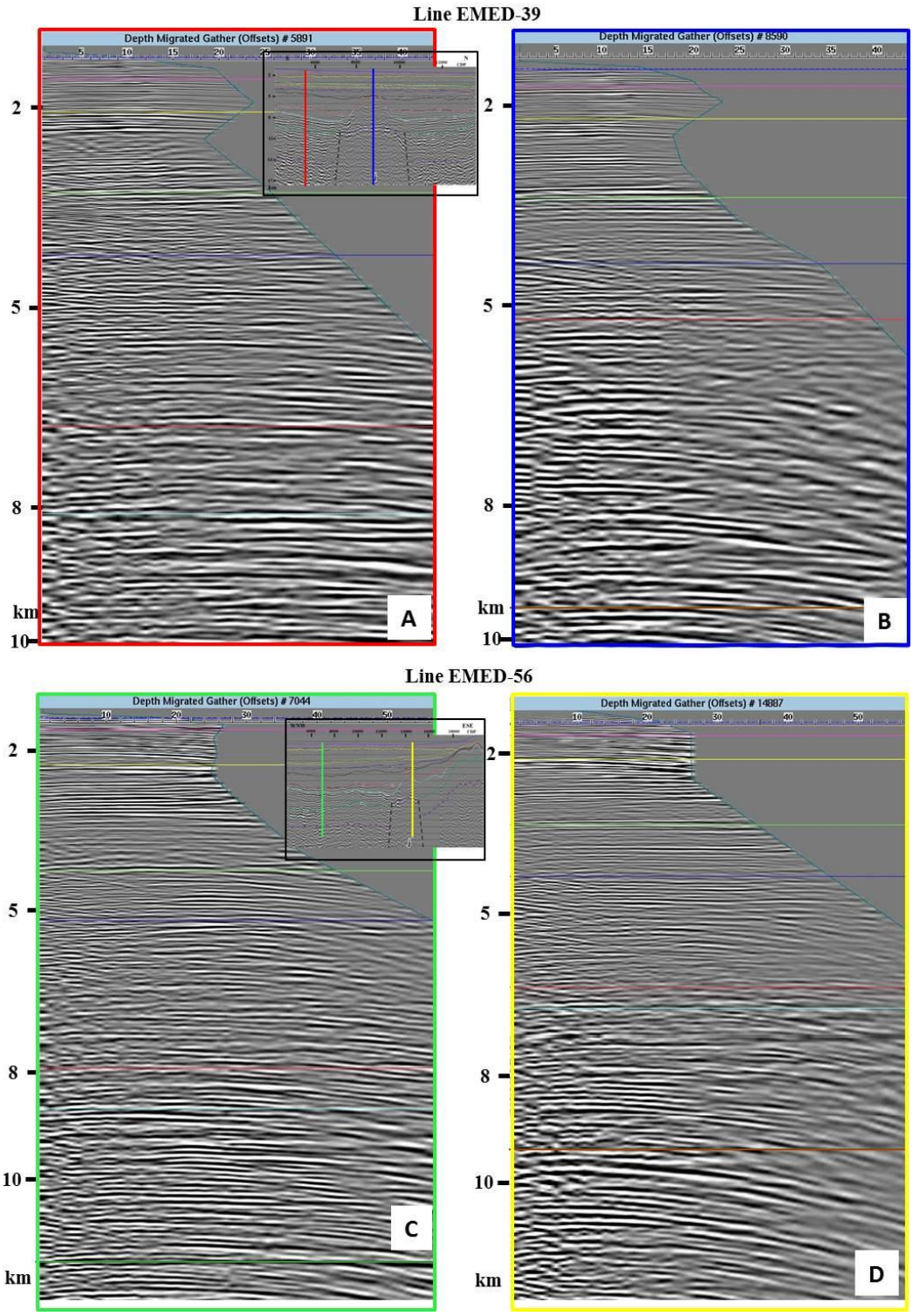

Figure 3.1: Selected CIG (Common Image Gather) displaying flat reflectors along lines EMED-39 (A and B) and Line EMED-56 (C and D) down to >10 km. Insets display location of the CIG on the seismic line according to the vertical colored lines: A) Red: south of Jonah high. B) Blue: above Jonah high. C) Green: west of Jonah high. D) Yellow: above Jonah high. For more detailed location refer to Figs. 3.3 and 3.7 respectively and for line location refer to Fig. 2.1. Horizontal colored lines represent the horizon's depth (see Fig. 2.2 for definition).

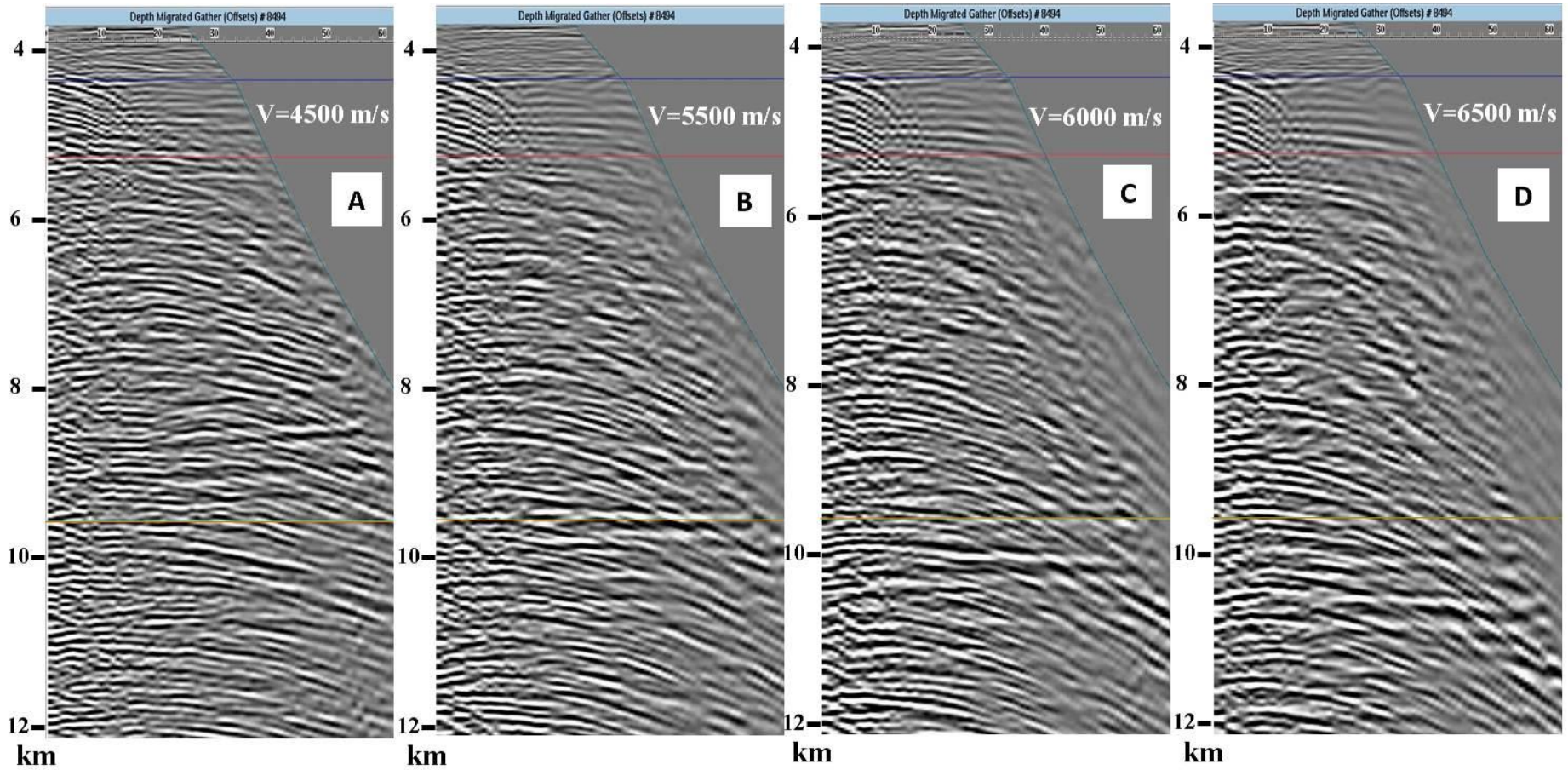
Depth Migrated Gather (Offsets) # 8494
V=4500 m/s
A
Depth Migrated Gather (Offsets) # 8494
V=5500 m/s
B
Depth Migrated Gather (Offsets) # 8494
V=6000 m/s
C
Depth Migrated Gather (Offsets) # 8494
V=6500 m/s
D
4
6
8
10
12
km

Figure 3.2: CIG (Common Image Gather) of line EMED-39 above Jonah high, after pre-stack depth migration using constant interval velocity below the Mid Miocene horizon (blue): A) V=4500 m/s, B) V=5500 m/s, C) V=6000 m/s, D) V=6500 m/s. Optimal velocity for the deep (>9 km) part of the CIG is 5500 m/s, displaying flat reflectors in the proximity of the Intra-Jonah horizon (light brown at ~9.8 km). Horizontal colored lines represent the horizon's depth (see Fig. 2.2 for definition).

3.2 Depth sections and velocity models

Interpretation of horizons was performed throughout the basin on time migrated sections, which was based on correlation to formation tops at selected wells. The interpretation of some horizons is supported by data collected in previous works (Bar, 2009; Steinberg, 2011). The interpreted horizons (section 2) are displayed in figure 2.2. The top of the basement was marked solely on the processed seismic sections in order to constrain the bottom part of the velocity models (lower boundary condition). Profound explanation for the interpretation of the horizons is presented in the analysis of the structural highs in the Levant basin (Ch. 4), while description of the Intra-Jonah (11) and top of Jonah (12) is presented in the analysis of Jonah high (Ch. 5).

The deep (>15 km) geological setting of the Levant basin in the depth domain is illuminated for the first time by the depth migrated sections crossing the Jonah high from various directions (Figs. 2.1, 3.3-3.7). The seismic depth sections show that although the base Pliocene is extensively faulted and deformed, the base Messinian horizon in contrary is relatively flat (for example the yellow and green horizon, Fig. 3.6A). The high velocity (~4200 m/s) of the Messinian evaporate section in compare to the sequence beneath it or above it (~2700 m/s, Figs. 3.3B-3.7B) combined with the intensively faulted and deformed Pliocene horizon (yellow) create strong local lateral velocity variation and creates a "pull-up" effect that causes the base Messinian horizon to appear deformed in the time domain sections. Noteworthy, this artifact

affects the whole section underneath the base Pliocene. Thus in the time domain, the section underneath the base Pliocene is deformed. However, the pre-stack depth migration resolves these lateral velocities variation and relocate (migrate) the seismic data, as expressed by the flat base Messinian horizon (Figs. 3.3A-3.7A). Further detailed comparison between time domain sections and depth sections processed here is presented in Ch. 5.

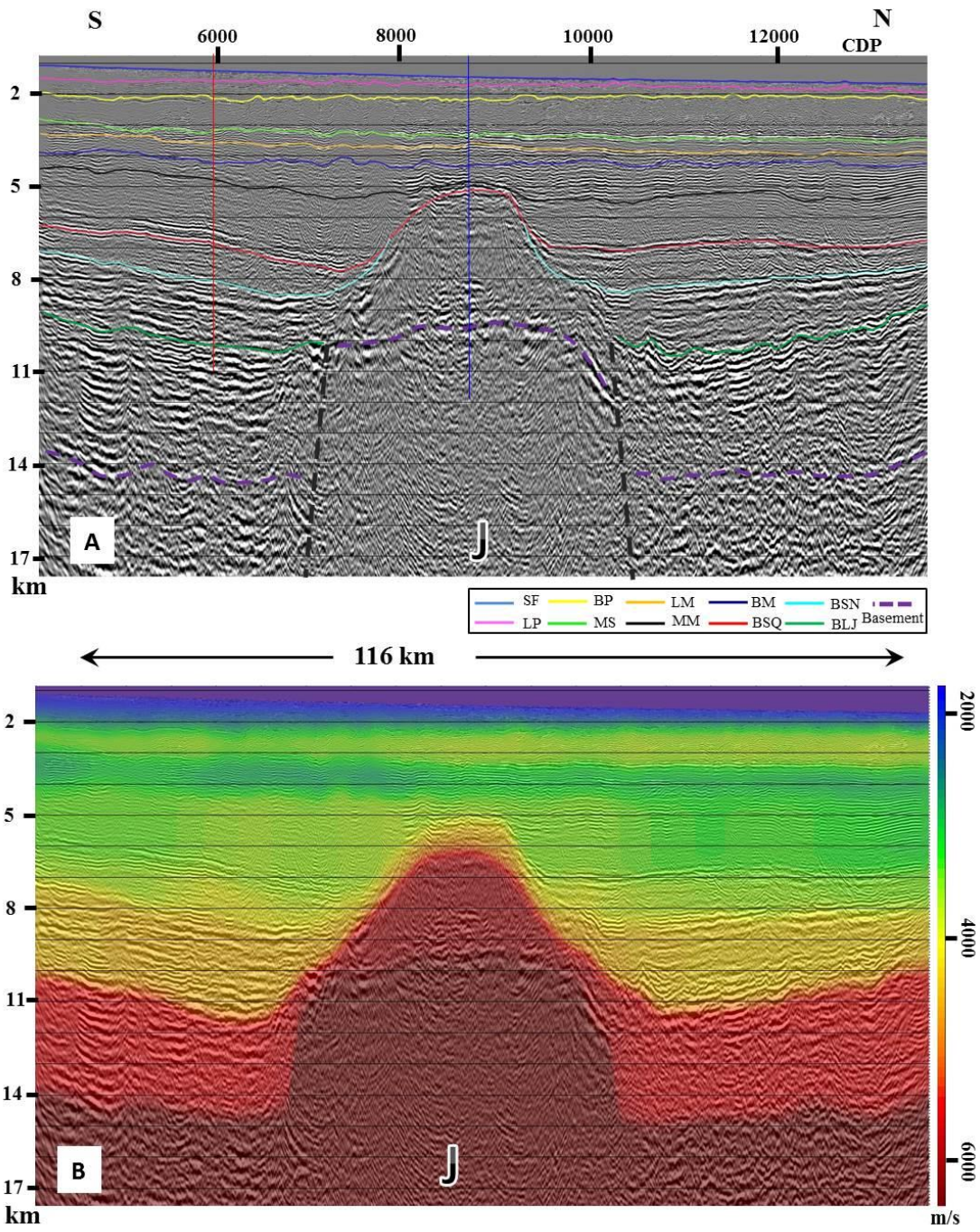

Figure 3.3: Interpreted line EMED-39 (for location see Fig. 2.1). A) Pre-Stack Depth Migrated section crossing Jonah high (marked by J and bounded by dashed gray lines), revealing an internal reflector at ~10 km depth. Also bundles of reflection are observed till ~14 km at the southern part of the section. Interpreted horizons are presented by color lines while red and blue vertical lines represent location of CIG (Common Image Gather) displayed in Figs. 3.1A and B respectively. B) Interval velocity model in depth.

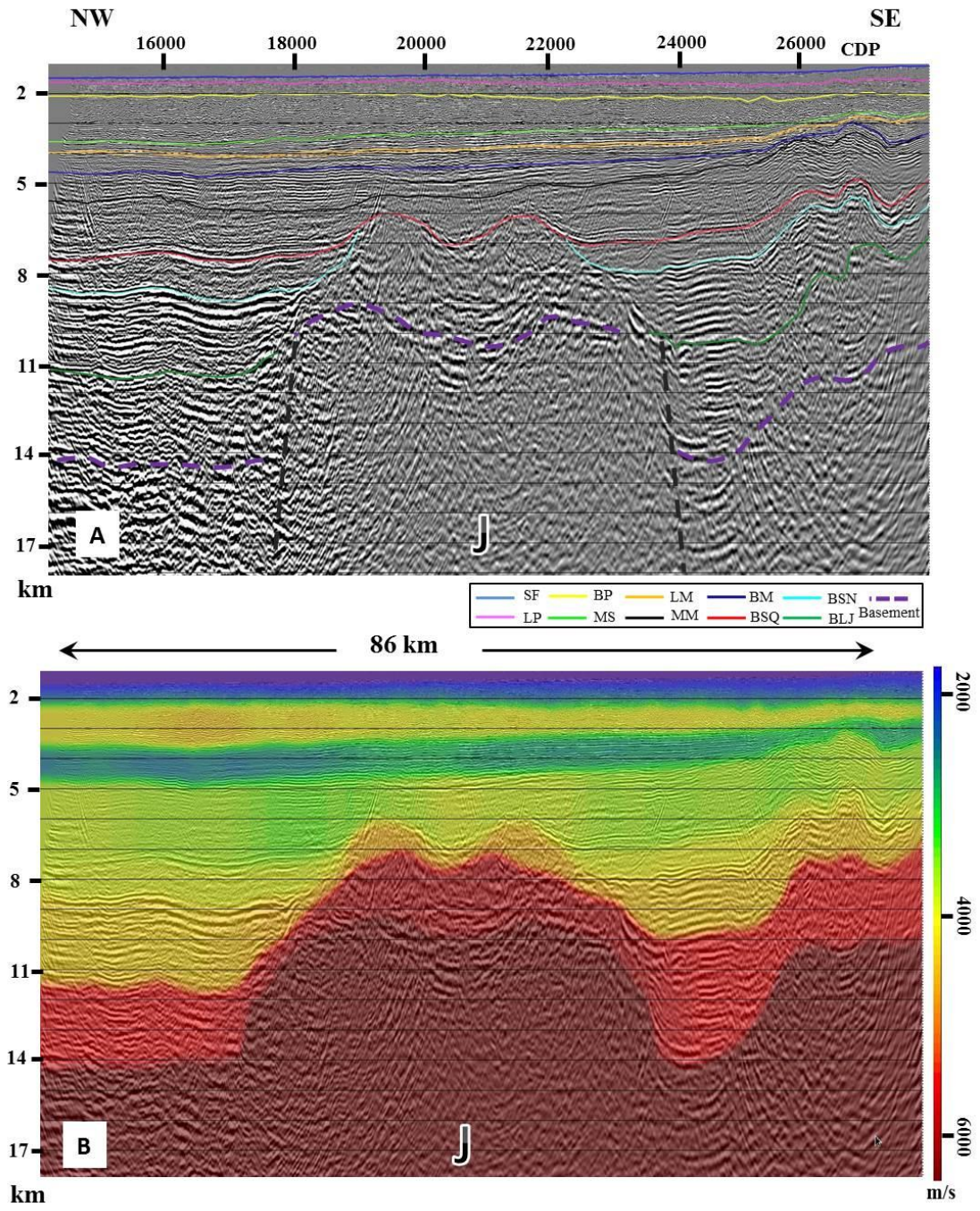

Figure 3.4: Interpreted line EMED-27A (for location see Fig. 2.1). A) Pre-Stack Depth Migrated section crossing Jonah high (marked by J and bounded by dashed gray lines) oblique to its southern part. Bundles of reflectors are observed till ~14 km south-east of Jonah high. B) Interval velocity model in depth.

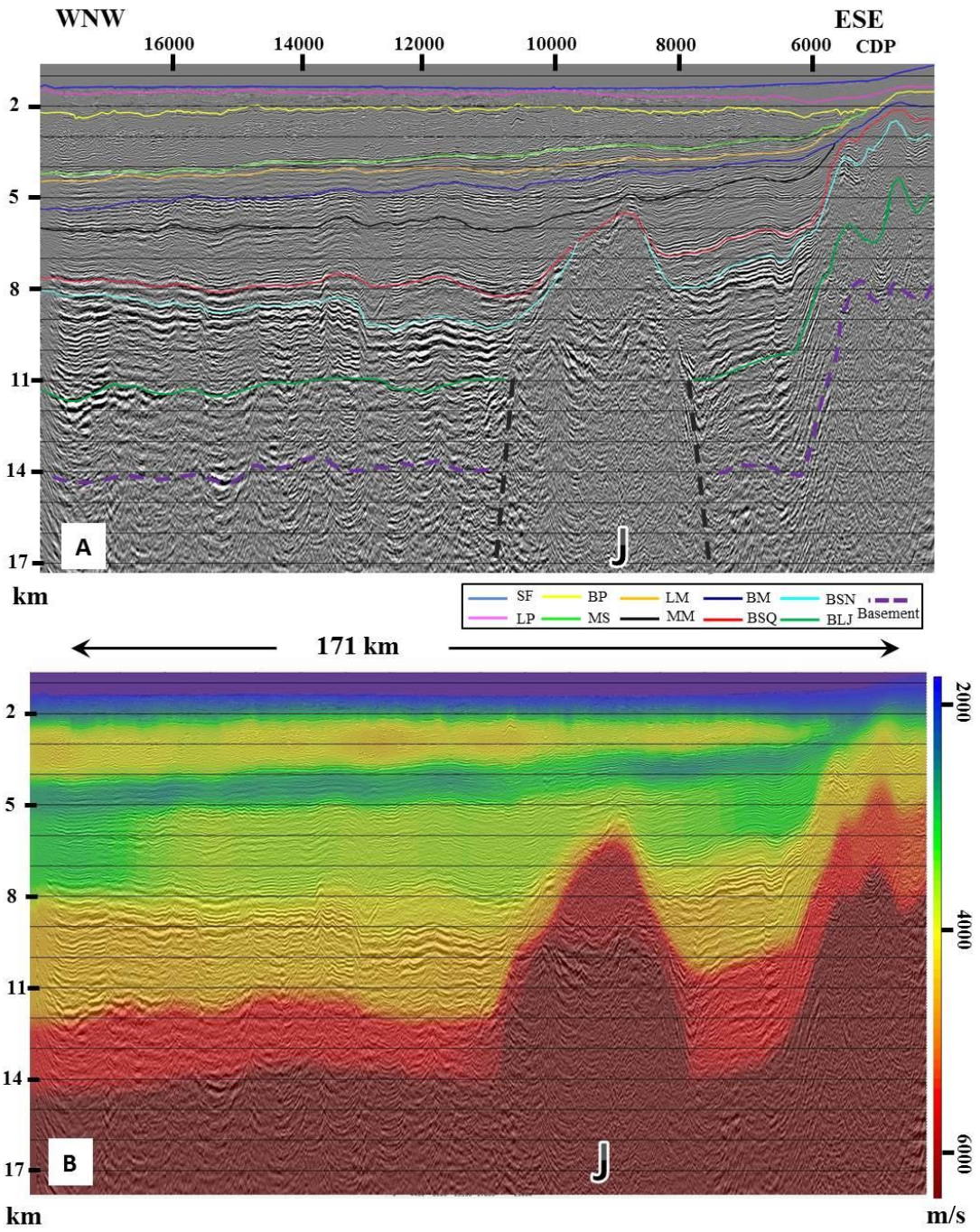

Figure 3.5: Interpreted line EMED-52 (for location see Fig. 2.1). A) Pre-Stack Depth Migrated section crossing Jonah high (marked by J and bounded by dashed gray lines) along its southern tip. B) Interval velocity model in depth.

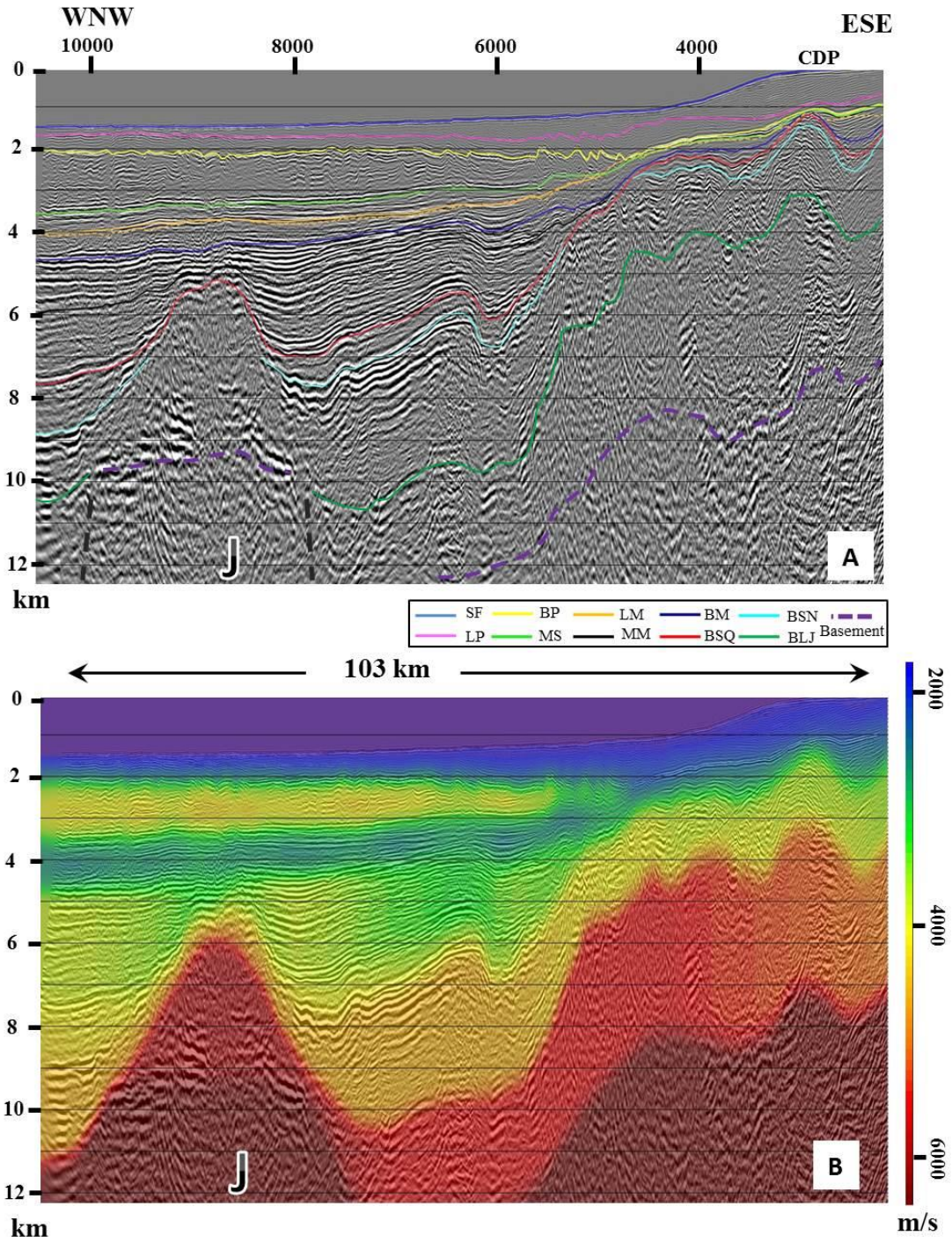

Figure 3.6: Interpreted line IS-4045 (for location see Fig. 2.1). A) Pre-Stack Depth Migrated section crossing Jonah high (marked by J and bounded by dashed gray lines) along its southern tip. B) Interval velocity model in depth.

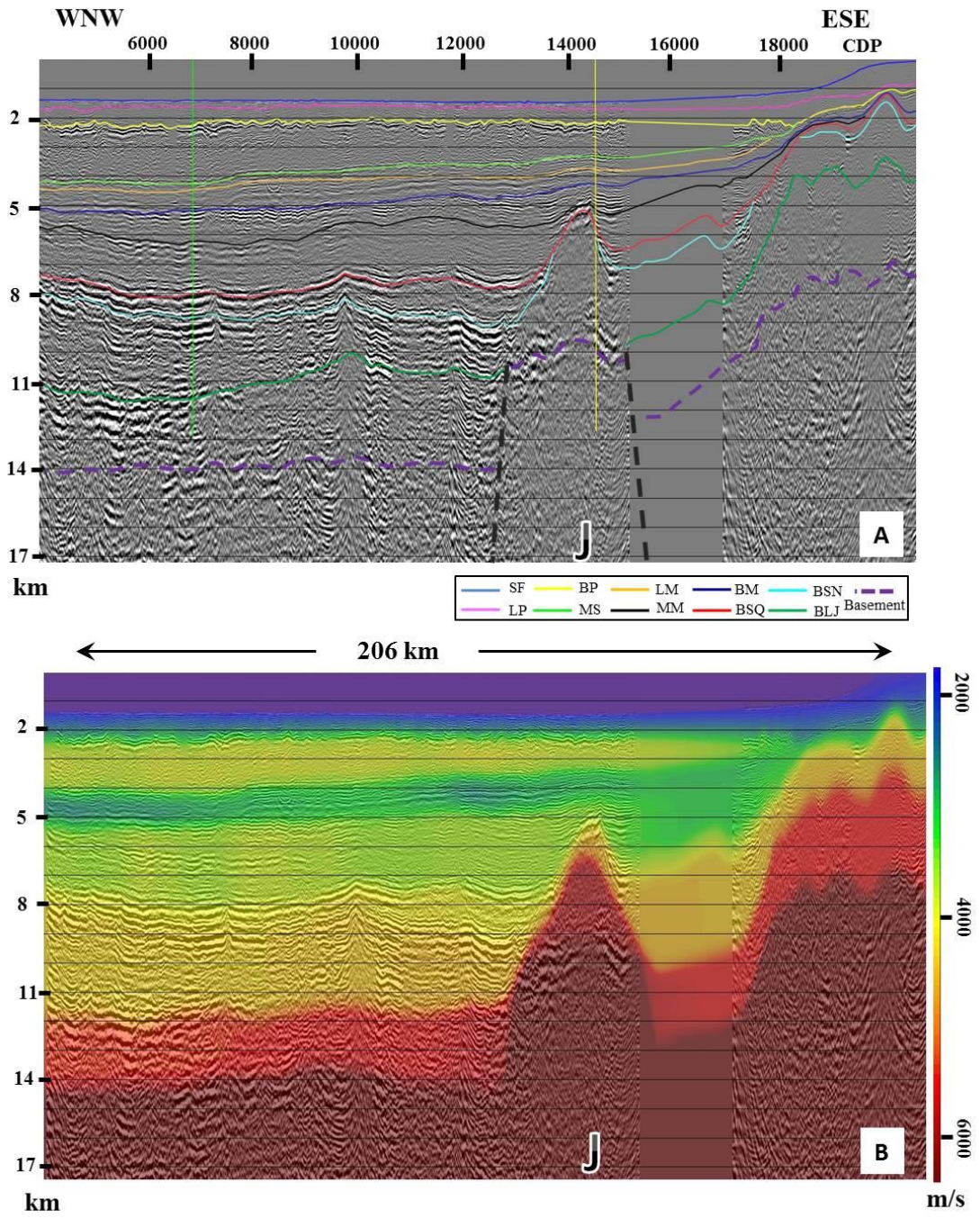

Figure 3.7: Interpreted line EMED-56 (for location see Fig. 2.1). A) Pre-Stack Depth Migrated section crossing Jonah high (marked by J and bounded by dashed gray lines). Corrupted field tape prevents imaging between CDP 15000 and 17000. Interpreted horizons are presented by color lines while green and yellow vertical lines represent location of CIG (Common Image Gather) displayed in Figs. 3.1C and D respectively. B) Interval velocity model in depth.

3.3 Interval velocity maps

Interval velocities of each horizon, as computed along the seismic lines, were gridded and smoothed to create an interval velocity map of the entire study area (Fig. 3.8). The grids were computed solely based on velocity information collected along the seismic lines and were extrapolated for the entire study area. Therefore they might suffer from artifacts that are due to the vast extrapolation. For convenience, the location of the seismic lines is plotted on each interval velocity map. Figure 3.8 display the various velocity maps which were used for converting structural maps in time to structural maps in depth. These structural maps are presented and discussed in chapter 4. The slight variation in Sea-floor velocities (Fig. 3.8A) are attributed to small changes in the salinity of the water. The section bellow the seafloor down to the base Pliocene is characterized by spatially uniform velocities (~1700 m/s) and with slight increasing of velocities with depth (Fig. 3.8B, C). The interval velocity of the base Messinian (Fig. 3.8D) reveals a jump in the velocities to an average of ~4200 m/s, which characterizes the evaporate section. The low velocities in the eastern part of the map are due to the extent of extrapolation eastward where the Messinian is absent from the shallow water and coastal area. Ignoring the eastern part of the map, the velocity of the Messinian horizon ranges from ~3900 to 4400 m/s. Apart from the eastern part of the map, interval velocity of the base Messinian ranges from ~3900 to 4400 m/s. These variation are attributed to the presence of clastic sediments in the evaporate section which are characterized by lower velocities. The section bellow the base Messinian horizon is characterized by lower velocities (~2170-3075 m/s) for the Late Miocene and Middle Miocene, Fig. 3.8E, F) as expected from clastic sediments. Bellow the Middle Miocene velocities increase with depth to ~ 3300 m/s, especially in the central and western part of the basin, where the base Saqiye and base Santonian

horizons reaches depth of 6-8 km (Figs. 3.3-3.7). Onshore wells that penetrated the Late Jurassic and Cretaceous section reveal a wide range of velocities (~2500-5500m/s), altogether the interval velocity maps of the deep horizons correspond to this range and might suggest the presence of hard carbonate rocks buried at >6 km depth.

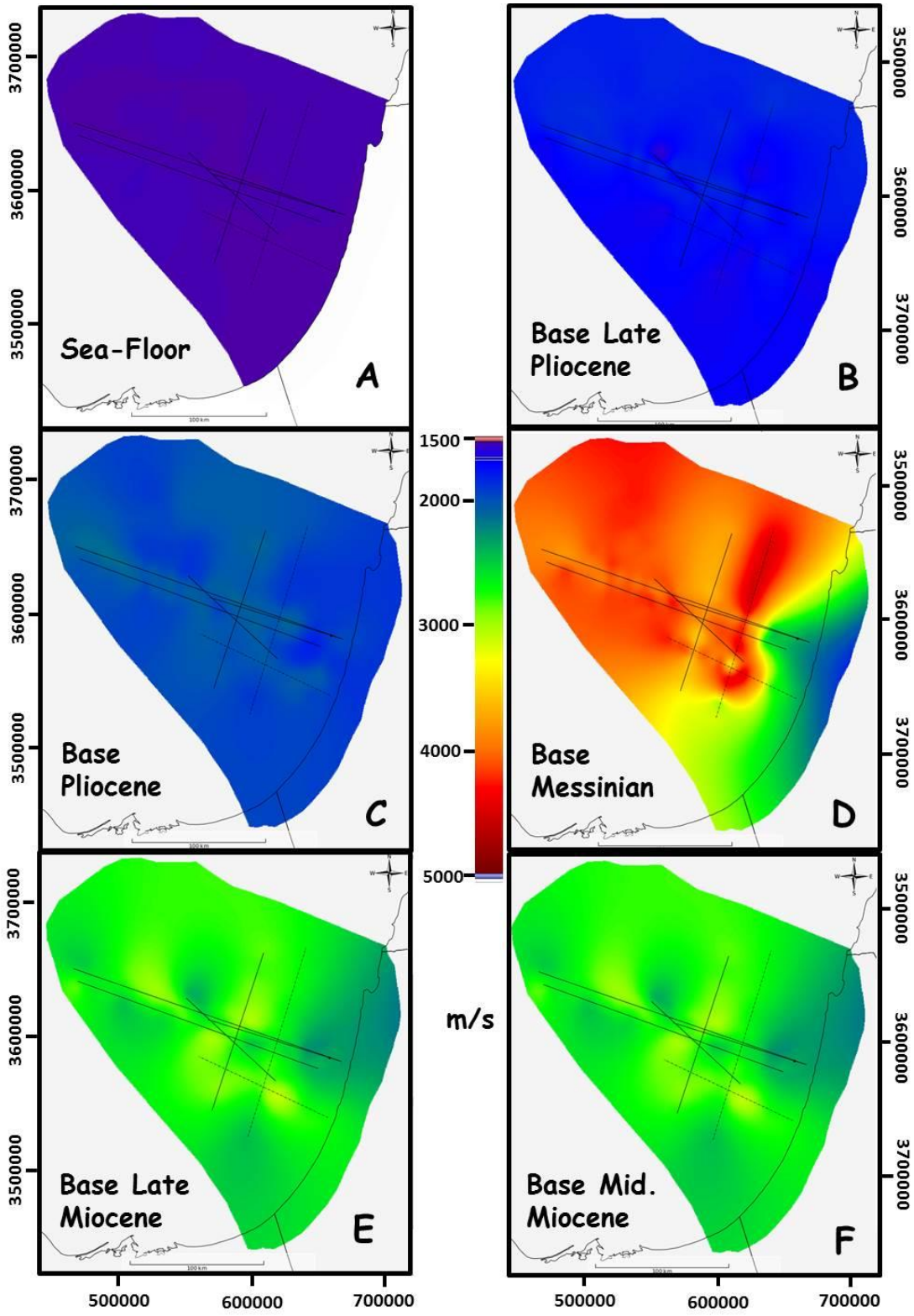
Sea-Floor
A
Base Late Pliocene
B
Base Pliocene
C
Base Messinian
D
Base Late Miocene
E
Base Mid. Miocene
F
1500
2000
3000
4000
5000
m/s
3700000
3600000
3500000
500000
600000
700000

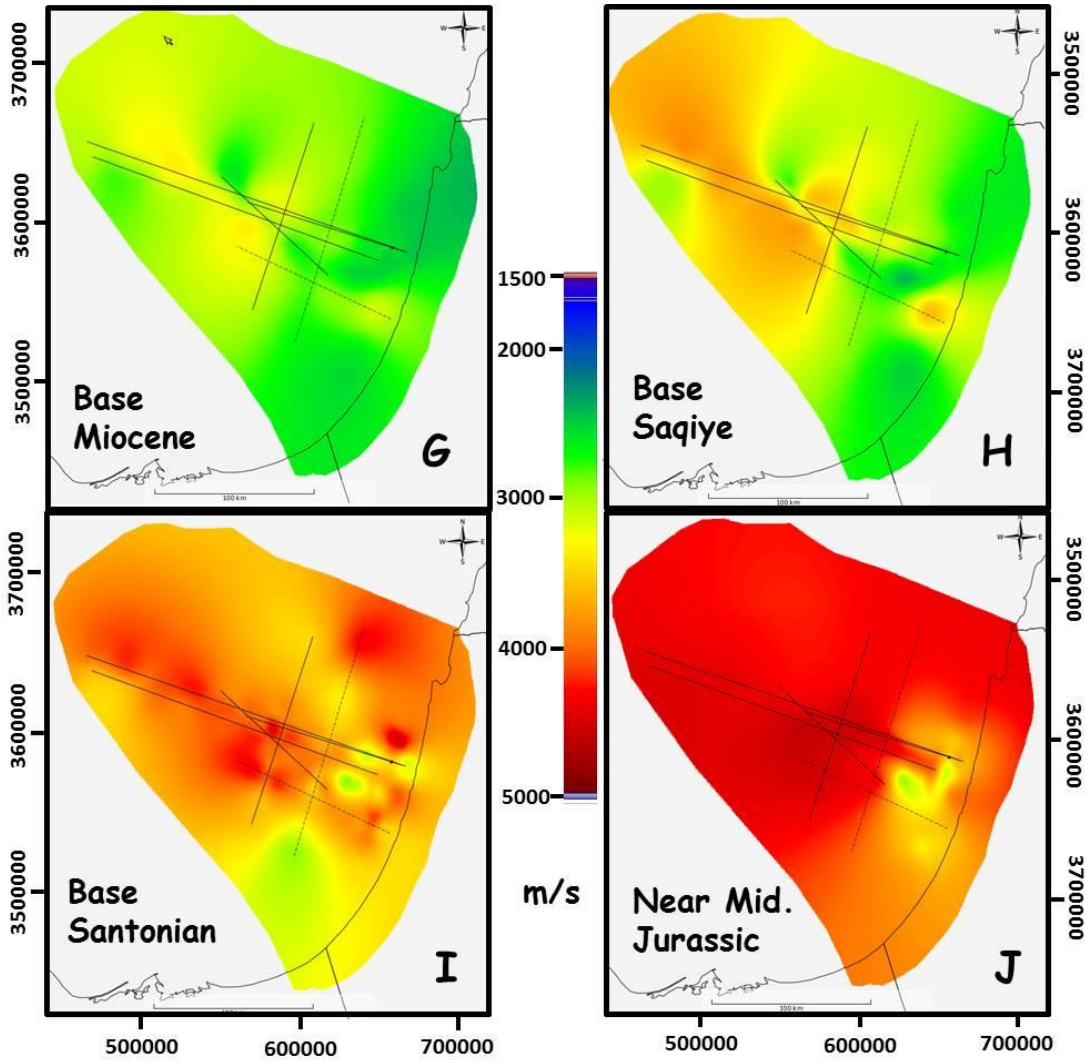

Figure 3.8: Interval velocity models created along the processed lines (black lines) were combined with modified velocity models (Marig, 2015) (dashed lines). Subsequently to compute the interval velocity maps of each horizon. A) Sea-floor velocity ranges from 1500 m/s to 1540 m/s. These velocities were constrained by performing a moveout correction on the time gathers with constant velocity of 1490-1520 m/s by step of 5 m/s. Velocities were determined in the time gathers according to the flatness of the sea-flor reflector. B) Base Late Pliocene display velocities that range from ~1588 to 1880 m/s, which are typical for unconsolidated sediments. C) Base Pliocene velocities ranges from ~1800 to 2140 m/s. D) Base Messinian velocities ranges from ~2000 to 4400 m/s, with low velocities in the eastern part (see text for explanation). E) Base Late Miocene and F) Base Middle Miocene display velocities that range from ~2170 to 3075 m/s. Lower velocities in the north east corner are extrapolation artifacts. G) Base Miocene display relatively uniform velocities that range from ~2380 m/s to 3365 m/s. H) Base Saqiye display velocities that range from ~2415 to 3850 m/s. I) Base Santonian display velocities that range from ~2940 to 4500 m/s, the base Santonian has a relatively uniform velocity of ~3700 m/s (except for some local velocity highs). J) Base Late Jurassic display velocities that range from ~3000 to 4580 m/s. Maps are presented in WGS 1984 UTM 36N coordinate system. Note that the interval velocity map of the base Late Miocene (E) was copied from the interval

velocity map of the base Middle Miocene (F). In addition, interval velocity map of the base Miocene (G) was computed calculating the mean between the base Saqiye (F) and the base Middle Miocene (H) maps. Computation of the mean account for the velocity gradient (slight increase of velocity with depth) observed below the Middle Miocene horizon.

4. Structural highs in the Levant basin

4.1 Introduction

The Levant basin hosts a variety of structural elements. A series of narrow and elongated anticlines and monoclines are primarily observed in the shallow eastern part of the basin (Figs. 2.1, 4.1). These folds, usually oriented NNE are comparable in their dimension and orientations to onshore folds of the Syrian Arc; a ~1000 km Late Cretaceous onshore fold system extending from the Palmyra Mountains in Syria through Israel, down to Sinai and Egypt (Krenkel 1924; Picard, 1959). The deeper part of the basin hosts fewer structures. The Tamar and Dalit gas bearing anticlines (Fig. 1.1) are narrow and long (~16 km by 23 km and 11 km by 22 km respectively), akin in their structure and orientation to the folds in the shallow part of the basin. Other structure, such as the Leviathan and Jonah highs, are larger and different in their geometry and extent (Fig. 4.1).

An exceptionally thick sedimentary section (up to 15 km) in the Levant basin preserves evidence for sedimentary and tectonic evolution during >250 m.y (since the Late Paleozoic – Early Mesozoic). In this chapter we take advantage of the continuous stratigraphic record of the offshore Levant basin and the dense seismic network (>500 seismic lines) to explore the tectonic evolution of the basin and its implication to the Syrian-arc system and other regional deformation phases. In particular, we aim to answer how long folding continued, how far west did it extent and how the orientation of folding vary with time and space.

In what follow we present a basin-wide interpretation between the Israeli coastline and the Eratosthenes seamount, based on ten interpreted horizons bounding upper Jurassic to recent deposits. We map the different structures and for each one of them we determined the timing of its generation, orientation and its evolution

episodes. Ages of activity were deduced from thickness variations that were examined along seismic cross sections that provided 2D details, and from nine isopach maps that illustrate the tectonic evolution of the basin and its sedimentary filling history in 3D.

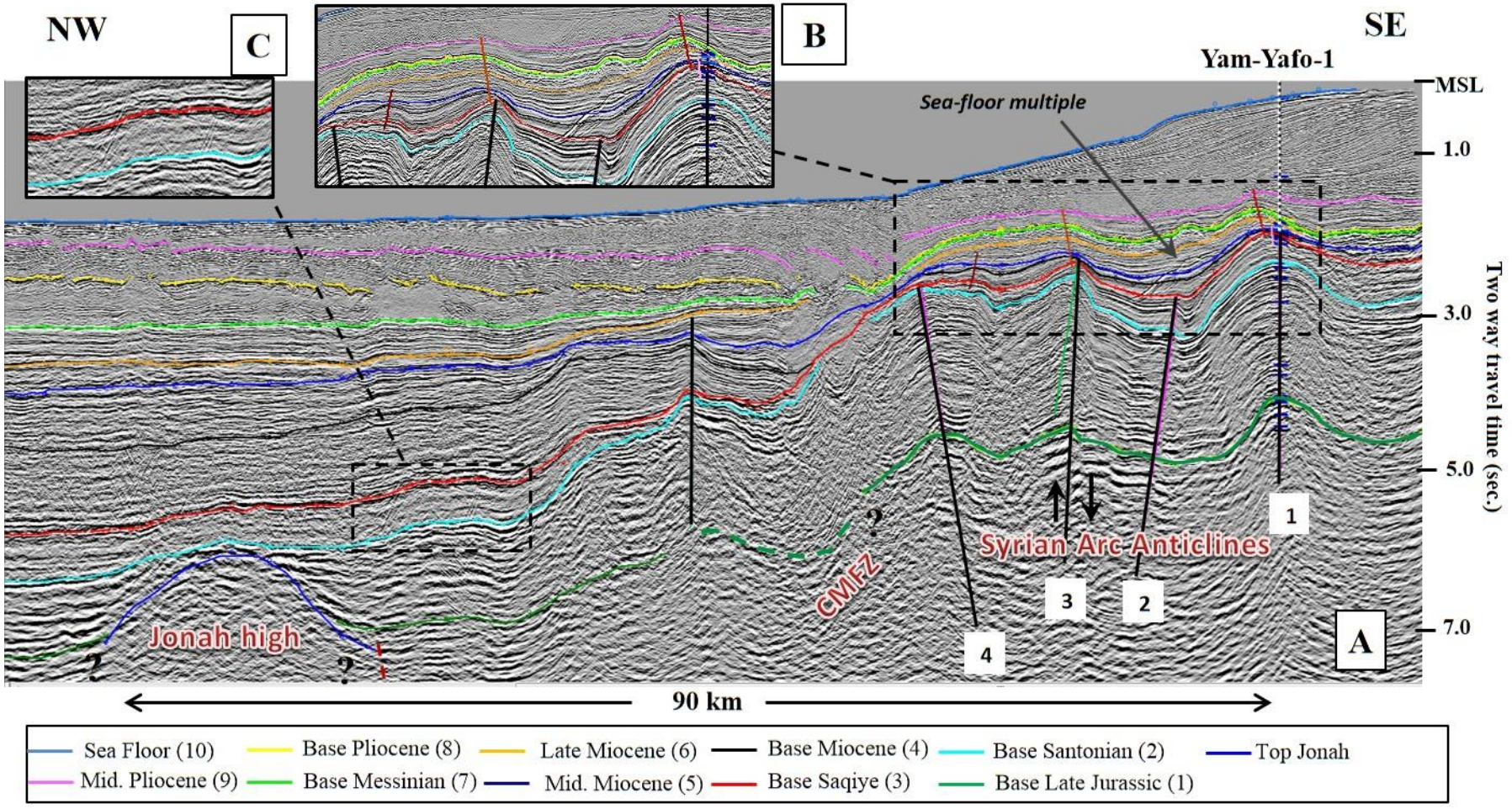
NW
C
B
SE
Yam-Yafo-1
MSL
1.0
3.0
5.0
7.0
Two way travel time (sec.)
Sea-floor multiple
Syrian Arc Anticlines
CMFZ
Jonah high
1
2
3
4
A
90 km
Sea Floor (10)
Base Pliocene (8)
Late Miocene (6)
Base Miocene (4)
Base Santonian (2)
Top Jonah
Mid. Pliocene (9)
Base Messinian (7)
Mid. Miocene (5)
Base Saqiye (3)
Base Late Jurassic (1)

Figure 4.1: A) Line IS-2035, time-migrated regional section showing the seismic horizons discussed in text (according to Fig. 2.2) and typical "Syrian Arc" folds in the shelf area. Location in Fig. 2.1. Folds activity varies between base Santonian (turquoise) till base Late Pliocene (pink) horizons. Black lines indicate the projection of the fold's axial plane on the cross-section. Brown lines represents secondary fold's axial plane that developed since the Miocene (axes migration discussed in text). Enlargement B) displays Early Pliocene folding along two folds as expressed by the thinning of this section toward fold's crests. Enlargement (C) displays lack of reflectors within the Santonian – Late Eocene section (between the turquoise and red horizons). The unclear borders of the Jonah high are denoted by question marks. Note that this line crosses the southern flank of the Jonah high; hence the top of Jonah structure is lower compared to the cross sections of figures 3.3, 3.4 and 5.3. CMFZ denotes Continental Margin Fault Zone after Gvirtzman and Steinberg (2012).

4.2 Seismic interpretation

Regional interpretation of four horizons (base Late Jurassic, base Santonian, base Late Miocene and base Late Pliocene) was carried out in this study together with rechecking and modification of six horizons previously interpreted by Steinberg et al. (2011). An overall interpretation of ten horizons dividing the Cenozoic and Mesozoic section was conducted on more than 500 2D time-migrated seismic reflection lines with a total length of ~27,000 km and was tied to more than 30 wells. Figure 2.2 lists the ten horizons and their ages.

Special care was given to the two deepest horizons: base Santonian (turquoise) and base Late Jurassic (green), which were penetrated only in the shelf area and only by several wells (e.g. Yam-Yafo-1 well in Fig. 4.1). The continental margin fault zone (CMFZ, Gvirtzman and Steinberg, 2012) that creates a ~2 km high structural step challenges the interpretation of these horizons from the shelf area (across the CMFZ step) to the deep basin (Fig. 4.1). Therefore, we based our correlation on the distinct seismic appearance of the section bounded between the base-Santonian and the base-

Saqiye (base-Late Eocene in the deep basin) horizons, which is characterized by scarcity of internal reflectors and by prominent thickness variation along the Syrian Arc folds (Fig. 4.1). Differing from other units in the deep basin, which are well stratified, the Santonian to Mid Eocene section has almost no internal reflections (Fig. 4.1). It is therefore a unique section easily distinguishable throughout the entire deep Levant basin. The lack of Santonian and Eocene section (white polygons denoted by 'tr' and 'nd' in Fig. 4.2B) is interpreted as truncated in the shelf area, probably by the base Saqiye unconformity (Gvirtzman et al., 2008), and as non-deposition over the Jonah high.

The deepest horizon interpreted in this work is the base Late Jurassic (BLJ, Fig. 2.2, 4.2A). In the shelf area and onshore this horizon is constrained by several wells, and is most probably the lateral continuation of the top Zohar Formation that is approximately the transition from Middle to Late Jurassic. The continuation of this horizon to the deep basin seems possible though somewhat uncertain as shown in Fig. 4.1.

In contrast to the problems arising with the deep horizons, the base Late Miocene and base Late Pliocene horizons, encounter different obstacles (Fig. 4.2F, H). For example, the base Late Miocene horizon can be easily interpreted over most of the deep basin, however in the shelf area it converges with the base Messinian horizon because the Late Miocene section thins below seismic resolution or missing (Bar, 2009). Therefore, its interpretation on the shelf area is mostly based on borehole data. The Early Pliocene section is highly faulted and folded at the foot of the continental slope due to the halo-kinetic deformation of the underlying Messinian evaporates. North of the Delta-1 well (Fig. 2.1), the base-Late-Pliocene horizon was not

interpreted due to the complexity of sedimentary structures created when the salt evacuated these areas (Fig. 4.2H).

In addition to mapping regional horizons, the irregular top of the Jonah high (blue horizon, Figs. 4.1, 2.2) and an intra-Jonah reflector (orange horizon, Fig. 2.2) were mapped locally. Special difficulties arise while interpreting the intra-Jonah reflector on the time-migrated sections as it is poorly imaged. It should therefore be regarded as a marker for internal reflections (which probably hint for a stratified body) rather than a consistent horizon (for details see Ch. 5). Altogether a set of 10 structural maps depicting various structural elements in the basin are presented bellow (Fig. 4.2).

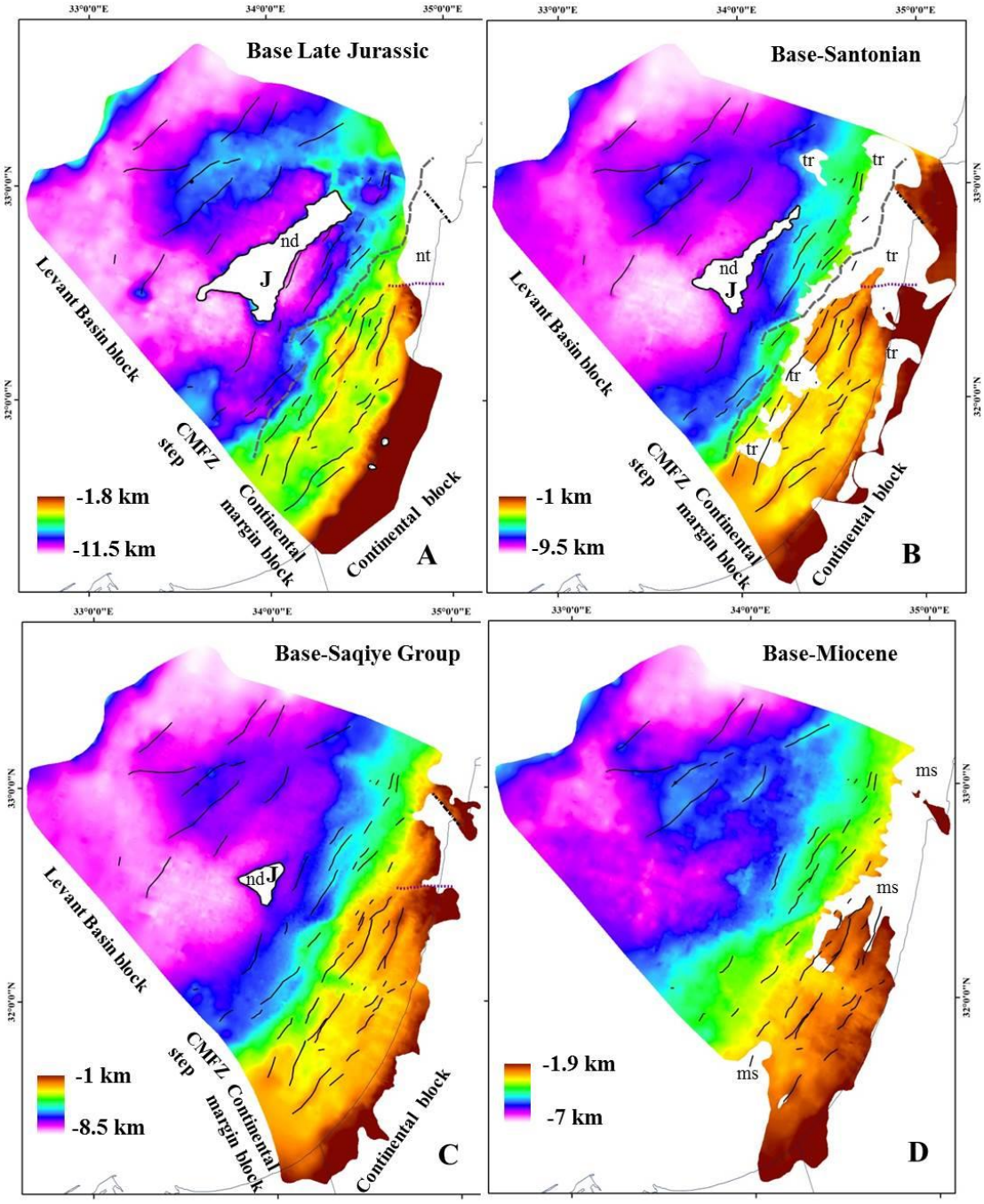
Base Late Jurassic
nd
J
nt
Levant Basin block
CMFZ step
Continental margin block
Continental block
-1.8 km
-11.5 km
A
Base-Santonian
tr
nd
J
Levant Basin block
CMFZ step
Continental margin block
Continental block
-1 km
-9.5 km
B
Base-Saqiye Group
nd
J
Levant Basin block
CMFZ step
Continental margin block
Continental block
-1 km
-8.5 km
C
Base-Miocene
ms
Levant Basin block
CMFZ step
Continental margin block
Continental block
-1.9 km
-7 km
D

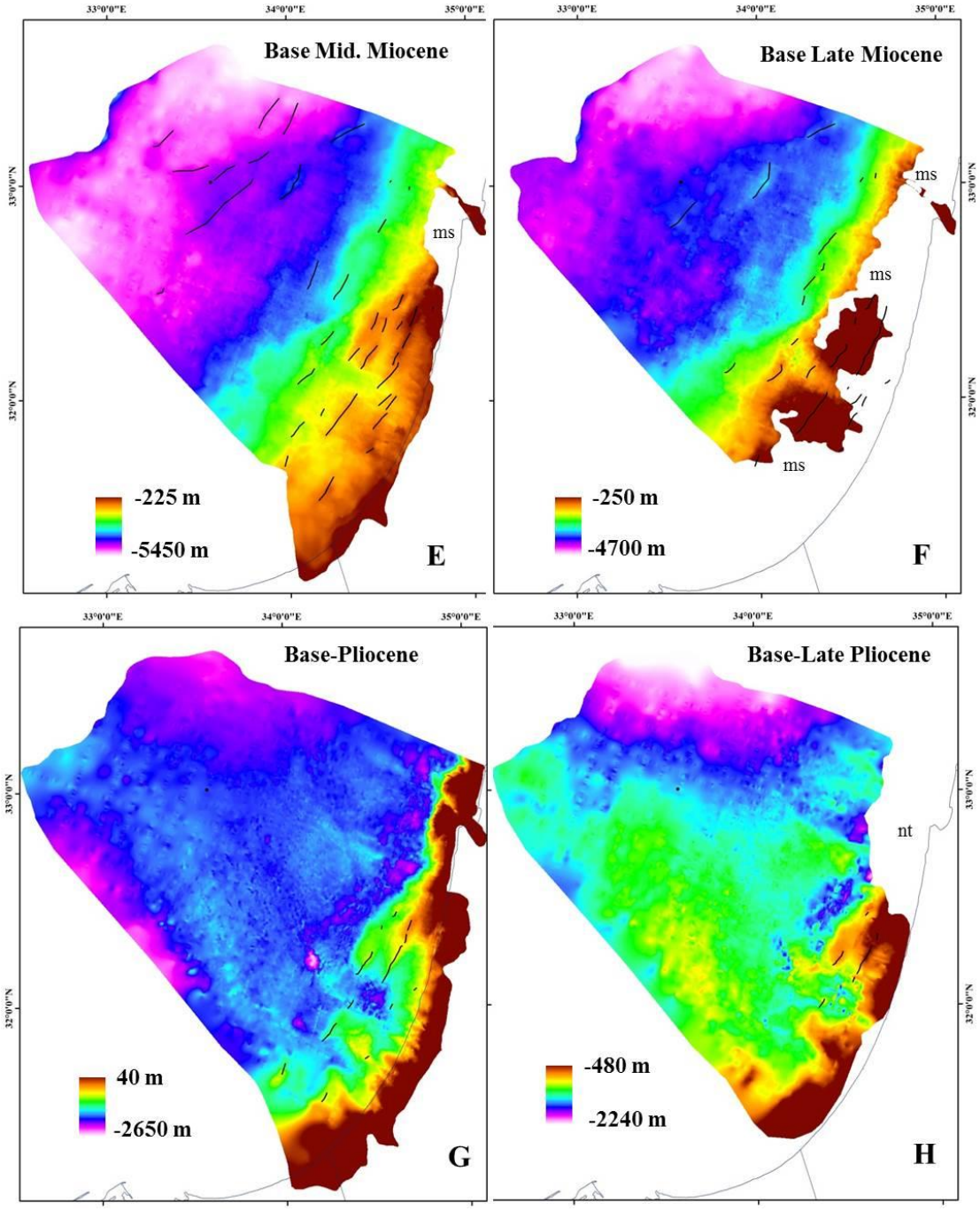

Figure 4.2: Structural maps displaying the major structures in the basin. A) Base-Late Jurassic, note that due to poor imaging at the deep north eastern part of the basin (offshore Carmel) the horizon was not interpreted (nt). B) Base Santonian ('tr' – truncated, 'nd' – not deposited), C) Base Saqiye Group unconformity. The boundary is diachronic changing from Mid-Late Eocene in the basin to Pliocene on land. D) Base Miocene, note that it is partially missing (ms) in the shelf area. E) Base Middle Miocene. F) Base Late Miocene, G) Base Pliocene. H) Base Late Pliocene (note due to complex deformation in the north eastern part, the base Late Pliocene was not interpreted (nt). Black lines – folds. Dashed gray line – the western boundary of the CMFZ. Dotted purple line – Or-Akiva fault. Dotted black line – Carmel fault. Black dot – Leviathan-1 well. For simplicity, the CMFZ, Or-

Akiva, and Carmel faults are only marked on A and B. The gradual burial of the Jonah high (J) from the Late Jurassic to Early Miocene (maps A-D) is discussed in Ch.5.

4.3 Main Structures

Two major structural steps are prominent in Fig. 4.2: the CMFZ step with a vertical offset of ~2 km and the coastal plain step with a vertical offset od ~1.5 km (Gvirtzman et al., 2008; Steinberg et al., 2011; Gvirtzman and Steinberg, 2012; Bar et al., 2013). These structural steps distinguish three major blocks constituting the Levant basin and its continental margin: the deep basin block, the continental margin block, and the coastal plain block (mostly beyond the study area).

This chapter focuses on elongated folds (black lines in Fig. 4.2), which represent a post rift contractional phase. In the continental margin block these folds are very common ranging from ~1 km to 50 km length and with a typical distance of ~5-10 km between axes (typical Syrian Arc structures). In the basin block these folds are less common and more widely spaced. In addition, the basin hosts two other prominent structures that do not resemble the folds in their geometry and their size: the Jonah high in the center of the basin (Fig. 4.2) will be analyzed in details in chapter 5, and the Leviathan high, (Fig. 4.2) which seems to be a large basement block reactivated in the post rift phase, is described in section 4.6.

4.4 Folds analysis

The gradual thinning of the Late Mesozoic and Cenozoic section towards the fold's crest suggests that onset of folding and pulses of activity varied among the folds as depicted on the cross-section of the continental margin block (Fig. 4.1). During the

Late Miocene and Early Pliocene secondary folds evolved up to 3 km westward of the main anticline crest (brown line Fig. 4.1, fold no.1 representing the projection of the axial plane on the cross section). Gathering all the 72 fold axes, which were interpreted on each of the structural maps (Fig. 4.2), in a single map present a robust picture (Fig. 4.3) of folding activity. But how exactly the folds evolved through time is best determined by an analysis of thickness variation along 2D seismic lines crossing each fold's axis plane. This analysis enables us to distinguish between phases of activity, while the subsequent ispoach analysis enables further to understand their spatial evolution on a broader scale.

The examination of a 2D section crossing the continental margin is illustrated in Fig. 4.4 by showing flattened sections. Flattening the base-Santonian horizon reveals relatively flat reflectors beneath it along folds 1, 2 and 3 and some tilted and or faulted reflectors beneath folds no. 4 and 3, suggesting that folding activity post-date the beginning of the Santonian (Fig. 4.4a), whereas tilting or faulting in the area of fold no. 4 and 2 occurred prior its deposition. Conversely, flattening of the base-Saqiye horizon (red) reveals a thinning pattern within the Santonian - Eocene section that clearly express syn-deformational deposition (all internal layers are thinning and thickening as in Fig. 2.10D). This pattern is observed across folds No. 1, 2, and 3, and especially across fold No. 3 (Fig. 4.4b). In addition to original thickness variations, fold no. 4 located at the edge of the CMFZ is truncated by repeated erosion events. Flattening of the overlying horizons further reveals syn-depositional thickness variations till the Late Pliocene section. Overall, the folding activity started after the beginning of the Santonian, it ceased along fold no. 2 during the Oligocene (Fig. 4.4c). Since the Middle Miocene (Fig. 4.4d) secondary folding evolved westward of folds No. 1 and 3 and eastward to fold No. 4 (brown line, Figs. 4.1 and 4.4). A last

phase of folding activity is recorded in the Early Pliocene sediments which thin gradually toward the secondary folds axis (folds 1 and 3, Fig. 4.1, and Fig. 4.4g). This analysis was carried on all the folds in the basin. However, in the absence of internal layers where very minor thickness variations of the section is observed, assessing the fold's activity was speculated and hence the folds were denoted as suspected to be active. This occurs mostly in the Late Miocene and Early Pliocene sections.

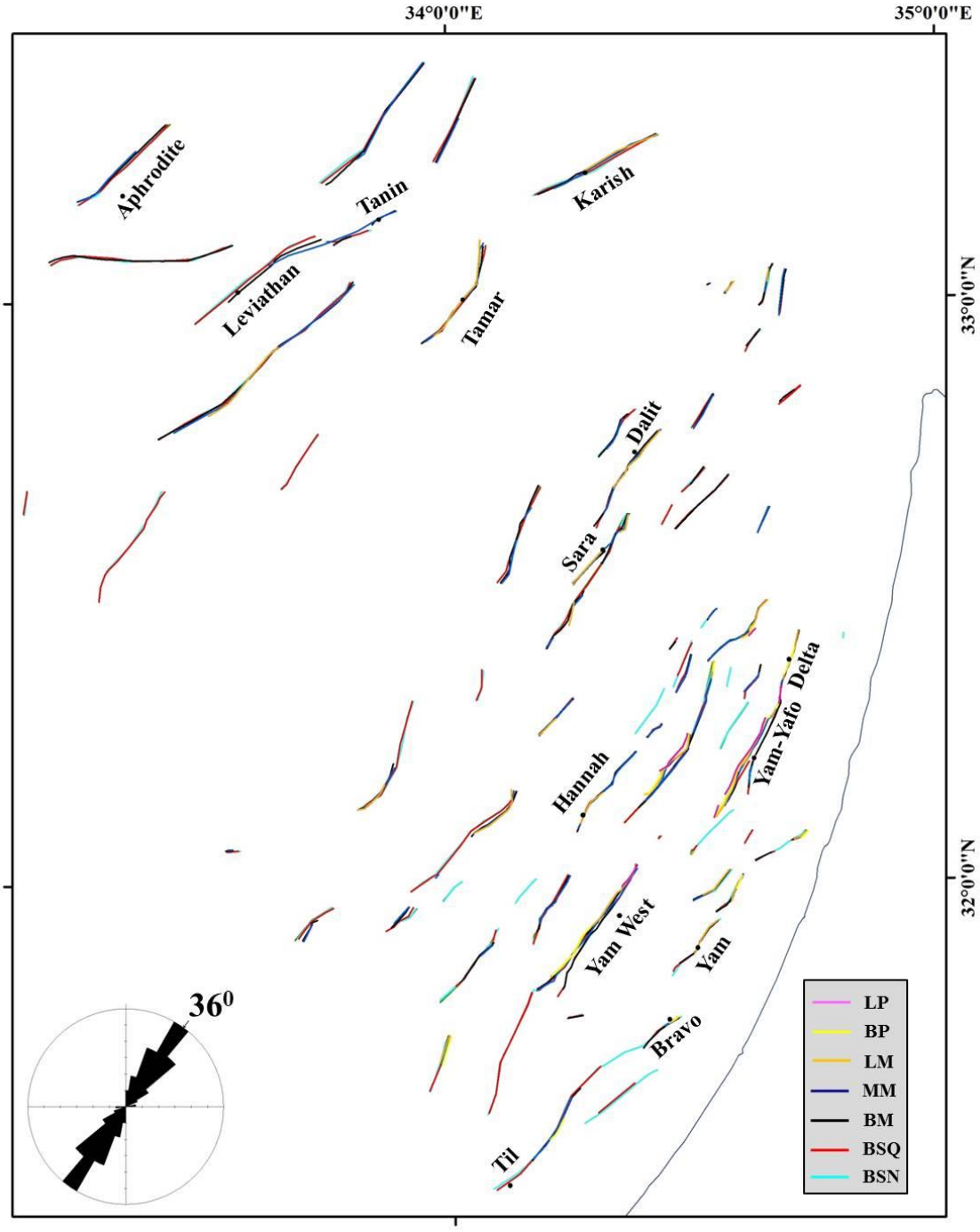

Figure 4.3: Folds axis map compiled from amalgamation of the fold axis in each of the structural maps of figure 4.2. Folds axis are color coded according to the horizons (see Fig. 4.1). Noteworthy, this map does not refer to the timing of folding since folding could occur after the deposition of the horizon. Black dotes – wells, major folds were named according to the wells drilled nearby.

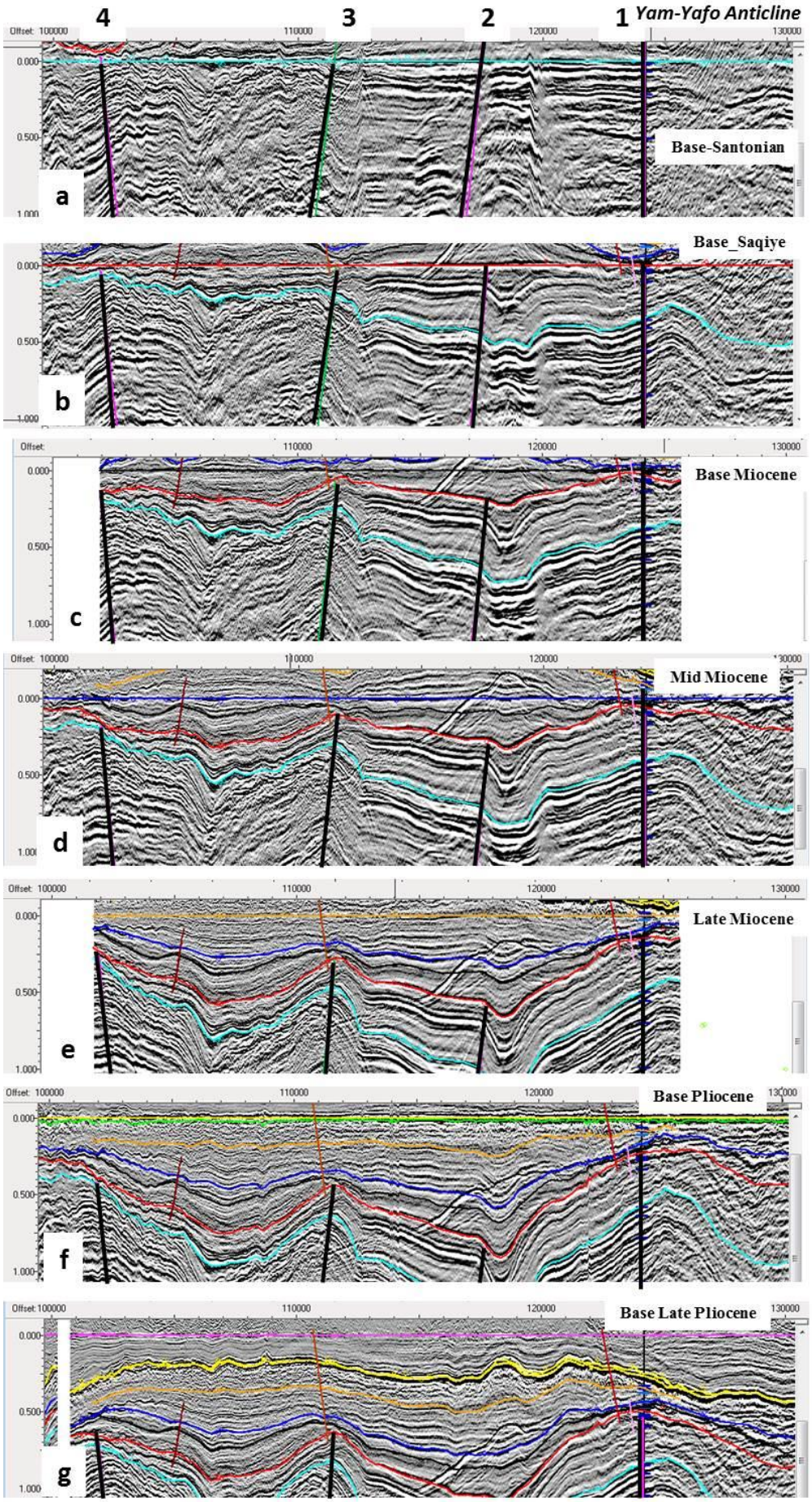
4
3
2
1
Yam-Yafo Anticline
Offset: 100000
110000
120000
130000
0.000
0.500
1.000
Base-Santonian
a
Base_Saqiye
b
Base Miocene
c
Mid Miocene
d
Late Miocene
e
Base Pliocene
f
Base Late Pliocene
g

Figure 4.4: Flattened time seismic section of line IS-2035 (same as Fig. 4.1). a) Base Santonian horizon (turquoise) flattened showing unfolded section below it (tilted and or faulted reflectors are observed near folds no. 4 and 2, without any thickness variation). This indicates that folding activity started after the beginning of the Santonian. b) Base Saqiye unconformity (red) flattened. The thinning pattern within the Santonian-Eocene section along folds 1, 2, 3 indicates syn-tectonic Santonian-Mid Eocene deposition. Abrupt thinning along fold no. 4 hints for younger erosion. c). Base Early Miocene (black) and d) Base Middle Miocene (blue) flattening, show slight thickness variations below them and indicate ongoing folding during the Late-Eocene, Oligocene and Early Miocene. e) Base Late Miocene (orange) flattened indicating declination of folding in the Middle Miocene which continues in the Late Miocene (f). g) Base Late Pliocene (pink) flattening indicating Early Pliocene folding activity along the secondary folds (brown lines) that develop west of fold 1 and 3 respectively. Fold numbers and color code are according to Fig. 4.1. In general, this analysis illustrates the ongoing activity along the folds since the Santonian till the Late Pliocene, while during the Middle and Late Miocene it declined and migrated to secondary axis (brown axis).

The deep Levant basin host fewer folds than the shelf area (Fig. 4.2). Some of them are gentle and relatively symmetric (Tamar, Fig. 4.5c), some are asymmetric (Aphrodite, Fig. 4.5d, T1 and T2, Fig. 4.5b) and some are monoclinic (Fig. 4.5e, and f). Analysis of thickness variation reveals that during the Santonian folding started solely along the monoclines bordering the Leviathan high (Fig. 4.5.e, f). Along the other folds thickness variations mainly begins in the Early Miocene section (between the black and blue horizons) and decrease in the Middle Miocene section (between the blue and orange horizons). This pattern is observed in Figure 4.5b (T1 and T2 anticline) and in 4.5d (Aphrodite anticline) indicating strong activity in the Early Miocene that gradually decreased in the Middle Miocene. The Tamar anticline (Fig. 4.5.c) expresses a late phase of activity during the Late Miocene (not including the Messinian).

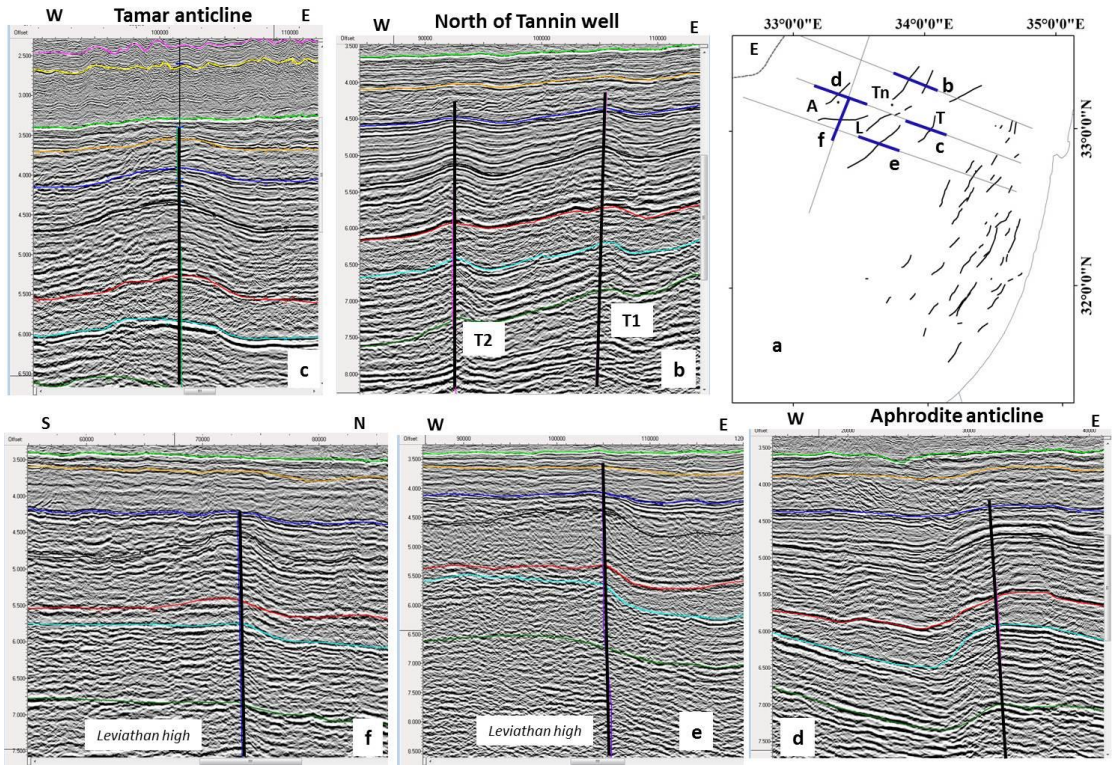

Figure 4.5: Examples of folds in the deep Levant basin, inset a) display the location of the time sections (blew lines) and the folds (black lines) from the base Miocene structural map (Fig. 4.2D). E – Eratosthenes, wells: A – Aphrodite, L - Leviathan-1, T- Tamar-1, Tn – Tanin-1. Horizon color code as in Figs. 2.2, 4.1.

4.5 Folding evolution in time and space

In order to gain a broader representation and understanding of thickness variations through time and space, isopach maps were computed and examined (Fig. 4.6). The Late Jurassic to base Santonian sequence (i.e. Late Jurassic to Turonian, Fig. 4.6A) predates the folding and represents the passive margin phase of the basin after the Early Mesozoic rifting and before the Late Cretaceous contractional phase (details in the geologic background Sec. 1.4). Obviously, this isopach shows no correlation with folding; rather it reflects the thick passive margin deposition along the continental margin and the thinner condensed section in the deep basin. Except for the pre-folding isopach (A), all the other maps (B-I) depict series of anticline and

synclines in the shelf and deep basin since the Santonian till the Early Pliocene. Combining the 2D fold analysis presented above (Sec. 4.4) with thickness variations observed in the isopach yields a set of maps each representing a specific period with the folds that were active at that time (Fig.4.7). These maps demonstrate the fold's evolution in time and space. In what follow a description of folding activity throughout the basin in each period is presented.

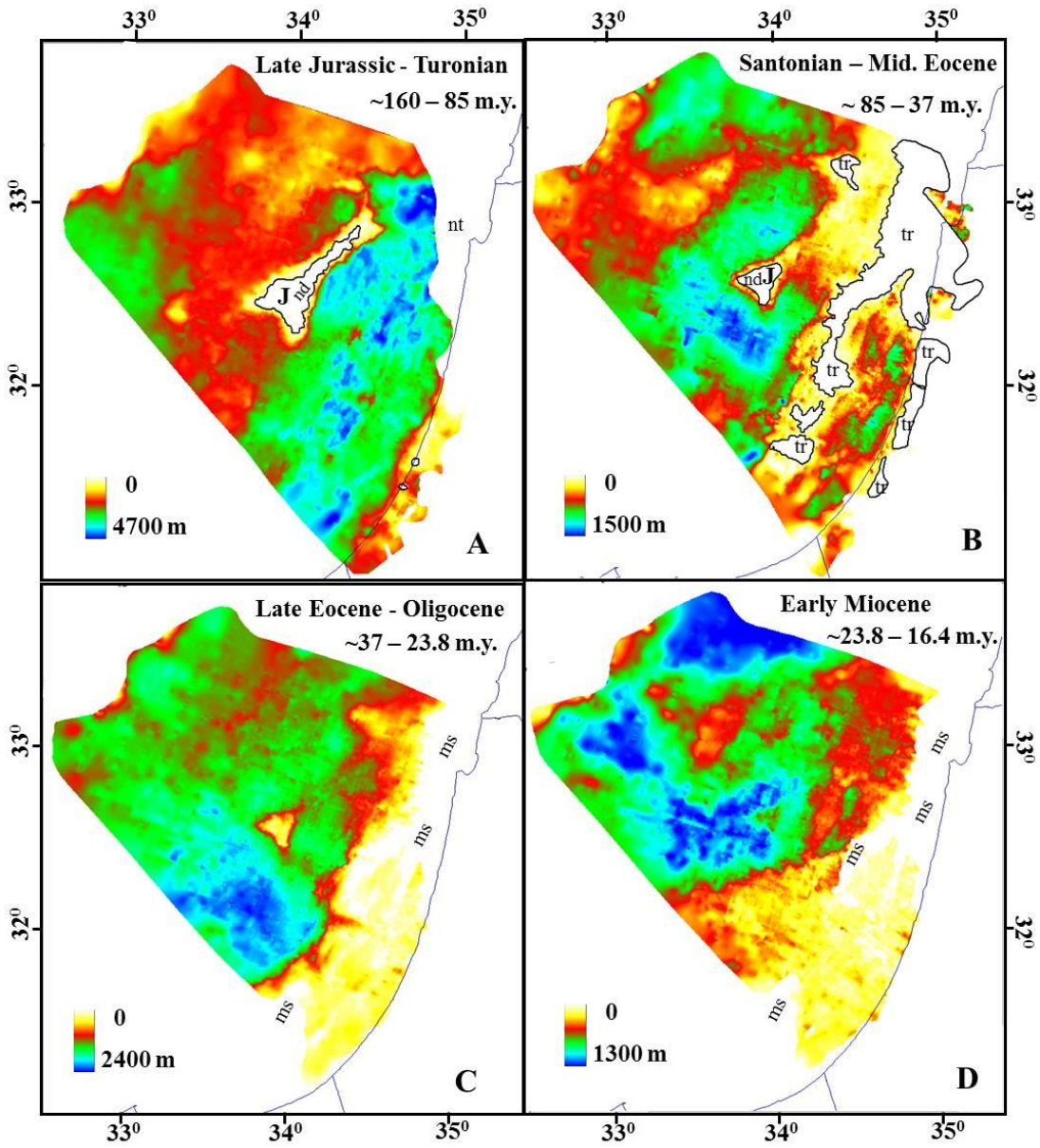

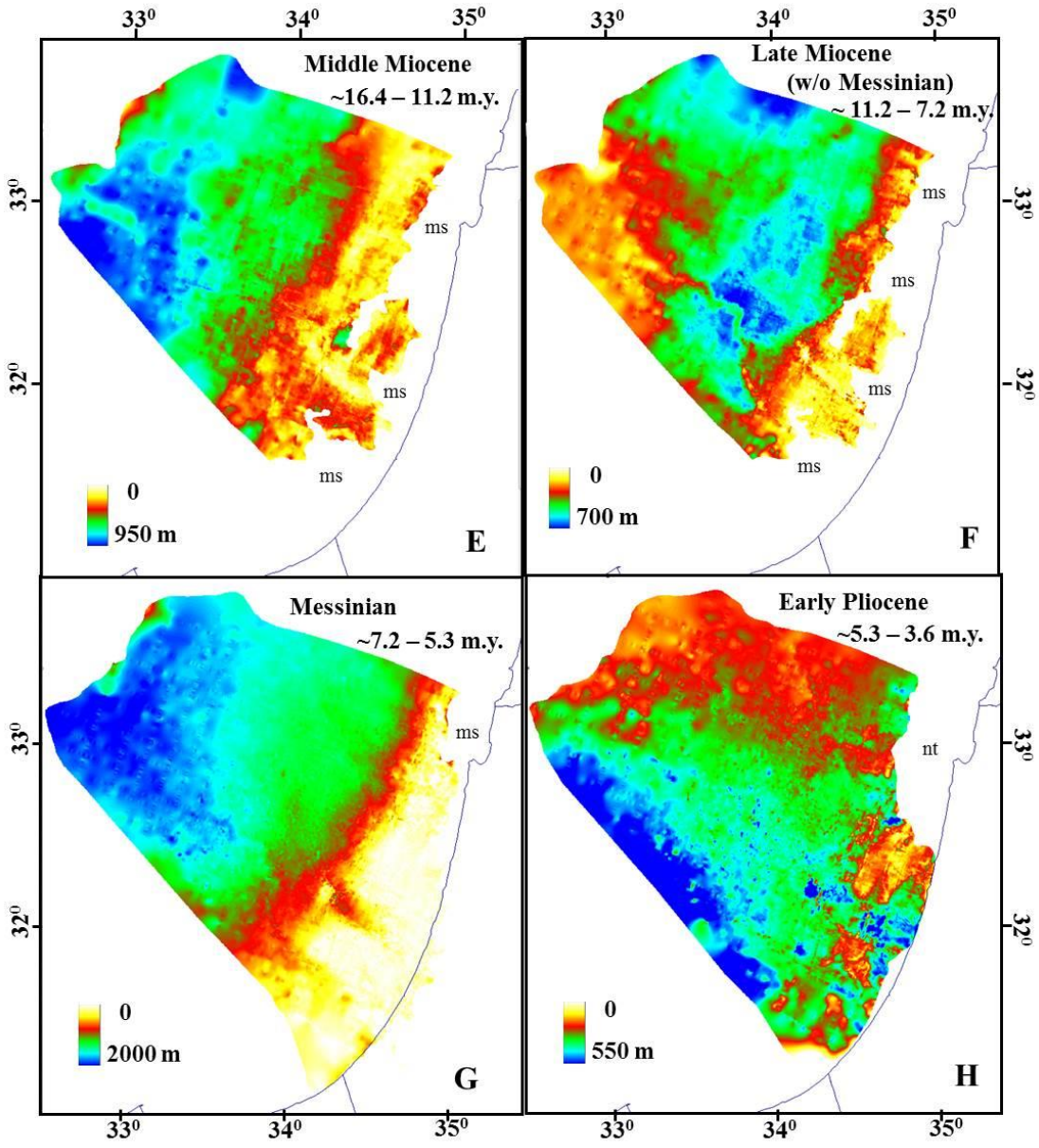
33⁰
34⁰
35⁰
32⁰
Middle Miocene
~16.4 – 11.2 m.y.
ms
ms
ms
0
950 m
E
Late Miocene
(w/o Messinian)
~ 11.2 – 7.2 m.y.
ms
ms
ms
ms
0
700 m
F
Messinian
~7.2 – 5.3 m.y.
ms
0
2000 m
G
Early Pliocene
~5.3 – 3.6 m.y.
nt
0
550 m
H

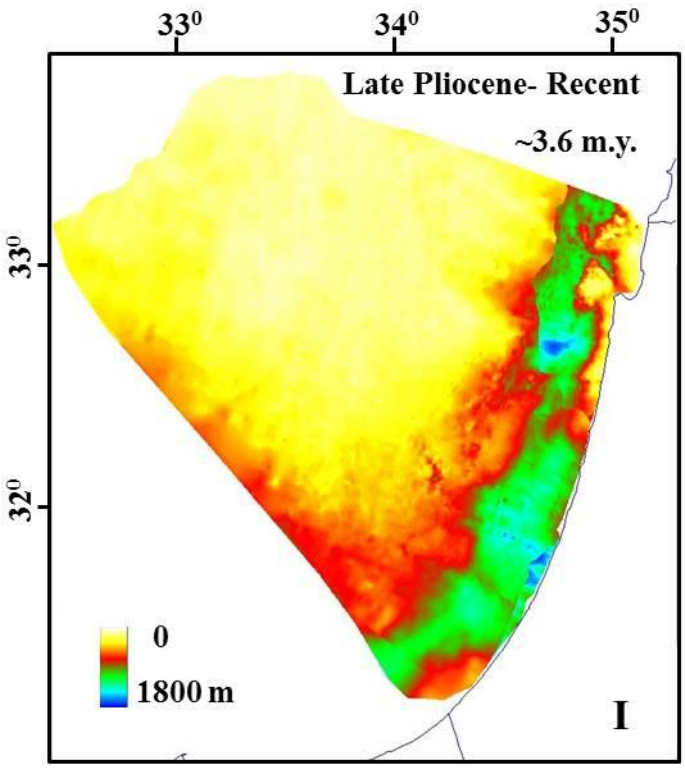

Figure 4.6 Isopach maps computed from the structural maps of Fig. 4.2: A) Base Late Jurassic – Base Santonian. Where base-Santonian is missing (white polygons in Fig. 4.2B) the base-Saqiye structural map was used for computation. Note, a large depocenter is located east of Jonah high (J). B) Base-Santonian – Base Saqiye (note series of synclines in the nowadays shelf area and the thinning of the section along the Leviathan high). C) Base Saqiye – Base Miocene, series of synclines is restricted to the nowadays shelf area and major progradation of sediments in the south east (at the depocenter location). D) Base Miocene – Base Middle Miocene. E) Base Middle Miocene – Base Late Miocene. F) Base Late Miocene – Base Messinian, depicting the mold of a channel flowing from south east to northwest (see Sec. 4.7). G) Base Messinian – Base Pliocene. H) Base Pliocene – Base Late Pliocene. I) Base Late Pliocene – Sea floor. Where the base Late Pliocene was not interpreted ("nt", Fig. 4.6H), the base Pliocene structural map was used for computation, therefore, representing a slightly exaggerated thickness for this section in that area. Abbreviations: nt- not interpreted; nd – not deposited; ms – missing; tr- truncated.

Forty four folds were formed from the beginning of the Santonian till the Late Eocene (Fig. 4.7A), 38 on the nowadays shelf and slope area and 6 in the deep basin (Fig. 4.7A). Noteworthy, the activity of 15 of those folds stopped after the Middle

Eocene and were never rejuvenated since. Folds orientation varies between north-east to north-northeast.

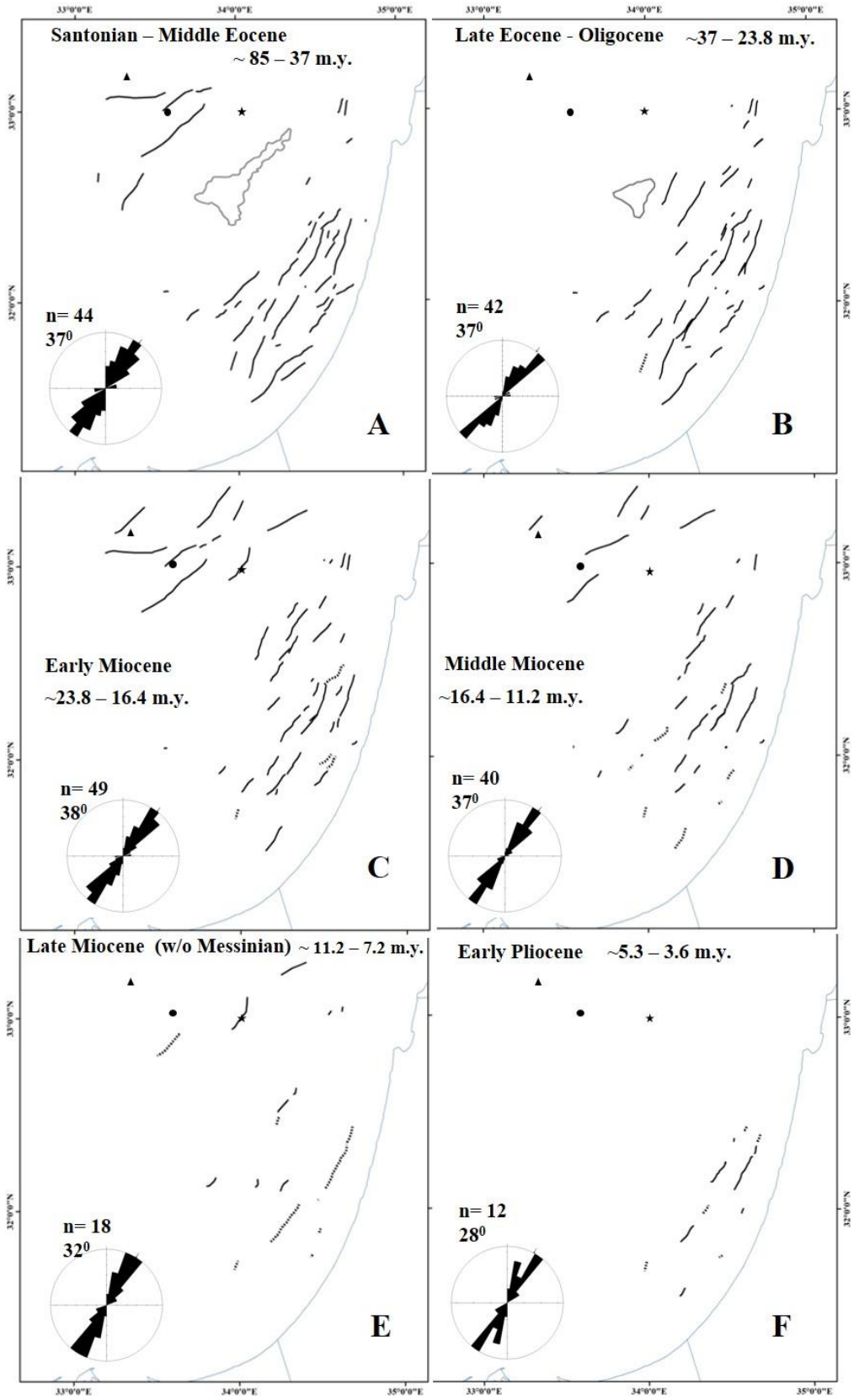

Figure 4.7: Active folds maps displaying folding activity through time and space. Rose diagram denote fold axis azimuth (n – number of folds). A) Santonian-Middle-Eocene (including), B) Late-Eocene – Oligocene, C) Early Miocene, D) Middle Miocene, E) Late Miocene, F) Early Pliocene. Black lines – active folds, black dotted lines – uncertain active folds. Gray polygon – the erosive boundaries of Jonah high in the beginning of the Santonian (A) and in the beginning of the Late Eocene (B) is presented for convenience. Folding west of Jonah high ceased during the Late-Eocene – Oligocene (B), it resumed in the Early Miocene and it diminished from the Late Miocene. Note that folds azimuth remain in the same direction for more than ~80 m.y. For Isopach maps displaying the active folds in each period refer to appendixes 1 to 6. Triangle – Aphrodite-1 well, circle – Leviathan-1 well, star – Tamar-1 well.

During the Late Eocene and all of the Oligocene intense folding activity continued in the continental margin block (Fig. 4.7B) and ceased in the deep basin. During this time 12 folds were formed, and altogether 42 folds were active in the eastern part of the basin, mostly striking to the north- east and some to the north-north-east. To the south, the Yam-West and the Yam-Yafo anticlines branch and form a fork like secondary folding (Figs. 4.3 and 4.7B). This secondary folding is best expressed in time sections, and continues through the early Miocene (Fig. 4.1).Towards the end of the Oligocene the activity on 7 of these folds stopped, and never rejuvenated since.

The Early Miocene period is characterized by intense tectonic activity on more than 49 folds (Fig. 4.7C). Some of the folds (e.g., the monoclines bordering the Leviathan high) which stopped their activity in the Late Eocene rejuvenated. Ten new folds, striking to the north- east and some to the north-north-east were formed in the deep basin (Fig. 4.7C). On the shelf area, the activity on the secondary folds along the Yam-West and Yam-Yafo anticlines continued, while the tectonic activity on the main fold axis ceased (Fig. 4.1, 4.4). Though the deformation migrated on those structures, the azimuth of the secondary folds didn't change much and they remain

almost parallel to the "original" main fold (Fig. 4.7C). Towards the end of the Early Miocene the tectonic activity on 12 folds stopped, and was never rejuvenated since.

During the Middle Miocene 40 folds (striking to the north-east to north-north-east) remained active throughout the basin and three ones rejuvenated (Fig. 4.7D). The Middle Miocene section displays minor thickness variation over the Aphrodite anticline and the Leviathan high (Figs. 4.5, 4.6E, 4.7), suggesting that tectonic activity started to diminish along those structures during the Middle Miocene. Towards the end of the Middle Miocene, the activity on 18 folds stopped, and never rejuvenated since.

Declining of folding activity continued in the Late Miocene with only 18 active folds at that time (e.g., the Tamar anticline, Fig. 4.5c, 4.7E). Nonetheless, a noticeable folding phase is observed in the shelf area during the Early Pliocene. In spite of salt-tectonic deformation during the Plio-Quaternary (e.g. Cartwright and Jackson, 2008) this Early Pliocene activity could be identified in the Early Pliocene, comprising ~9 folds (5 of which are suspected to be active), striking to the north-north-east (Fig. 4.7F).

Overall, a complex folding pattern and folding events characterizes the Levant basin, and although the Jonah high pre-dates this activity (as described in Ch. 5), the Leviathan high seems to be at least partially congruent to this activity. A brief description of this enigmatic high is presented below.

4.6 Leviathan high

The Leviathan high, observed in the structural maps of Fig. 4.2, is located in the deep Levant basin and was interpreted by Gardosh et al. (2008) as a basement high bounded by faults. The Leviathan structure is not observed in the Late Jurassic – base Santonian isopach (Fig. 4.6A), apparently indicating that it wasn't tectonically active during that time consistent with the ages of post-rift and pre-contraction phase (see geological background Sec. 1.4). Examining seismic sections crossing this structure shows that at some places the sub-Santonian section (below the turquoise horizon) is composed of incoherent reflectors (Fig. 4.5e) and in other places relatively flat bundles of reflectors are observed (Fig. 4.5f). The alternate appearance and disappearance of reflectors within the Leviathan structure, and its unclear boundaries at depth challenge the interpretation of Gardosh et al. (2008). The blurring of reflectors at places inside the structure may hint for volcanic flows similar to the Asher volcanic. Such volcanic flows can causes the blurriness observed in the structure while not disturbing the imaging of coherent reflectors underneath it. However, lack of magnetic anomalies (Rybakov et al., 2011) does not favor such possibility, unless the magmatism is granitic unlike the Asher Volcanics. Alternatively, amalgamation of coherent reflectors crossing the structure without coherent reflectors might result from facies changes across it, such as hard carbonates or reefs which tend to have a similar seismic appearance. The possibility of facies changes is in line with the observation that Leviathan is an ancient horst, slightly elevated from its surrounding, as expressed by the gently dipping away of the BLJ horizon (Figs. 4.5e, f), and also with the lack of spatial consistency of this phenomenon.

The Leviathan structure is associated with moniclinal folds at its boundaries (Figs. 4.5e, f). The Santonian-Eocene section thins towards these monoclines as observed in the seismic sections of Fig. 4.5 e, f, and in the isopach map of Fig. 4.6B, thus indicating tectonic activity during the first phase of folding. As explained above, during the Late-Eocene – Oligocene period these monoclines ceased to operate (Figs. 4.6C, 4.7B) and then renewed their activity in the Early Miocene (Figs. 4.6E, 4.7C). During the Middle and Late Miocene the western boundary of Leviathan ceased to operate while its eastern boundary continued. Since the Pliocene all activity in the deep basin ceased (as explained above).

Overall, the Leviathan high portrays a triangular wide shape differing from the elongated anticlines typical to Syrian Arc structures (Figs. 4.2, 4.6). Though its deeper boundaries are vague and obscure, it seems that this large structure is an early Mesozoic horst (Gardosh et al., 2008). However, unlike the Jonah high which was a prominent seamount until its complete burial during the Miocene (see Ch. 5), the Leviathan horst accumulated sediments continuously, at least since the Late Jurassic. Moreover, the Leviathan structure was reactivated during the contractional phase of the basin (unlike the Jonah high see Ch. 5) and distinct monoclines were formed at its boundaries.

Simultaneously to the evolution of the major structures such as the Leviathan high, Jonah high (Ch. 5) and the folds described above, the Levant basin accumulated more than 15 km of sediments. The above detailed interpretation of 10 horizons dividing the Mesozoic and Cenozoic section encompass more than 160 m.y of sedimentary filling history and provide an opportunity to review how sediments accumulated in the basin, where the major depocenter evolved in each period, and further understanding the factors controlling the accommodation space in the basin. In

what follows, a brief review of the sedimentary filling history in the Levant basin as portrayed by the nine isopach of figure 4.6 is presented.

4.7 Levant basin sedimentary filling history

During the Late Jurassic till the beginning of the Late Cretaceous sediment accumulated in the inherited horst and graben structure resulting from the Early Mesozoic rifting events (Fig. 4.6A). The Jonah horst remained a prominent high (see Ch. 5 for details) bounding the major depocenter to the west. More than 4 km of sediments accumulated west of the Israeli present coastline during this time span (~80 m.y.), whereas ~2 km of sediments accumulated relatively uniformly west of Jonah horst. Thus, passive margin conditions seem to prevail through the entire Levant area.

The complete burial of the Early Mesozoic horst and graben in the eastern part of the Levant basin was followed by a westward shift of the major depocenter. Bounded by the Jonah horst in the east and the Leviathan high in the west, this "L" shaped depocenter accumulated ~1.5 km of sediments during the Santonian till the Middle Eocene (Fig. 4.6B). The subsequent period, of the Late Eocene and Oligocene, marks major changes in the basin configuration. First, vast acceleration of sediment deposition occurred in the Oligocene and persisted through the Tertiary (Steinberg et al., 2011). Specifically more than 2.5 km of sediments accumulated during the Late Eocene-Oligocene which has promoted shelf build-up westward. Second, the uplift of the eastern margin of the Levant basin along the continental margin fault zone (Gvirtzman et al., 2008; Gvirtzman and Steinberg, 2012; Bar, 2009) is pronounced, and has further localized the depocenter southward of the Jonah high (Fig. 4.6C). During the Early Miocene more than 1.3 km of sediments accumulated throughout the

basin, burying the Jonah high and localizing the depocenter south-west of it (Fig. 4.6D). Gradual westward thickening of the Middle Miocene section points to a regional westward tilting of the entire Levant basin. Burial of the Leviathan high further located the basin depocenter in the west (Fig. 4.6E). During the Late Miocene, sediments accumulated mainly in the central part of the basin, and truncation of the upper part of the section occurred in the west by the overlying Messinian horizon.

The late Miocene (without the Messinian) isopach (Fig. 4.6F) display the mold of a prominent channel, flowing (from 34^0E, 32^0N) westward for more than 100 km and its issuing alluvial fan (to 33^0E, $32^0$30'N). The channel erodes the upper part (~100 m) of the Late Miocene section and marks the onset of the Messinian event. Whether this channel was a submarine channel such as turbidities current delivering sediments to the deep basin or a subaerial channel incising the exposed (if indeed) Mediterranean seafloor, its flowing direction to the west express the direction of the lowest area in the Levant basin at that time. This however is in contrast to the nowadays bathymetry which deepens to the north (toward Cyprus) as depicted by the >200 km turbidities channel flow (Gvirtzman et al., 2014). During the Messinian, the Levant basin accumulated more than 2 km of evaporates (Fig. 4.6G). The major depocenter was localized in the western part of the basin where erosion of the upper part of the Late Miocene - Tortonian took place (Fig. 4.6F).

The Early Pliocene depocenter was located in the south and western part of the basin pointing towards the Nile alluvial cone (Fig. 4.6H). This suggests that the depocenter location was dictated by the subsidence driven by the flexural loading of the Nile's alluvial fan. Note that for the first time in the basin's history, the sedimentary section thins gradually to the west and north-west of the basin, reflecting the "starved basin" condition that prevailed in the deep basin. This feature however is

much more pronounced in the later period from the Late Pliocene till nowadays where the major depocenter is localized in the Jaffa basin (Fig. 4.6I) (Gvirtzman et al., 2008; Steinberg et al., 2011). During the Late Pliocene till recent, the Israeli shelf builds-up (Fig. 4.6I), locating the depocenter along the eastern border of the basin suggesting it is controlled by sediment supply mainly from the Nile alluvial fan. The Late Pliocene-Pleistocene section gradually thins towards the north-west in the deep basin, portraying the "starved basin" conditions there.

Overall sediment accumulation in the Levant basin was controlled during the Late Jurassic till Santonian by subsidence of the grabens inherited from the previous rifting phase. The subsequent folding episodes mainly affected sediment accumulation in the nowadays shelf area, whereas the bulk of sediments accumulation (the depocenter location) was controlled by subsidence of the areas bordering the Jonah, Leviathan and the CMFZ. During the Middle Miocene, sediment accumulation was controlled by the westward tilting of the entire Levant, while later on, during the Plio-Pleistocene sediment accumulation was controlled by sediment supply from the Nile cone and the eastern Levant area.

4.8 Synthesis

Folding activity in the Levant basin started after the Santonian marking the end of the quiet period that followed the Early Mesozoic rifting stage. The onset of an extensive folding activity is recorded through a vast area at the borders of the Levant continental margin and further inland: Western Egypt, Sinai, Israel, Lebanon and Syria (Guiraud and Bosworth, 1997; Bosworth et al., 1999). The Santonian to Late Eocene folds evolved in the current shelf and deep basin (Fig. 4.7A). During the Late-

Eocene and Oligocene folding activity was limited to the eastern part of the basin - east of Jonah horst. Extensive folding in the deep basin was renewed in the Early Miocene (Fig. 4.7). Folding activity continued during the Middle Miocene (Fig. 4.7), however only one new fold started its activity. While folding activity diminished along most of the folds in the Late Miocene, it continued along 18 folds. As folding activity declined, the remaining active fold's segments become shorter, stressing the difficulty to measure accurately their azimuth (on a map view). Moreover, assessing their timing of activity also becomes harder; hence we classified some of the folds which are susceptive to be active during the Early Pliocene but included them in the rose diagrams. Nevertheless, Early Pliocene folds azimuth of 28^0 slightly varies from the mean general fold's azimuth of ~38^0.

Altogether folding activity in the Levant basin indicate that the Syrian Arc Fold belt extend westward offshore Israel >200 km into the Levant basin. A complex pattern of folding activity is recorded since the Santonian, where folds activity ceased on some folds while new ones were formed. Also during the Late Eocene till Oligocene the Jonah high and CMFZ marks the western boundary of activity. As tectonic activity diminished in the Late Miocene it was restricted to the eastern part of the basin where activity continued till the Early Pliocene.

Two fundamental observations are presented: first, folding activity that started in the Santonian-Eocene time continued till Early Pliocene. Second, folds orientation (azimuth) remain uniform through more than 80 m.y., new folds that formed after the Late Eocene have similar orientation (azimuth) as older-Santonian ones.

4.9 Discussion

The idea that Syrian Arc deformation belt originated by far field stress related to the African plate motion has been widely accepted (Chaimov et al., 1992; Eyal, 1996; Guiraud and Bosworth, 1997; Brew et al., 2003; El-Motaal and Kusky, 2003). Bosworth et al. (1999) suggested that the Santonian shortening correspond to the significant change in the poles of opening of the North Atlantic. The Syrian Arc deformation also corresponds to the East Alpine and northern Carpathian nappes which collided with the eastern parts of the Helvetic shelf (Ziegler, 1990). Although this orogenesis was far to the north, it is postulated that it has generated far-field compressional stresses that were transmitted south (Bosworth et al., 2008). In what follows, we will integrate the timing and spatial extent of folding in the Levant basin with plate scale major tectonic events that shaped this area.

4.9.1 Timing of deformation and plate re-organization

The thick sedimentary section in the Levant basin indicate about 80 m.y. of folding activity. The Santonian – Middle-Eocene section records an intensive folding throughout the basin, similarly to onshore observations. Generation of folds and reactivation of existing folds continue till the Pliocene, but two main phases of decreasing activity can be recognized (the Late-Eocene –Oligocene and the Late Miocene). The Late-Eocene – Oligocene section shows that activity is restricted to the eastern part of the basin (east of Jonah high). This diminishing of activity in the western part of the basin is correlated with the development of an extensive fault zone (<20 km wide) along the margins of the Levant basin (CMFZ, Figs. 4.1, 4.2) which accommodated the early stage of the African-Arabian breakup (Gvirtzman and Steinberg, 2012). Activity along the CMFZ during the Oligocene generated vertical separation of more than 2 km across the basin. It is likely that this mainly vertical

separation has also accommodated a great part of the horizontal shortening during that time. In this case, the CMFZ and the nearby area acted as large scale shock absorber by crumpling and accommodating the imposed shortening, similarly to the Cyrenaica area (Bosworth et al., 2008), leaving the area of Jonah high and west of it to reside in a strain shadow. Interestingly, although the activity of the CMFZ has affected the entire lithospheric structure (Gvirtzman and Steinberg, 2012), when activity along it ceased (Early Miocene), folding similar to the Santonian phase resumed in the central and western part of the Levant basin (west of Jonah high).

During the Late Miocene a marked decrease of folding intensity occurs in the entire basin alongside with the development of new plate boundaries north and east of the basin. To the north, the Cyprus subduction boundary evolved accommodating the northward drift of the African plate beneath Eurasia (Robertson, 1998a,b); and to the east the Dead Sea Transform evolved accommodating the same motion relative to the Arabian plate (Garfunkel, 1981; Garfunkel, 1998). However, in spite the fact that much of the motion of Africa is accommodated along these two plate boundaries, folding in the Levant continental margin continued in the shelf area till the Late Pliocene (Fig. 4.7). Moreover, despite the formation of new plate boundaries, Pliocene folding continued in similar orientation as previously.

Observations of NNE-SSW Pliocene folding are also reported onshore along the Israeli coastline, Judea Mountains and the Dead Sea apparently indicating WNW-ESE compression (Eyal, 1996). According to Eyal (1996) the onshore NNE trending folds are not associated with the Dead Sea transform stress field, because this would have produce ENE-WSW structures. Instead, they represent a

.

Our results from the offshore show NE trending folds for more than 80 m.y. and hence cannot be solely explained by far field stress, because such stresses should have been rotated together with the Afro-Arabian motion since the Late Cretaceous. We alternatively suggest that the Levant basin was affected by the interplay of far field stresses resulting from plate motion and pre-existing continental weak lineaments as discussed below.

4.9.2 Spatial distribution of the Syrian Arc Folds

We presented here observations showing that folds in the Levant basin include structural elements similar to the onshore Syrian Arc folds that extend > 200 km from the Israeli and Sinai coastline. This wide deformational zone lines up with a series of compressional structures (folds) observed from Morocco to Syria dating as early as the Santonian (Guiraud and Bosworth, 1997; Guiraud, 1998). The fold belt is related to the onset of shortening along the northern margin of Gondwana during the Santonian as demonstrated in north-east Libya (Papanikolaou et al., 2004; El-Hawat and Abdulsamad, 2004), north-central Egypt and Sinai (Bartov et al., 1980; Moustafa and Khalil, 1990; Moustafa, 2013), the Levant (Eyal and Reches, 1983; Bruner, 1991; Mart, 1994; Druckman et al., 1995; Walley, 1998), Palmyrides and northeastern Syria (Chaimov et al., 1992; Brew et al., 2003). These compressional structures reflect the scissor like closure of the Tethys, when Africa-Arabia had experienced a counterclockwise rotational northward drift (Guiraud and Bosworth, 1997). Further collision of Africa with Eurasia resulted in a compressional regional stress field which is thought to initiate inversion along early Mesozoic basin such as the Cyrenaica basin N-E Libya (Papanikolaou et al., 2004; El-Hawat and Abdulsamad, 2004), and the

Palmyrides in Syria (Chaimov et al., 1992). We therefore point out that most of this fold zone developed on the margin of the African plate.

The development of several Syrian Arc folds was suggested to originate by reactivation of late Paleozoic-early Mesozoic normal faults as reverse faults (Freund et al., 1975; Cohen et al., 1990). Seismic studies from offshore Sinai, to Palmyrides, Syria, reported reactivation of Early Mesozoic normal faults during the Santonian – Maastricht in a reverse motion forming fold related faults over the upper part of the section while the lower part exhibited reverse faulting (Druckman et al., 1995; Bruner, 1991; Chaimov et al., 1992; Gardosh et al., 2008; Yousef et al., 2010). However, the present analysis of the Levant basin suggest that reactivation of normal fault as reverse faults might explain only a few folds (see Fig. 4.1), whereas most of the folds are not associated with buried faults that penetrate the upper (post-rift) sedimentary sequence. Perhaps interpreting deeper horizons expressing the syn-rift period would have reveal the existence of normal faults. Such faults striking to the NNE, as presented in Triassic to Early Jurassic faults map of Gardosh et al. (2010), might have influenced the folding orientation. But the inability to identify fault surfaces beneath most of the folds does not support the fault inversion theory, and hints for a complex mechanism.

Combining these observations with the observation that the wide (>200 km) deformation belt accompanies the north margin of the African plate from Morocco to Syria lead us to suggest that this is a plate margins phenomenon. That is, during the Tethys closure, weak old lineaments in the previously extended crust were preferably deformed. This 200 km wide belt is characterized by thick sedimentary section similarly to other pan-African domains that had experienced Santonian shortening (Guiraud and Bosworth, 1997).

Accordingly the irregular geometry of the northeast African margin has exerted a controlling influence on the inhomogeneous strain pattern affecting the east Mediterranean (Bosworth et al., 2008). On a smaller scale, the observation that the folds in the Levant basin evolved relatively in a constant (NNE ~38^0) orientation over > 80 m.y. expresses the local NE trend of the continental margin, as revealed by the Triassic to Early Jurassic faults map of Gardosh et al. (2010).

The analysis and findings described in this chapter were published in Tectonophysics (Sagy et al., 2015).

5. The Enigma of the Jonah high

5.1 Introduction

This chapter focuses on the Jonah high, located 80 km west of the Israeli coastline in the southeastern part of the Mediterranean Sea (Figs. 5.1, 4.1). Seismic reflection surveys reveal a triangular, ~18 km-wide structure, buried under more than 3 km of Late Tertiary sediments and a mound topped by sub-horizontal bundles of reflectors (Folkman and Ben-Gai, 2004; Gardosh et al., 2008). The Jonah high, one of the most prominent structures in this basin, is quite enigmatic and attractive both for tectonic research and for hydrocarbon exploration. Its dome shape, as displayed on seismic sections, reveals a non-reflective internal structure that does not show folded beds (Fig. 4.1). In addition, it is associated with one of the largest magnetic anomalies in the Levant basin (Rybakov et al., 2011). Interestingly, only a small positive gravity anomaly is observed (Rybakov et al., 1997; Gardosh et al., 2008) and extrusive or intrusive boundaries typical to magmatic bodies are not identified in the seismic images (Fig. 4.1). Finally, the difference between its non-reflective internal structure and its reflector-rich surrounding is prominent, but distinct faults were not recognized (Fig. 4.1).

Several suggestions for the origin of the Jonah high, with different profound implications for our understanding of the regional tectonics, were offered in the literature, without providing a detailed analysis. Folkman and Ben-Gai, (2004) suggested that the Jonah high is a deep-seated (8 km) igneous intrusion that was

formed concurrently with the Syrian Arc structures. Considering its location tens of kilometers west of the main fold belt, the Jonah high has implications for the extent and nature of this deformation zone. Alternatively, Rybakov et al. (2011) suggested a Mesozoic and Cenozoic volcanic edifice that is located in the transition zone between the eastern Mediterranean oceanic crust and the continental crust of the Arabian plate. This alternative raises the question of the age of magmatic activity: is it related to the magmatism of Early Mesozoic rifting (Garfunkel, 1998; Robertson, 1998); to Early Cretaceous intra-plate magmatic activity previously identified in the hinterland (Garfunkel, 1989); or to Cenozoic magmatism related to the Arabia-Africa breakup? Gardosh et al. (2008) hypothesized that the Jonah high is an Early Jurassic horst, overlain by an extrusive volcanic cone of Late Cretaceous to Early Tertiary age.

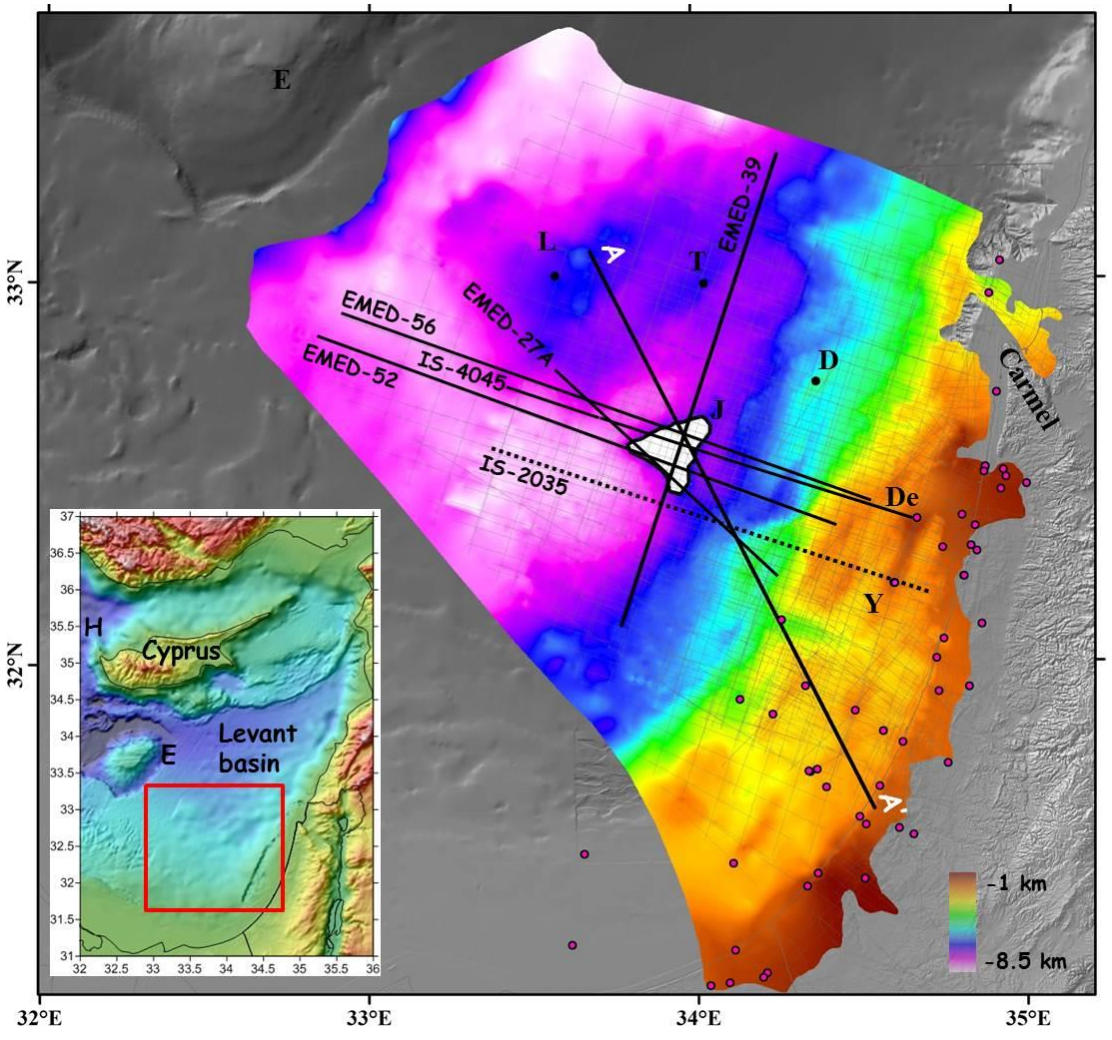

Figure 5.1: Location map. Colored map is the Base Saqiye Group unconformity surface. White polygon denotes the part of the Jonah high (J) where the lower Saqiye Gr. (Late Eocene-Oligocene) is missing. Gray background is bathymetry from Hall (1993). Regional bathymetry map (inset) is taken from ETOPO 11 (Amante and Eakins, 2009). Black lines are the depth-migrated seismic sections. Doted black line is a representative time-migrated section (Fig. 4.1). Fine gray mesh represents all seismic lines used for interpretation. AA' is a regional section used for gravity and magnetic modeling (Fig. 5.7). Dots are wells used for correlation. Abbreviation: L-Leviathan, T-Tamar, D-Dalit, De-Delta-1, Y-Yam-Yafo-1, E-Eatosthenes seamount, H-Herodotus Basin.

Noteworthy, in light of the recent giant gas discoveries in the Levant basin within structural highs, such as Dalit, Tamar and Leviathan (Fig. 5.1), understanding the origin of the Jonah high (horst, fold or magmatic body), its age and rock composition, could have major implications for hydrocarbon exploration. The possibility that the Jonah structure rose above the ancient surrounding seafloor for tens or even a 100 m.y. and may have been covered by carbonate reefs further emphasizes its importance as a reservoir regardless of its origin.

In respect to these contradicting scenarios we present a detailed analysis based on newly processed seismic data (presented in chapter 3) and interpretation of the Jonah high. We examine the geometric relationship between the Jonah structure and the well-resolved reflectors around it. Particularly we search for indications of syndepositional folding (thickness variations), syndepositional intrusion (deformed and deflected structures) and gradual burial of an existing seamount (onlapping strata). Eventually we test the consistency of our geological model with magnetic and gravity data.

5.2 Jonah high and its internal structure

Improving the accuracy of depth imaging depends on the ability to resolve detailed velocity variations in the vertical and lateral directions. This final interval velocity model should represent the true subsurface velocity characteristics, and it is used for the final migration process. In order to constrain the velocity model below the top of the Jonah high where reflectors are sparse and mostly incoherent, we performed several runs of pre-stack depth migration using a constant velocity of 4000 m/s, 4500 m/s, 5000 m/s, 5500 m/s, and 6000 m/s below the dark blue horizon (Mid-Miocene). Results for line EMED-39 and line EMED-56 (Fig. 5.2) indicate that the thick reflector inside the Jonah high appears much better (coherent) using velocities greater than 5500 m/s. However, outside the Jonah structure, lower velocities (<5000 m/s) are required to gain a better image of the deep part of the section. The velocities for the down part of each seismic line were defined according to these constant velocity panels, and were combined with the results from the iterative process of velocity analysis to yield a final interval velocity model in depth (an example for line EMED-39 is displayed in Fig. 5.3C).

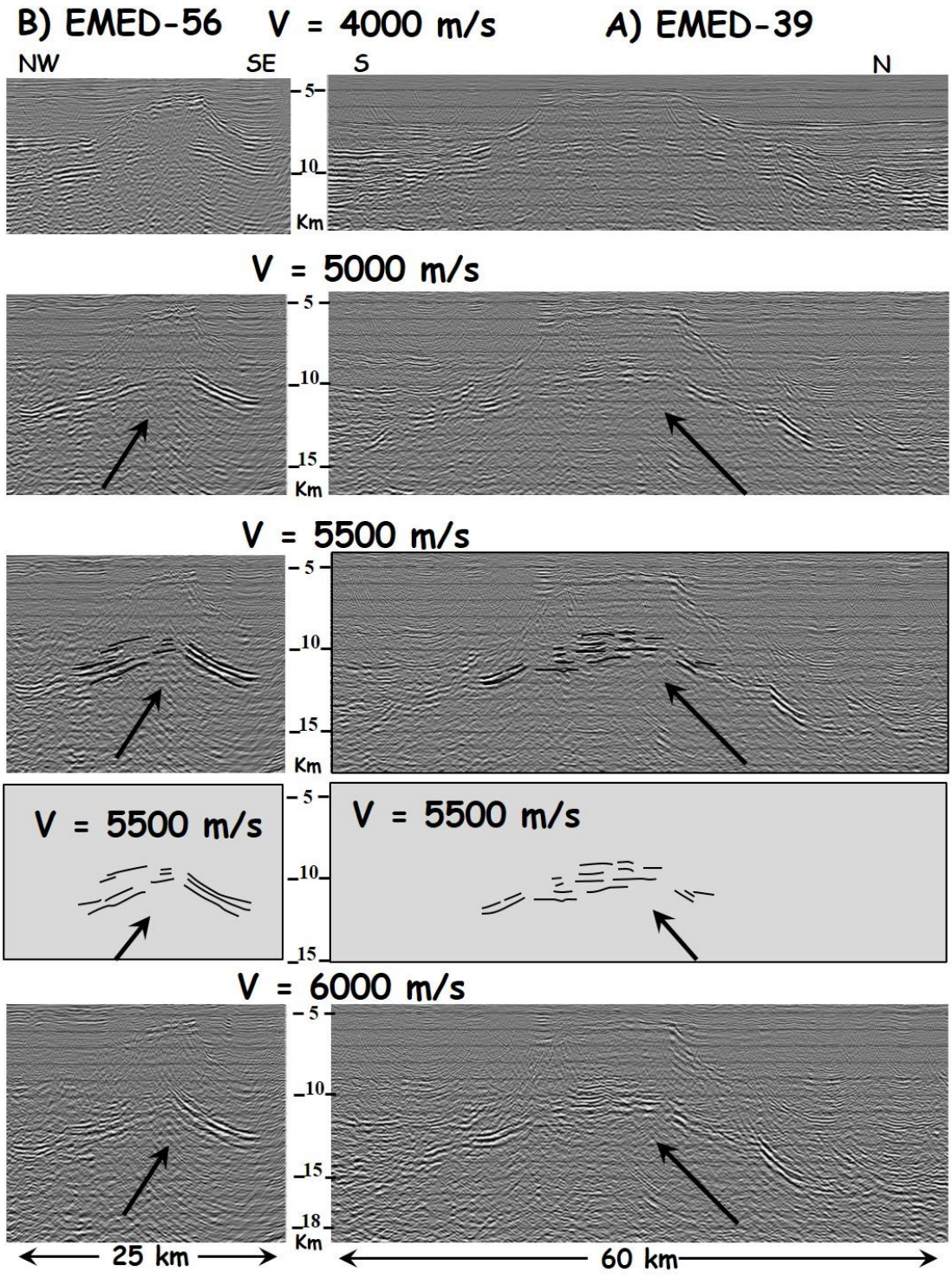

Figure 5.2: Depth-migrated sections using constant velocity below the base Mid-Miocene horizon (dark blue in Figs. 4.1, 5.3) for line EMED-39 (A) and line EMED56 (B) (location in Fig. 5.1). The intra-Jonah reflectors denoted by black arrows are unclear with low velocity of about 4000 m/s (topmost panels), start to appear using velocity of 5000 m/s (second from top); and seem most prominent, coherent and continuous while using velocity of 5500 m/s (third from top). For comparison to time-migrated section see figure 5.3A.

The importance of depth migration for interpreting the Jonah structure is illustrated by line EMED-39 crossing it from south to north (Fig. 5.3). A comparison between the time-migrated section (Fig. 5.3A) and the depth-migrated section (Fig. 5.3B) reveals first that the shallower part of the Jonah structure is laterally narrower (15 km) in the depth section than in the time section (20 km, Fig. 5.3A). Moreover, the top of the Jonah high (blue horizon) appears folded in the time section, while it appears relatively flat in the depth section. Second, the depth migration sharpens the differences between the structure and its surrounding rocks even at a depth of >11 km, enabling a better delineation of its deep boundaries and indicating that it is much wider (~40 km) than its topmost part (~15 km). Third, the depth migration highlights a thick and nearly flat reflector within the structure itself at a depth of ~10 km. Differing from the time section, in which this vague reflector is concave and seems like a folded layer, the depth migrations reveal that this layer is flat.

The interval velocity model constrained by our depth domain analysis (Fig. 5.3C) displays low velocities of ~1600 m/s in the Plio-Quaternary section (down to the yellow reflector), sharply jumps to ~4200 m/s in the Messinian evaporite layer (down to the harlequin green horizon), drops back to ~2600 m/s below the evaporites, and then gradually rises to about 3800 m/s at the base Saqiye Group unconformity (red horizon, Mid-Late Eocene). From this unconformity downwards the velocity within the Jonah structure increases abruptly to 5500 m/s at a depth below 6 km and to about 6500 m/s below 10 km. Thus, the Jonah high creates a strong lateral velocity contrast to its surroundings, where velocity jumps from ~3500 m/s to ~ 5000 m/s at depths of 7-8 km and from ~5000 m/s to ~6500 m/s at 10 km depth and greater. This strong lateral velocity variation further emphasizes the importance of performing pre-stack depth migration in order to obtain a correct structural cross section of the subsurface.

Noteworthy, since seismic velocity of 6500 m/s is typical to igneous rocks, the boundary between 5500 m/s and 6500 m/s may represent the top of the crystalline crust, which is ~15 km deep in the basin and ~10 km deep within the Jonah high.

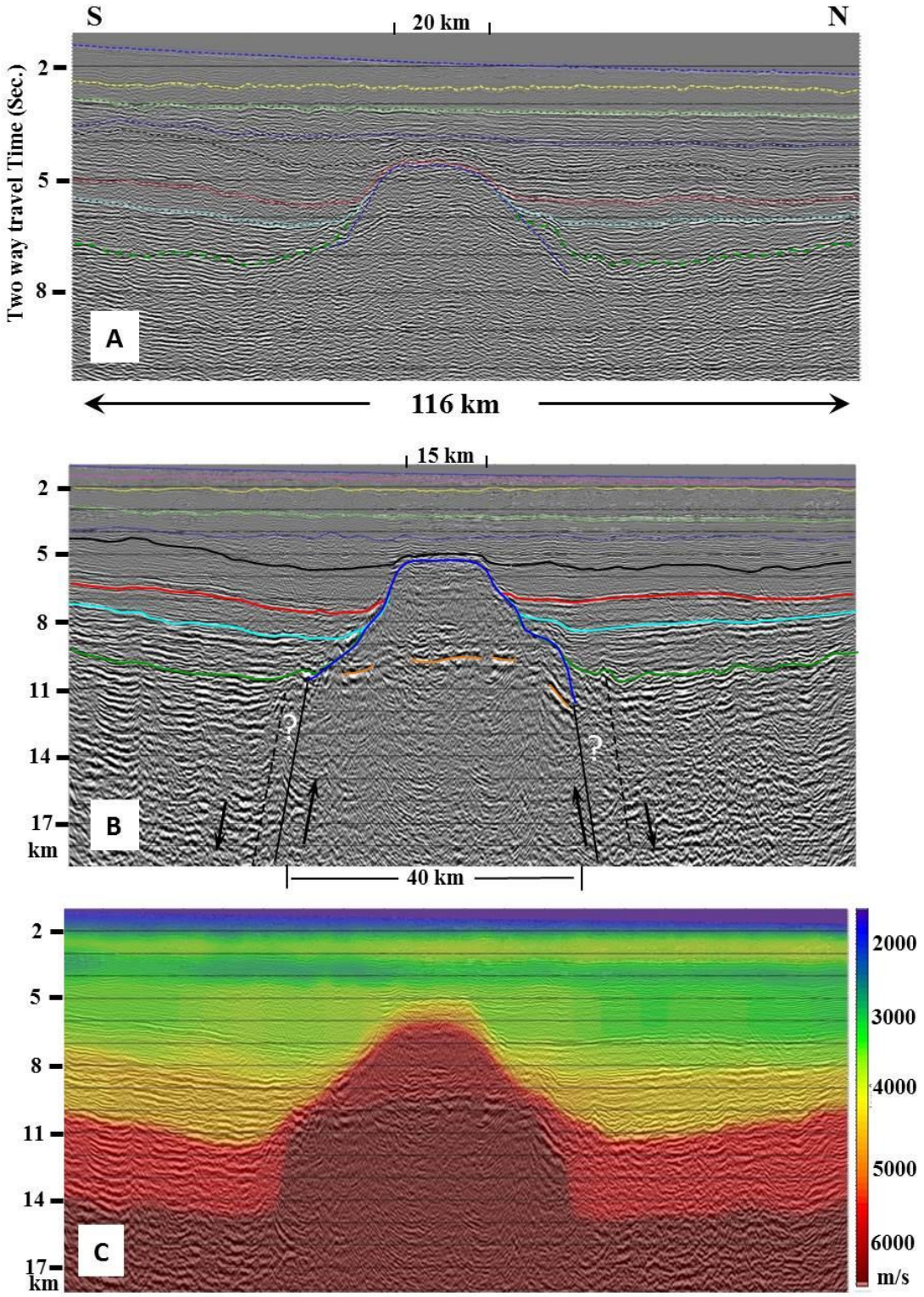

Figure 5.3: Line EMED-39 crossing the Jonah high from south to north (location in Fig. 5.1). A) Time-migrated section. B) Depth-migrated section (this study). C) Interval velocity model in depth (this study). The abrupt termination of all reflectors towards the Jonah structure indicates the existence of faults, but their exact location is uncertain (question marks) as further shown in figure 5.6. For legend refer to figure 4.1.

5.3 Jonah boundaries

The contrast between the reflector-rich surrounding and the internal chaotic appearance of the Jonah high is marked by the blue horizon, which appears as an irregular erosive surface (Figs. 4.1, 5.3, 5.4). A detailed interpretation of the depth-migrated seismic lines crossing the Jonah high reveals high-frequency, well-bedded, parallel reflectors onlapping the mid to upper part of the Jonah high and gradually burying it (Fig. 5.4). These onlapping relations are observed at least from the green horizon (near Mid-Late Jurassic) up until the base Miocene reflector (black horizon on Fig. 5.4), that is within a 5 km-thick section representing more than 120-140 m.y.

Interestingly, unlike the syntectonic thickness variations associated with Syrian Arc structures (Fig. 4.1, inset and Fig. 5.5A), no syntectonic thickness variations are observed in the thick and long-lived package adjacent to the Jonah high (Figs 5.4C, 5.5B). Onlapping geometries such as depicted in figure 5.5B are consistently observed in depth-migrated sections crossing the Jonah structure. The reflectors onlap the Jonah structure (marked in yellow, Fig. 5.4C), and the section wedges out such that thinning occurs only in the vicinity of the Jonah high's flanks, similarly to the EFG triangle in figure 5.5b and not farther away. At places the reflectors are slightly dipping away from the structure, suggesting some differential compaction. The un-deformed reflectors approaching the upper part of Jonah high and covering it rules out the possibility of any re-activation. Hence, these geometrical relationships indicate that

while the Syrian Arc structures were active in the Santonian-Eocene (Eyal, 1996; Walley, 1998; Brew et al., 2003), the Jonah high was a giant seamount at that time that was slowly buried but not reactivated. This conclusion does not mean that regional basin-wide thickness variations did not occur. For instance, the Lower Cretaceous package (between the green and turquoise horizons) is thicker southeast of the Jonah high, whereas the Upper Cretaceous package (turquoise to red horizons) is thicker in the northwest (Fig. 5.4B). These regional variations are not related,

however, to the Jonah high .

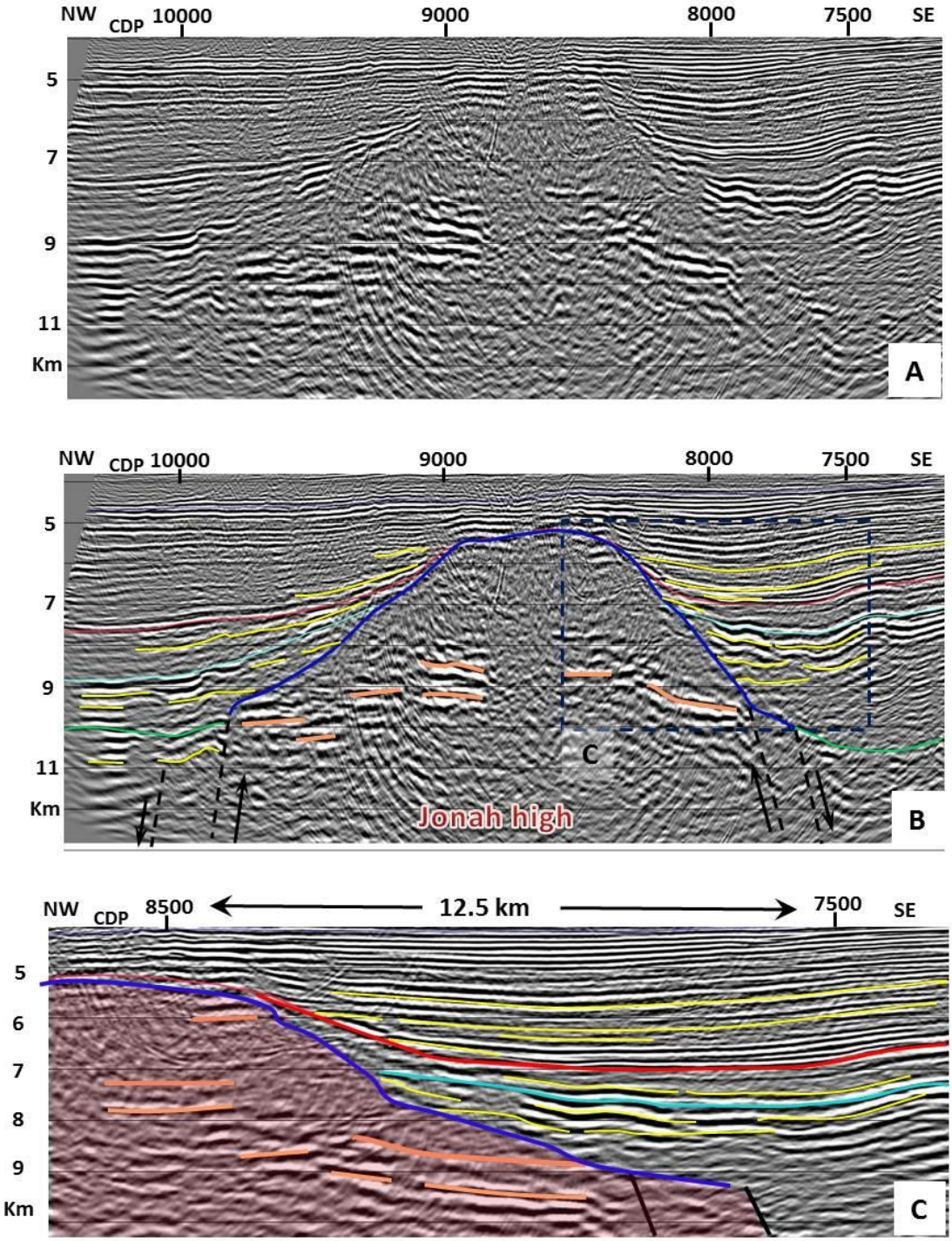

Figure 5.4: Parallel reflectors onlapping the Jonah high indicating gradual burial of a pre-existing seamount (depth-migrated section of line IS-4045, location in Fig. 5.1). A) Non-interpreted section, B) interpreted section, C) close-up on the eastern flank of the Jonah high with nearly no vertical exaggeration. This image represents the geometry with minimal distortions and shows no syndepositional thickness variations in layers approaching the structure (further explanation in Fig. 5.5). Exact fault location is uncertain as in figure 5.2.

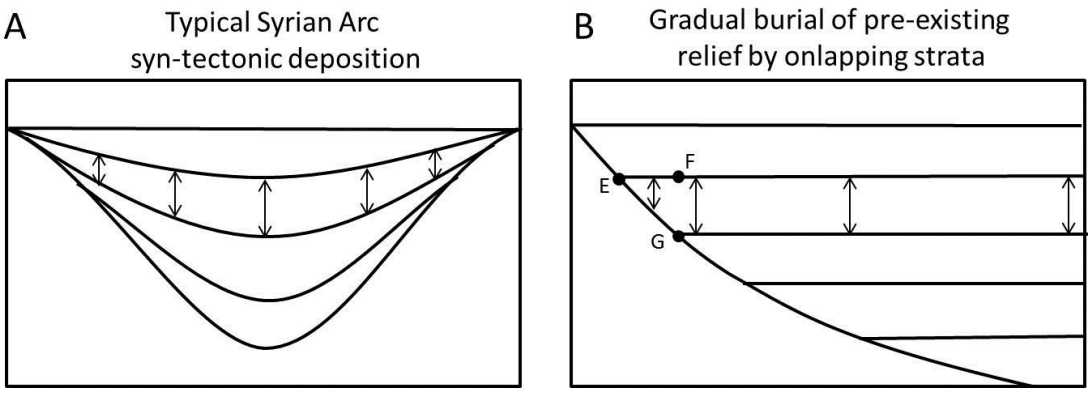

Figure 5.5: Cartoon exemplifying the difference between syn- and post-tectonic thickness variations. A) Thickness variations resulting from syntectonic deposition in which units change their thickness all along. This type of variation is typical to Syrian Arc folds as shown in figure 4.1. B) Thickness variations resulting from gradual burial of a pre-existing bathymetric relief, where thinning is limited only to the EFG triangle. This type of variation characterizes the ancient Jonah seamount.

The deep boundaries of the Jonah high below the green horizon are not at all clear in the available seismic data. The existence of many coherent reflectors on both sides of the structure and their abrupt ending (Figs. 5.3, 5.4, 5.6) hints at the existence of faults bounding a horst. But distinct faults are hard to identify in the seismic sections. We marked faults on each interpreted time-migrated line bearing in mind that its exact location is uncertain (as shown in Figs. 5.3, 5.4). We then further checked fault locations in a map view to see if their spatial orientation is reasonable in terms of fault bending and spatial continuity. Results indicate at least three fault systems (Fig. 5.6): the western side comprises two sub-parallel faults trending northeast; the eastern side comprises three sub-parallel faults trending north-northeast; the southern side comprises two en-echelon faults trending east-west; the northern side is less clear and probably less steep.

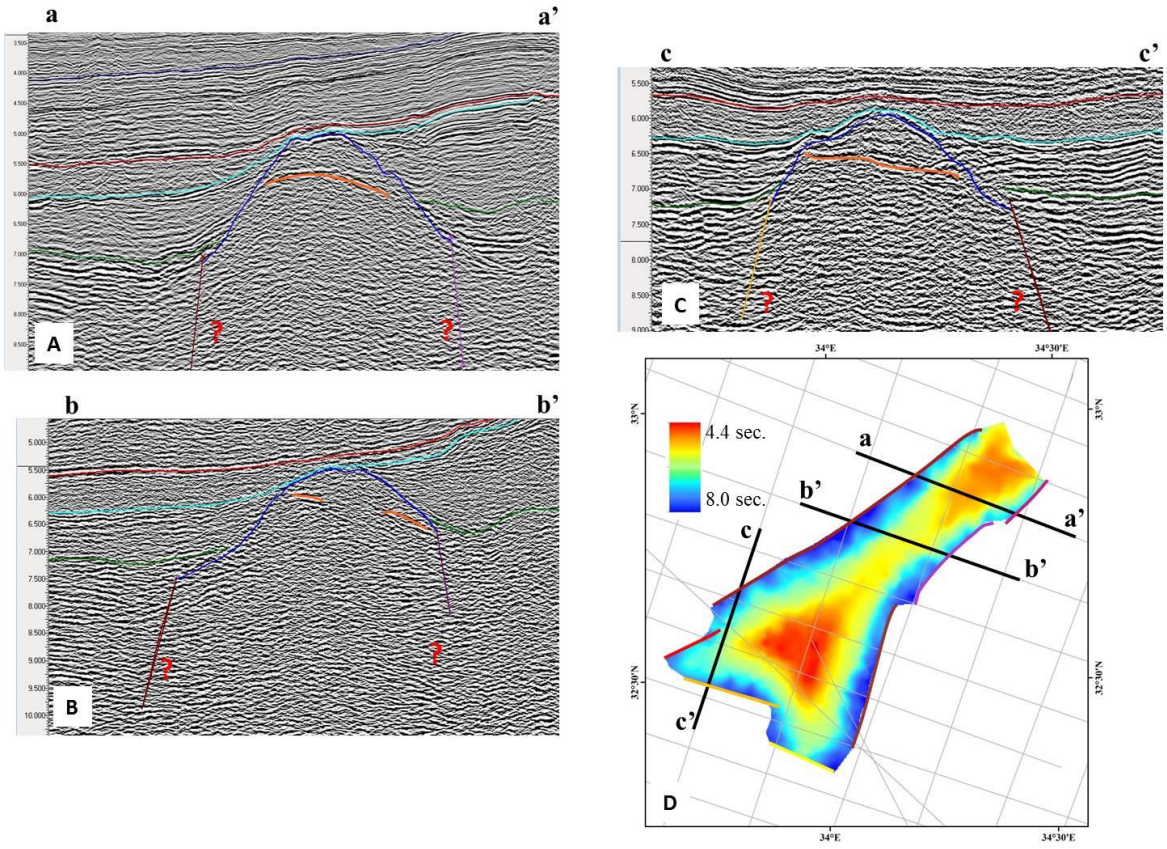

Figure 5.6: A-C) Selected time-migrated sections across the Jonah structure illustrating how its faulted boundaries appear in seismic data and how they were mapped. D) Two-way travel time structural map of the top Jonah horizon. Note that, exact location of faults is hard to determine in specific lines (see question marks in a, b and c). The resulting map shows that the western boundary comprises two en-echelon faults trending NE, the eastern boundary comprises three faults trending NNE to NE, and the southern side comprises two en-echelon WNW trending faults. Legend as in figure 4.1.

5.4 Burial history

The burial history of the Jonah high is shown by a set of structural maps (Fig. 4.2A-D) representing the Mid-Late Jurassic transition (green horizon, ~160 Ma), beginning of the Santonian (turquoise horizon, 85 Ma), the Mid-Late Eocene transition (red horizon, 37 Ma), and beginning of the Miocene (black horizon, 24 Ma). This set of maps shows that the Jonah high began as an elongated ~35x75 km seamount (bigger than Mt. Carmel), continuously decreased to a 15 km wide triangle

in the beginning of the Oligocene, and finally was entirely covered by sediments in the Early Miocene. Moreover, the fact that the lower part of the Jonah structure is much wider than its upper part (40 km at >11 km depth to 15 km at a depth of 6 km, Fig. 5.3B) combined with the winding shape observed in the various structural maps (Fig. 4.2A-D) suggests that at least since the Late Jurassic it had undergone erosion and its boundary walls retreated, having typical dips of $16^0 – 20^0$ and at places up to 32^0 .

Based on onlapping relations described above, the lack of Cretaceous and Early Tertiary sediments over the high structure is considered as non-deposition over a high seamount, unlike the missing Santonian-Eocene section east of the Jonah high (Fig. 4.2B), which is interpreted as representing younger erosion (Gvirtzman et al., 2008). The internal flat reflector (the orange horizon) observed within a reflector free body is interpreted as denoting the top of a basement high. Underneath it no reflectors are observed as typical for crystalline rocks, while above it the non-reflectiveness is attributed to perhaps carbonate reefs buildups (the upper part of Jonah high is discussed in Sec. 5.61).

5.5 Gravity and magnetic modeling

Our analysis clearly indicates that the Jonah high was a big seamount and that it is not a Syrian Arc fold. In addition, its internal flat reflection and its deep boundary faults strongly suggest that it is an Early Mesozoic horst and not a volcano. But since the horst characteristics are less obvious in the deep part of the seismic data, and since the strong magnetic anomaly is frequently associated with magmatic bodies, we checked if the horst model can explain the observed magnetic and Free Air gravity

anomalies without any addition of a magmatic body. The main challenge in this modeling was to check whether a basement high with reasonable magnetic susceptibility value can generate the observed magnetic anomaly of about 130 nT. A secondary mission was to find out what was needed to produce the relatively small gravity anomaly of about 25 mgal.

The cross section in Figure 5.8, which is perpendicular to the Jonah high, is based on the following information: (1) Stratigraphic units down to the green horizon (near mid-late Jurassic) were taken from the present study; (2) Top basement horizon on the depth sections was interpreted from this study; (3) The Moho was compiled from Segev et al. (2006), Netzeband et al. (2006), Ben-Avraham et al. (2002) and Garfunkel (1998); (4) Fine tuning and smoothing of the Moho NW of Jonah high at a depth to ~21 km was determined by trial and error; (5) Slight deepening of the Moho under the Jonah high to a depth of ~23.5 km was determined by trial and error. This is consistent with crustal thickening under big horst and continental fragments, though for local isostasy a thicker crust is required (discussed below); (6) The intra-crustal boundary between the lower and upper crust is consistent with Garfunkel (1998) and was refined by trial and error; (7) Magnetic and gravity data are from the 2001 survey of TGS-Nopec Geophysical Company L.P. (Fig. 5.1); (8) Density was taken as 2.9 gr/cm3 for the lower crystalline crust and 2.75 gr/cm3 for the upper crystalline crust. Mantle density was taken as 3.3 gr/cm3; (9) Densities for the sedimentary section range from 2.0 gr/cm3 near the sea bed to 2.6 gr/cm3 at depth. Messinian salt density was taken as 2.05 gr/cm3, and seawater density was taken as 1.03 gr/cm3; (10) Densities of the upper part of the Jonah high were chosen by trial and error and yielded 2.65 gr/cm3, which may represent consolidated old pre-rift sediments or younger hard carbonates that had built around an ancient seamount; (11) Declination

(4.3720) and inclination (47.800) values for magnetic modeling were calculated according to the present Earth's field in the Levant basin (using the latest International Geomagnetic Reference (IGRF)); (12) Magnetic susceptibility for all sediments was taken as zero. Susceptibility of the lower and upper crystalline crust was chosen by trial and error and found to be 0.006 and 0.005 (cgs units) respectively. This value is considered extremely high (but possible) for acid igneous rocks and quite high for most basic igneous rocks (Dobrin and Savit, 1960).

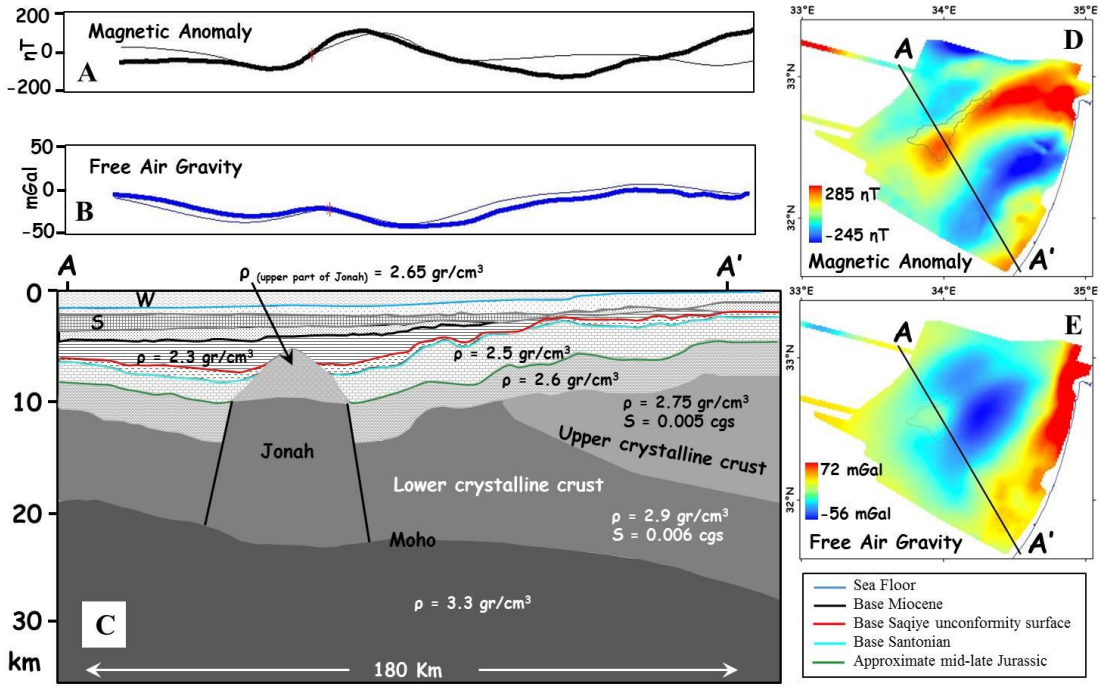

Figure 5.7: Magnetic and gravity model of section AA' crossing the Jonah high. For location refer to figure 5.1. A) Measured (thick line) and modeled (thin line) magnetic anomaly. B) Measured (thick line) and modeled (thin line) gravity anomaly. C) Geological cross-section based on this study plus rock densities and magnetic susceptibility values from the literature (see section 5.5 for details). Abbreviations: W-water, S- Messinian salt. D) Magnetic anomaly map and E) Gravity anomaly map from the 2001 survey of TGS-Nopec Geophysical Company L.P. The misfit of measured and modeled curves in the SE part of the section is attributed to the Hebron magnetic anomaly (Folkman and Yuval, 1976; Garfunkel, 1989), not modeled here.

Modeling results (Fig. 5.7) first indicates that considering the above values of magnetic susceptibility, the magnetic anomaly associated with the Jonah high can be

explained by a basement high. Noteworthy, our model does not try to solve the Hebron magnetic anomaly (Folkman and Yuval, 1976; Rybakov et al., 1995; Garfunkel, 1989) in the eastern part of the Levant area (~ 50 km south-eastward to the Israeli shoreline), which is beyond the scope of this paper.

Second, modeling results indicate that the free air gravity field in the Levant basin comprises of a long ~150 km wavelength regional component superimposed by a shorter <50 km component. The slight discrepancy between the observed and modeled gravity NW of Jonah high is due to the long wavelength component, which is mostly affected by the depth of the Moho. On the other hand, the short wavelength gravity anomaly associated with the Jonah structure is mainly caused by the relatively dense rocks on the top of the structure. Theoretically, this positive effect may be compensated by the negative effect of crustal thickening (local isostasy). However, crustal thickening larger than suggested by the model is inconsistent with the observation, because it widens the anomaly. Accordingly, we suggest that the Jonah horst is not compensated locally (see discussion).

To demonstrate the sensitivity of our modeling to the chosen density values, we note that changing the density of the rocks on top of the Jonah structure from 2.65 gr/cm^3 to 2.7 gr/cm^3, affect the modeled gravity by < 3 %; and similarly changing the density of the lower crust by ±5 gr/cm^3 causes a maximal change of ± 5 mGal.

5.6 Discussion

5.6.1 History of the Jonah horst and seamount

Differing from previous studies that speculated various possibilities for the origin of the Jonah high, we find that it is an ancient horst that produced a prominent long-lasting seamount in the deep Levant basin.

In order to determine the amount of vertical displacement and the age of faulting that produced the Jonah high (horst), a correlation of the internal reflector (denoted by the orange horizon in Figs. 5.3, 5.4, 5.6) with one of the deep reflectors within the basin (around the Jonah high) is needed. Unfortunately due to the limitation of the seismic data and lack of penetrating wells, such correlation is impossible. Yet, considering that rifting on land had ceased in the Mid-Late Jurassic and that the green horizon, approximately of the same age, is not faulted, we suggest that faulting around the Jonah horst also ceased in the Mid-Late Jurassic. In that sense the Jonah high is a time equivalent of the onshore horsts (Late Paleozoic to Early Mesozoic). However, differing from several onland Early Mesozoic horsts claimed to have been reactivated by Syrian Arc folding in Cretaceous and Tertiary times (Bruner, 1991; Eyal, 1996; Walley, 1998; Guiraud, 1998; Gardosh et al., 2008), no signs for post Jurassic tectonism is observed in the Jonah structure .

The paleo-height of the Jonah seamount relative to its surrounding seafloor is also difficult to reconstruct. Assuming that the lowermost horizon in the velocity model of figure 5.3C approximately represents the top of the crystalline basement (~15 km in the basin), correlation of this horizon with the orange horizon within the Jonah structure (at a depth of ~10 km) reveals a vertical offset along the southern fault (at line EMED-39) of nearly 5 km (Fig. 5.3B). However, this does not necessarily mean

that the Jonah seamount was 5 km above its surrounding seafloor, because sedimentation in the deep basin and erosion of the seamount frequently decrease bathymetric differences. On the other hand, since carbonate buildup may sometimes increase the height of a seamount, the vertical differences between its top (blue horizon) and surrounding reflectors is also not useful for paleo-height reconstruction. Nevertheless, assuming that the orange reflector predates rifting, the 1-1.5 km vertical difference between the green and orange reflectors (Figs. 5.3, 5.4) sets a minimal constraint on the height of the seamount in the Late Jurassic. The ~ 5 km sediments comprising the upper part of Jonah (Fig. 5.4B, 5.7C) can be either compacted pre-rift sediments or hard carbonates that build up following its uplift. It also might be a combination of both: pre-rift sediments overlained by carbonate buildup as expressed by the observed spars reflectors in figures 5.3B and 5.4. We cannot differ from carbonate build up which might have underwent diagenetic processes such as dolomitzation and hence increasing their density to ~2.67 gr/cm3, or to compacted pre-rift sediments having similar density. This high density and correspondingly high velocity (~5000 m/s, Fig. 5.3C) in the upper part of Jonah high rules out the possibility of shally sediments (Rybakov et al., 2011) or even mud diapirs (Ben-Gai and Druckman 2013). In both case, the implication of these observations and assumptions is that the top most part of Jonah high was probably at shallow water depth and might even be intermittently exposed. Removal of pre-rift sediments on top of Jonah horst might have occurred via erosional processes either due to exposure or to submarine shallow erosion.

The ~ 5 km sediments comprising the upper part of Jonah (Figs. 5.3B, 5.7C) between the orange and blue reflectors can be pre-rift sediments, hard carbonates that build up during or after rifting, or a combination of both possibilities. Typical slope

angles of carbonate reefs are in the range of 10^0 to 30^0 with maximum angle slope reaching 45^0 (Roehl and Choquette, 2012) which are in accordance to the observed slopes at the upper part of the Jonah high, though at places the original slopes of a presumed carbonate reef build up might be altered due to erosion and walls retreat. These different scenarios cannot be resolved from the seismic data, but relatively high (2.65 gr/cm^3) density that is required to explain the observed gravity anomaly supports dolomitic nature and thus hints for shallow waters. If this is correct, the top of the Jonah structure may have been occasionally exposed and truncated.

Altogether, we estimate that in the Late Jurassic, a few tens of millions of years after the end of rifting, the height of the Jonah seamount relative to its surrounding seafloor was at least 1-1.5 km. It remained quite high much longer in spite of sedimentation around it, because its top kept growing upwards by a carbonate buildup. Otherwise, it is quite difficult to explain why it wasn't buried until the Miocene .

Interestingly, coeval with its upward growth, the Jonah seamount was continuously eroded and its walls retreated tens of kilometers laterally (Fig. 4.2). This lateral retreat is consistent with the curved winding shape of its boundaries that indicates submarine incisions of its walls similar to the present shape of the Eratosthenes seamount (Fig. 5.1) and also to its ancient buried walls (Klimke and Ehrhardt, 2014).

5.6.2 The discrepancies of a magmatic model

We have shown that the magnetic anomaly associated with the Jonah high can be explained by a basement high, if the crystalline crust in the Levant basin is characterized by considerably high magnetic susceptibility that usually characterizes basic rocks. This conclusion, however, should be carefully examined, because of its broad petrologic and tectonic implications. An alternative magnetic model might include high susceptibility magmatic intrusion within a low susceptibility crust. However, since such intrusion is not detected in the seismic material, a deep body within the crust should be considered and a deeper magnetic source may not explain the observed magnetic anomaly .

Another difficulty with the intrusion model is that most Early Mesozoic magmatic bodies detected onshore are concentrated in structural lows, not in horsts. For instance, the Asher Volcanics (Steinitz et al., 1983; Garfunkel, 1989; Korngreen and Benjamini, 2001) are found in the Asher basin (northern Israel) and not in the Maanit, Gaash-Meged and Gevim highs (Gardosh and Druckman, 2006). The reason for concentrating volcanic flows in topographic depressions is obvious, but the coincidence of basaltic flows with horsts is much less favorable.

5.6.3 Early Mesozoic extension

The formation of the Levant basin in the Late Paleozoic and Early Mesozoic with its thinned ~20 km crust (Makris et al., 1983; Ben-Avraham et al., 2002) involved separation of small splinters such as the Eratosthenes block (Garfunkel, 2004) having a ~27 km crustal root (Welford et al., 2015). Similarly, the Jonah horst is interpreted as additional fragment of the stretched Levant continental crust (Fig. 5.7C). However, differing from the Eratosthenes comprising a thicker middle crust and thinner lower

crust to its northeast (Welford et al., 2015), the Jonah block consist of a one layered lower continental crust and is lacking a significant crustal root as indicated by gravity modeling (see above). This apparently suggests regional isostatic compensation typical to a relatively rigid crust, consistent with slight tilting and flexing of the sub-basins in both side of the Jonah structure (Fig. 5.7C). Both Jonah high and the Eratosthenes exhibit a strong magnetic anomaly, while the Eratosthenes is interpreted as comprising localized magmatic intrusion (Welford et al., 2015), the Jonah high is interpreted as a basement high lacking any magmatic intrusion.

A fundamental implication of the horst and graben structure in the midst of the deep Levant basin is that the lithosphere was not ruptured during the Early Mesozoic rifting and no oceanic crust was produced. Generally oceanic crust is formed in the post rift phase, hence we would expect the formation of horst and graben to predate it. This observation is consistent with the general opinion that the crust under the Levant basin is a thinned continental crust (Woodside, 1977; Hirsch et al., 1995; Netzeband et al., 2006; Gardosh et al, 2010). Though Netzeband et al. (2006) proposed a two layer thinned continental crust based on two refraction lines acquired in the northern and southern Levant basin, our study suggests that the Levant basin comprises one layer thinned lower continental crust similarly to previous study by Garfunkel (1998). Nevertheless, a first order estimation of the stretching factor can be obtained by calculating the crustal thinning ratio relative to the ~35 km thick crust in southern Jordan (Ginzburg and Gvirtzman, 1979; Ginzburg and Folkman, 1980; Makris et al., 1983; Garfunkel 1998). Accordingly, ~20 km crystalline crust near the coastline, 10 km in the deep Levant basin and 15 km in the Jonah horst implies a stretching factor β of 1.75, 3.5 and 2.3, respectively. Noteworthy, thermal equilibrium of the Levant

margin was nearly achieved in the Santonian, ~100 m.y. following the Early Mesozoic rifting event in the area (Bar, 2009).

6. Conclusions

1. Syrian Arc folds extend westward offshore Israel by more than 200 km.

2. Folding started in the Santonian and continued for more than 80 m.y. till the Early Pliocene.

3. Strain orientation in the Levant basin remained relatively constant over more than 80 m.y. although its intensity was attenuated since the Late Miocene.

4. During the Oligocene the CMFZ acted as a large scale shock absorber accommodating horizontal shortening within it and along the continental margin block, while forming a strain shadow west of it.

5. Pliocene folding preserve a NNE-SSW orientation, similar to older Santonian folding, although new plate boundaries evolved along the DST and the Cyprus subduction zone (located 60-100 km east and north of the Levant basin respectively). Thus suggesting that deformation in the Levant basin was affected by the interplay of far field stresses resulting from plate motion and pre-existing (Late Paleozoic – Early Mesozoic) continental weakness lineaments.

6. Africa's northeastern margins that were shaped during the Tethyan rifting dictated the boundary condition during Tethyan closure. In the area studied here, this boundary condition dictated the direction of folding for over >80 m.y.

7. The Jonah structure is an Early Mesozoic horst. It was a prominent seamount, which lasted > 120 m.y until the Early Miocene, and was never reactivated tectonically. In that sense it is a small continental fragment, similar to the adjacent Eratosthenes block, in the midst of a thinned continental crust.

References

Adams, C.G., Gentry, A.W. and Whybrow, P.J., 1983. Dating the terminal Tethyan event. In: J.E. Meulenkamp (Editor), Reconstruction of marine paleoenvironments. Utrecht Micropaleontological Bulletins, Utrecht, pp. 273-298.

Allen, P.A. and Allen, J.R., 2013. Basin analysis: Principles and application to petroleum play assessment. John Wiley & Sons, 632 pp.

Amante, C. and Eakins, B.W., 2009. ETOPO1 1 Arc-Minute Global Relief Model: Procedures, Data Sources and Analysis NOAA Technical Memorandum NESDIS NGDC-24, pp. 19

Bar, O., 2009. The shaping of the continental margin of central Israel since the Late Eocene – Tectonics, Morphology and Stratigraphy. PhD Thesis, Ben Gurion University, Be'er Sheva, 207 pp.

Bar, O., Gvirtzman, Z., Feinstein, S. and Zilberman, E., 2013. Accelerated subsidence and sedimentation in the Levant Basin during the Late Tertiary and concurrent uplift of the Arabian platform: Tectonic versus counteracting sedimentary loading effects. Tectonics, 32(3): 334-350.

Bartov, Y., Lewy, Z., Steinitz, G. and Zak, I., 1980. Mesozoic and Tertiary stratigraphy, paleogeography and structural history of the Gebel Areif en Naqa area, eastern Sinai. Israel Journal of Earth Sciences, 29: 114-139.

Becker, A., 1994. Bedding-plane slip over a pre-existing fault, an example: the Ramon Fault, Israel. Tectonophysics, 230(1): 91-104.

Bein, A. and Gvirtzman, G., 1977. A Mesozoic fossil edge of the Arabian Plate along the Levant coastline and its bearing on the evolution of the Eastern Mediterranean. In: B. Biju-Duval and L. Montadert (Editors), International Symposium on the structural history of the Mediterranean Basin. Editions Technipin, Split (Yugoslavia), pp. 95-110.

Ben-Avraham, Z., 1978. The structure and tectonic setting of the Levant continental margin, Eastern Mediterranean. Tectonophysics 46, (3): 313–331.

Ben-Avraham, Z., Ginzburg, A., Makris, J. and Eppelbaum, L., 2002. Crustal structure of the Levant Basin, eastern Mediterranean. Tectonophysics, 346(1): 23-43.

Ben-Gai, Y., Druckman, Y., 2013. Mega-Scale Swells and Diapirs in the Deep Levant Basin, Eastern Mediterranean, and their Association with Recent World-Class Gas Discoveries. AAPG Search and Discovery Article #90161©2013 AAPG European Regional Conference, Barcelona, Spain, 8-10 April 2013.

Bonen, D., 1980. The Mesozoic basalts of Israel. PhD Thesis, Hebrew University, Jerusalem.

Bosworth, W., Guiraud, R. and Kessler, L.G., 1999. Late Cretaceous (ca. 84 Ma) compressive deformation of the stable platform of northeast Africa (Egypt): Far-field stress effects of the "Santonian event" and origin of the Syrian arc deformation belt. Geology, 27(7): 633-636.

Bosworth, W., El-Hawat, A.S., Helgeson, D.E. and Burke, K., 2008. Cyrenaican "shock absorber" and associated inversion strain shadow in the collision zone of northeast Africa. Geology, 36(9): 695-698.

Brew, G., Best, J., Barazangi, M. and Sawaf, T., 2003. Tectonic evolution of the NE Palmyride mountain belt, Syria: the Bishri crustal block. Journal of the Geological Society of London, 160(5): 677-685.

Bruner, I., 1991. Investigation of the subsurface in the northern Negev, Israel, using seismic reflection techniques, Tel Aviv University, Tel Aviv, 105 pp.

Buchbinder, B., 1996. Miocene carbonates of the eastern Mediterranean, the Red Sea and the Mesopotamian basin: Geodynamic and eustatic controls. Concepts in Sedimentology and Paleontology, Vol. 5; Models for carbonate stratigraphy from Miocene reef complexes of Mediterranean regions, 89-96 pp.

Buchbinder, B. and Zilberman, E., 1997. Sequence stratigraphy of Miocene-Pliocene carbonate-siliciclastic shelf deposits in the eastern Mediterranean margin (Israel): effects of eustasy and tectonics. Sedimentary Geology, 112: 7-32.

Cartwright, J.A. and Jackson, M.P.A., 2008. Initiation of gravitational collapse of an evaporite basin margin: The Messinian saline giant, Levant Basin, eastern Mediterranean. Geological Society of America Bulletin, 120(3-4): 399-413.

Chaimov, T.A., Barazangi, M., Alsaad, D., Sawaf, T. and Gebran, A., 1992. Mesozoic and Cenozoic Deformation Inferred from Seismic Stratigraphy in the Southwestern Intracontinental Palmyride Fold-Thrust Belt, Syria. Geological Society of America Bulletin, 104(6): 704-715.

Cohen, Z., Kaptsan, V. and Flexer, A., 1990. The Tectonic Mosaic of the Southern Levant - Implications for Hydrocarbon Prospects. Journal of Petroleum Geology, 13(4): 437-462.

De Sitter, L.U., 1962. Structural development of the Arabian Shield in Palestine. Geol. Mijnbouw, 41(3): 116-124.

Dercourt, J. et al., 1986. Geological Evolution of the Tethys Belt from the Atlantic to the Pamirs since the Lias. Tectonophysics, 123(1-4): 241-315.

Derin, B. and Gerry, E., 1979. Devora 2A, Stratigraphic Log, Isr. Inst. Petrol. Energy.

Derin, B., Lipson, S. and Gerry, E., 1982. Asher Atlit 1, Stratigraphic Log, Isr. Inst. Petrol. Energy.

Dobrin, M.B. and Savit, C.H., 1960. Introduction to geophysical prospecting, 4. McGraw-hill New York.

Druckman, Y., Giller, D., Fleischer, L., Gelberman, E. and Wolf, O., 1995. Subsurface geology and structural evolution of the northwestern Negev, southern Israel. Israel Journal of Earth Sciences, 44: 115-135.

Dvorkin, A. and Kohn, B.P., 1989. The Asher Volcanics, northern Israel: petrography, mineralogy, and alteration. Israel Journal of Earth Sciences, 38(2-4): 105-123.

Ebinger, C.J. and Sleep, N.H., 1998. Cenozoic magmatism throughout east Africa resulting from impact of a single plume. Nature, 395(6704): 788-791.

El Hawat, A.S. and Abdulsamad, E.O., 2004. The geology of Cyrenaica: a field seminar, Sedimentary Basins of Libya Symposium, 3rd, Geology of East Libya, Binghazi, pp. 501-520.

El-Motaal, E.A. and Kusky, T.M., 2003. Tectonic evolution of the intraplate s-shaped Syrian Arc fold-thrust belt of the Middle East region in the context of plate tectonics, The 3rd International Conference on the Geology of Africa, pp. 139-157.

Eyal, Y., 1996. Stress field fluctuations along the Dead Sea Rift since the middle Miocene. Tectonics, 15(1): 157-170.

Eyal, Y. and Reches, Z.E., 1983. Tectonic analysis of the Dead Sea Rift region since the Late-Cretaceous based on mesostructures. Tectonics, 2(2): 167-185.

Fleischer, L. and Varshavsky, A., 2002. A lithostratigraphic data base of oil and gas wells drilled in Israel. OG/9/02, The Ministry of National Infrastructures, Earth Sciences Research Administration, Oil and Gas Unit, Jerusalem.

Fleischer, L., Gafsou, R., 2003. Structural map on top Judea Group. Geophys. Inst. Isr. Map 753/312/2003.

Flexer, A., Freund, R., Reiss, Z. and Buchbinder, B., 1970. Santonian paleostructure of the Galilee. Israel Journal of Earth Sciences, 19: 141-146.

Folkman, Y. and Yuval, Z., 1976. Aeromagnetic map of Israel. Institute for Petroleum Research and Geophysics, Holon.

Folkman, Y. and Ben-Gai, Y., 2004. The "Jonah" buried seamount; intrusive structure in the southeastern Levant Basin offshore Israel, Annual Meeting of Israel Geological Society, Israel.

Freund, R., Garfunkel, Z., Zak, I., Goldberg, M., Weissbrod, T., Derin, B., Bender, F., Wellings, F.E., Girdler, R.W., 1970. The Shear along the Dead Sea Rift [and Discussion]. Philos. Trans. R. Soc. A Math. Phys. Eng. Sci. 267, 107–130. doi:10.1098/rsta.1970.0027.

Freund, R., Goldberg, M., Weissbrod, T., Druckman, Y. and Derin, B., 1975. The Triassic-Jurassic structure of Israel and its relation to the origin of the Eastern Mediterranean. Geological Survey of Israel Bulletin, 65.

Frizon de Lamotte, D., Raulin, C., Mouchot, N., Wrobel-Daveau, J.C., Blanpied, C. and Ringenbach, J.C., 2011. The southernmost margin of the Tethys realm during the Mesozoic and Cenozoic: Initial geometry and timing of the inversion processes. Tectonics, 30(3).

Gardner, G.H.F. and Society of Exploration, G., 1985. Migration of seismic data. Society of Exploration Geophysicists.

Gardosh, M. and Druckman, Y., 2006. Stratigraphy and tectonic evolution of the Levantine Basin, offshore Israel. In: A.H.F. Robertson and D. Mountrakis (Editors), Tectonic development of the eastern Mediterranean. GSL Special Publications. The Geological Society of London, London, pp. 201-227.

Gardosh, M., Druckman, Y., Buchbinder, B. and Rybakov, M., 2008. The Levant Basin offshore Israel: stratigraphy, structure, tectonic evolution and implications for hydrocarbon exploration - revised edition. Report GSI/4/2008, Geological Survey of Israel.

Gardosh, M.A., Garfunkel, Z., Druckman, Y. and Buchbinder, B., 2010. Tethyan rifting in the Levant Region and its role in Early Mesozoic crustal evolution. In: C. Homberg and M. Bachmann (Editors). Evolution of the Levant Margin and Western Arabia Platform since the Mesozoic. The Geological Society of London, Special Publications, pp. 9-36.

Garfunkel, Z., 1981. Internal structure of the Dead Sea leaky transform (rift) in relation to plate kinematics. Tectonophysics, 80(1-4): 81-108.

Garfunkel, Z., 1989. Tectonic setting of Phanerozoic magmatism in Israel. Israel Journal of Earth Sciences, 38: 51-74.

Garfunkel, Z., 1998. Constraints on the origin and history of the eastern Mediterranean basin. Tectonophysics, 298: 5-35.

Garfunkel, Z., 2004. Origin of the Eastern Mediterranean basin: a reevaluation. Tectonophysics, 391(1): 11-34.

Garfunkel, Z. and Derin, B., 1984. Permian-early Mesozoic tectonism and continental margin formation in Israel and its implications for the history of the Eastern Mediterranean. Geological Society of London, 17(1): 187-201.

Ginzburg, A. and Gvirtzman, G., 1979. Changes in the crust and in the sedimentary cover across the transition from the Arabian platform to the Mediterranean Basin: evidence from seismic refraction and sedimentary studies in Israel and Sinai. Sedimentary Geology, 23: 19-36.

Ginzburg, A. and Folkman, Y., 1980. The crustal structure between the Dead Sea rift and the Mediterranean Sea. Earth and Planetary Sciences Letters, 51(1): 181-188.

Ginzburg, A. and Ben-Avraham, Z., 1987. The deep structure of the central and southern Levant continental margin, Annales Tectonicae, pp. 105-115.

Ginzburg, A., Benavraham, Z., Makris, J., Hubral, P. and Rotstein, Y., 1994. Crustal Structure of Northern Israel. Marine and Petroleum Geology, 11(4): 501-506.

Griscom, A. and Jachens, R.C., 1989. Tectonic history of the north portion of the San Andreas Fault system, California, inferred from gravity and magnetic anomalies. Journal of Geophysical Research: Solid Earth, 94(B3): 3089-3099.

Guiraud, R., 1998. Mesozoic rifting and basin inversion along the northern African Tethyan margin: an overview. Petroleum Geology of North Africa, 132: 217-229.

Guiraud, R. and Bosworth, W., 1997. Senonian basin inversion and rejuvenation of rifting in Africa and Arabia: synthesis and implications to plate-scale tectonics. Tectonophysics, 282(1): 39-82.

Gvirtzman, G., 1970. The Saqiye Group (Late Eocene to Early Pleistocene) in the Coastal Plain and the Hashefela regions, Geological Survey of Israel Report D/5/67. PhD (Hebrew abstract) Thesis, Geology department, Hebrew University, Jerusalem, 170 pp.

Gvirtzman, G. and Buchbinder, B., 1978. The Late Tertiary of the Coastal Plain and continental shelf of Israel and its bearing of the history of the Eastern Mediterranean. In: D.H. Ross and Y.P. Neprochnov (Editors), Initial Reports of the Deep Sea Drilling Project. US Government Printing Office, Washington, pp. 1195-1222.

Gvirtzman, G. and Steinitz, G., 1983. The Asher volcanics - an early Jurassic event in northern Israel. Israel Geological Survey Current Research, 1982: 28-33.

Gvirtzman, Z., 2004. Chronostratigraphic table and subsidence curves of southern Israel. Israel Journal of Earth Sciences, 53(1), 48-61.

Gvirtzman, Z. and Garfunkel, Z., 1998. The transformation of southern Israel from a swell to a basin: stratigraphic and geodynamic implications for intracontinental tectonics. Earth and Planetary Science Letters, 163: 275-290.

Gvirtzman, Z. and Steinberg, J., 2012. Inland jump of the Arabian northwest plate boundary from the Levant continental margin to the Dead Sea Transform. Tectonics, 31 TC4003.

Gvirtzman, Z., Zilberman, E. and Folkman, Y., 2008. The Jaffa Basin offshore central Israel Reactivation of the Levant passive margin during the late Tertiary and formation of. Journal of the Geological Society, 165: 563-578.

Gvirtzman, Z., J. Steinberg, O. Bar, B. Buchbinder, E. Zilberman, R. Siman-Tov, R. Calvo, L. Grossowicz, A. Almogi-Labin, and M. Rosensaft, 2011. Retreating Late Tertiary shorelines in Israel: Implications for the exposure of north Arabia and Levant during Neotethys closure. Lithosphere 3, (2): 95-109.

Gvirtzman, Z., Csato, I. and Granjeon, D., 2014. Constraining sediment transport to deep marine basins through submarine channels: The Levant margin in the Late Cenozoic. Marine Geology, 347(0): 12-26.

Hall, J.K., 1993. The GSI digital terrain model (DTM) project completed. Current Research - Geological Survey of Israel, 8: 47-50.

Hardy, C., Homberg, C., Eyal, Y., Barrier, E. and Mueller, C., 2010. Tectonic evolution of the southern Levant margin since Mesozoic. Tectonophysics, 494(3-4): 211-225.

Hawie, N., Gorini, C., Deschamps, R., Nader, F.H., Montadert, L., Granjeon, D. and Baudin, F., 2013. Tectono-stratigraphic evolution of the northern Levant Basin (offshore Lebanon). Marine and Petroleum Geology, 48, pp.392-410

Hensen, F.R.S., 1951. Observations on the geology of the petroleum occurences of the Middle East 3rd World Petroleum Congress, pp. 118-140.

Hirsch, F., Flexer, A., Rosenfeld, A. and Yellindror, A., 1995. Palinspastic and Crustal Setting of the Eastern Mediterranean. Journal of Petroleum Geology, 18(2): 149-170.

Honigstein, A., Flexer, A. and Rosenfeld, A., 1988. Tectonic activity in the Syrian Arc in Israel, as indicated by Senonian ostracodes. Neues Jahrbuch für Geologie und Palaeontologie, Monatshefte 3 (1988): 173-183.

Hsu, K.J., Cita, M.B. and Ryan, W.B.F. (Editors), 1973. The origin of the Mediterranean evaporites. DSDP Initial Report 13. US Gov. Printing office, Washington DC, 1203-1232 pp.

Klimke, J. and Ehrhardt, A., 2014. Impact and implications of the Afro-Eurasian collision south of Cyprus from reflection seismic data. Tectonophysics, 626: 105-119.

Korngreen, D. and Benjamini, C., 2001. Upper Triassic reef facies in the Asher-Atlit-1 borehole, northern Israel: Microfacies, cement stratigraphy and paleogeographic implications. Facies, 45: 1-23.

Kosloff, D., Sherwood, J., Koren, Z., Machet, E. and Falkovitz, Y., 1996. Velocity and interface depth determination by tomography of depth migrated gathers. Society of Exploration Geophysicists, 61(5): 1511-1523.

Krenkel, E., 1924. Der Syrische Bogen. Zentralbl. Mineral, 9: 274-281.

Krienitz, M. S., Haase, K. M., Mezger, K., van den Bogaard, P., Thiemann, V., and Shaikh-Mashail, M. A., 2009. Tectonic events, continental intraplate volcanism, and mantle

plume activity in northern Arabia: Constraints from geochemistry and Ar-Ar dating of Syrian lavas. Geochemistry, Geophysics, Geosystems, *10*(4).

Landa, E., Kosloff, D., Keydar, S., Koren, Z. and Reshef, M., 1988. Method for Determination of Velocity and Depth from Seismic Reflection DATA1. 36(3): 223-243.

Landa, E., Thore, P., Sorin, V. and Koren, Z., 1991. Interpretation of velocity estimates from coherency inversion. Society of Exploration Geophysicists, 56(9): 1377-1383.

Lowrie, W., 2007. Fundamentals of geophysics. Cambridge University Press.

Macgregor, D., 2011. Rift shoulder source to prodelta sink: The Cenozoic development of the Nile drainage system, AAPG International Conference and Exhibition, Milano, Italy, Italy.

Makris, J., Abraham, Z.B., Behle, A., Ginzburg, A., Giese, P., Steinmetz, L., Whitmarsh, R.B. and Eleftheriou, S., 1983. Seismic refraction profiles between Cyprus and Israel and their interpretation. Geophysical Journal International, 75(3), pp.575-591.

Marig, Y., 2015. A new look at the tectonic evolution of the Palmahim disturbance. Msc Thesis, Ben Gurion University of the Negev, Be'er Sheva, 115 pp.

Mart, Y., 1994. Ptolemais basin: The tectonic origin of a Senonian marine basin underneath the southeastern Mediterranean Sea. Tectonophysics, 234(1): 5-17.

Mart, Y. and Ben-Gai, Y., 1982. Some depositional patterns at continental margin of southeaster Mediterranean Sea. American Association of Petroleum Geologists Bulletin, 66(4): 460-470.

McMechan, G.A., 1989. A review of seismic acoustic imaging by reverse ÂÐtime migration. International Journal of Imaging Systems and Technology, 1(1): 18-21.

Mimran, Y., 1984. Unconformities on the eastern flank of the Fari'a anticline, and their implications on the structural evolution of Samaria (central Israel). Israel Journal of Earth Sciences, 33(1-2): 1-11.

Moustafa, A.R., 2010. Structural setting and tectonic evolution of North Sinai folds, Egypt. In: C. Homberg and M. Bachmann (Editors), Evolution of the Levant Margin and Western Arabia Platform since the Mesozoic. Geological Society of London, London, pp. 37-63.

Moustafa, A.R., 2013. Fold-related faults in the Syrian Arc belt of northern Egypt. Marine and Petroleum Geology, 48: 441-454.

Moustafa, A.R. and Khalil, M.H., 1990. Structural characteristics and tectonic evolution of north Sinai fold belts. In: R. Said, ed. (Editor), The Geology of Egypt. Balkema Publishers Rotterdam, Netherlands, pp. 381-389.

Netzeband, G. L., Gohl, K., Hübscher, C. P., Ben-Avraham, Z., Dehghani, G. A., Gajewski, D., and Liersch, P., 2006. The Levantine Basin—crustal structure and origin. Tectonophysics, 418(3), 167-188.

Papanikolaou, D., Barghathi, H., Dabovski, C., Dimitriu, R., El-Hawat, A., Ioane, D., Kranis, H., Obeidi, A., Oaie, C., Seghedi, A. and Zagorchev, I., 2004. TRANSMED Transect VII: East European Craton–Scythian Platform–Dobrogea–Balkanides–Rhodope Massif–Hellenides–East Mediterranean–Cyrenaica. W. Cavazza, FM Roure, W. Spakman, GM Stampfli and PAZ (eds)(Editors), The TRANSMED Atlas-The Mediterranean region from crust to Mantle. Berlin, Springer-Verlag, pp. 173.

Picard, L., 1959. 16. Geology and Oil Exploration of Israel, 5th World Petroleum Congress. World Petroleum Congress.

Quennell, A.M., 1958. The Structural and Geomorphic Evolution of the Dead Sea Rift. Quarterly Journal of the Geological Society114.1-4 (1958): 1-24.

Reches, Z.e., Hoexter, D.F. and Hirsch, F., 1981. THE STRUCTURE OF A MONOCLINE IN THE SYRIAN ARC SYSTEM, MIDDLE EAST ÂĐSURFACE AND SUBSURFACE ANALYSIS. Journal of Petroleum Geology, 3(4): 413-426.

Reshef, M., 1991. Depth migration from irregular surfaces with depth extrapolation methods. Geophysics, 56(1): 119-122.

Reshef, M. and Kosloff, D., 1986. Migration of common-shot gathers. Society of Exploration Geophysicists, pp. 324-331.

Ricou, L.E., 1994. Tethys Reconstructed - Plates, Continental Fragments and Their Boundaries since 260-Ma from Central-America to South-Eastern Asia. Geodinamica Acta, 7(4): 169-218.

Robertson, A.H.F., 1998a. Mesozoic-Tertiary tectonic evolution of the easternmost Mediterranean area: Integration of marine and land evidence. In: A.H.F. Robertson, K. Emeis, C. Richter and A. Camerlenghi (Editors), Proceedings of ODP Science Results, 160. Ocean Drilling Program, College Station, TX, pp. 723-782.

Robertson, A.H.F., 1998b. Tectonic significance of the Eratosthenes Seamount: a continental fragment in the process of collision with a subduction zone in the eastern Mediterranean (Ocean Drilling Program Leg 160). Tectonophysics, 298(1): 63-82.

Robertson, A.H.F. and Dixon, J.E., 1984. Introduction: aspects of the geological evolution of *the Eastern Mediterranean. Geological Society of London, 17(1): 1-74.*

Roehl, P.O. and Choquette, P.W., 2012. Carbonate petroleum reservoirs. Springer Science & Business Media.

Ryan, W.B.F. and Cita, M.B., 1978. Nature and distribution of Messinian erosional surfaces-Indicators of a several-kilometer-deep Mediterranean in the Miocene. Marine Geology, 27(3-4): 193-230.

Rybakov, M., Fleischer, L. and Goldshmidt, V., 1995. A new look at the Hebron magnetic anomaly. Israel Journal of Earth Sciences, 44(1): 41-49.

Rybakov, M., Goldshmidt, V. and Rotstein, Y., 1997. New regional gravity and magnetic maps of the Levant. Geophysical Research Letters, 24(1): 33-36.

Rybakov, M., Goldshmidt, V., Hall, J.K., Ben-Avraham, Z. and Lazar, M., 2011. New insights into the sources of magnetic anomalies in the Levant. Russian Geology and Geophysics, 52(4): 377-397.

Sagy, Y., Gvirtzman, Z., Reshef, M. and Makovsky, Y., 2015. The Enigma of the Jonah high in the Middle of the Levant Basin and its Significance to the History of Rifting. Tectonophysics (in press). doi:10.1016/j.tecto.2015.09.037.

Savostin, L.A., Sibuet, J.-C., Zonenshain, L.P., Le Pichon, X. and Roulet, M.-J., 1986. Kinematic evolution of the Tethys belt from the Atlantic Ocean to the Pamirs since the Triassic. 123(1): 1-35.

Scales, J.A., 1995. Theory of seismic imaging, 2. Springer-Verlag Berlin.

Schattner, U., 2010. What triggered the early-to-mid Pleistocene tectonic transition across the entire eastern Mediterranean? Earth and Planetary Sciences, 289(3): 539-548.

Schattner, U. and Ben-Avraham, Z., 2007. Transform margin of the northern Levant, eastern Mediterranean: From formation to reactivation. Tectonics, 26(5).

Schattner, U., Ben Avraham, Z., Lazar, M. and Huebscher, C., 2006. Tectonic isolation of theLevant basin off shore Galilee-Lebanon - eeffects of the Dead Sea fault plate boundary on the Levant continental margin, eastern Mediterranean. Journal of Structural Geology, 28: 2049-2066.

Segev, A., Rybakov, M., Lyakhovsky, V., Hofstetter, A., Tibor, G., Goldshmidt, V. and Avraham, Z.B., 2006. The structure, isostasy and gravity field of the Levant continental margin and the southeast Mediterranean area. Tectonophysics, 425(1), pp.137-157.

Sengor, A.M.C., 1979. The North Anatolian transform fault: its age, offset and tectonic significance. Geological Society of London, 136(3): 269-282.

Stampfli, G., Marcoux, J. and Baud, A., 1991. Tethyan Margins in Space and Time. Palaeogeography Palaeoclimatology Palaeoecology, 87(1-4): 373-409.

Stampfli, G.M., Mosar, J., Favre, P., Pillevuit, A. and Vannay, J.-C., 2001. Permo-Mesozoic evolution of the western Tethys realm; the Neo-Tethys East Mediterranean Basin

connection. In: P.A. Ziegler, W. Cavazza, A.H.F. Robertson and S. Crasquin-Soleau (Editors), Peri-Tethys memoir 6; Peri-Tethyan rift/wrench basins and passive margins. Ed. du Museum National d'Histoire Naturelle, Paris, pp. 51-108.

Steinberg, J., 2011. The rapid sedimentary filling of the Levant Basin alongside the Arabian-African breakup and the relationship to the deformation of its margin. PhD Thesis, the Hebrew University of Jerusalem, Israel, 120 pp.

Steinberg, J., Gvirtzman, Z. and Folkman, Y., 2010. New age constraints on the evolution of the Mt. Carmel structure and its implications on a Late Miocene extensional phase of the Levant continental margin. Journal of the Geological Society, 167: 203-216.

Steinberg, J., Gvirtzman, Z., Folkman, Y. and Garfunkel, Z., 2011. The origin and nature of the rapid late Tertiary filling of the Levant Basin. Geology, 39: 355-358.

Steinitz, G., Gvirtzman, G. and Lang, B., 1983. Evaluation of K-Ar ages of the Asher volcanics. Israel Geological Survey Current Research, 1982: 34-38.

Tearpock, D.J. and Bischke, R.E., 2002. Applied subsurface geological mapping with structural methods. Pearson Education.

Walley, C.D., 1998. Some outstanding issues in the geology of Lebanon and their importance in the tectonic evolution of the Levantine region. Tectonophysics, 298(1): 37-62.

Watts, A.B., 2001. Isostasy and Flexure of the Lithosphere. Cambridge University Press.

Woodside, J.M., 1977. Tectonic Elements and Deformation of Eastern Mediterranean. Transactions-American Geophysical Union, 58(6): 503-503.

Yilmaz, O., 2001. Seismic data analysis Processing, Inversion, and Interpretation of Seismic Data, 1. Society of Exploration Geophysicists Tulsa, Tulsa, 1000 pp.

Yousef, M., Moustafa, A.R. and Shann, M., 2010. Structural setting and tectonic evolution of offshore North Sinai, Egypt. Geological Society of London Special publications 341(1): 65-84.

Zhou, H.-W., 2014. Practical Seismic Data Analysis. Cambridge University Press.

Ziegler, P.A., 1990. Collision related intra-plate compression deformations in Western and Central Europe. Journal of Geodynamics, 11(4): 357-388.

Ziegler, P.A., Cloetingh, S., Guiraud, R. and Stampfli, G.M., 2001. Peri-Tethyan platforms: Constraints on dynamics of rifting and basin inversion. Memoires du Museum National d'Histoire Naturelle, 186: 9-49.

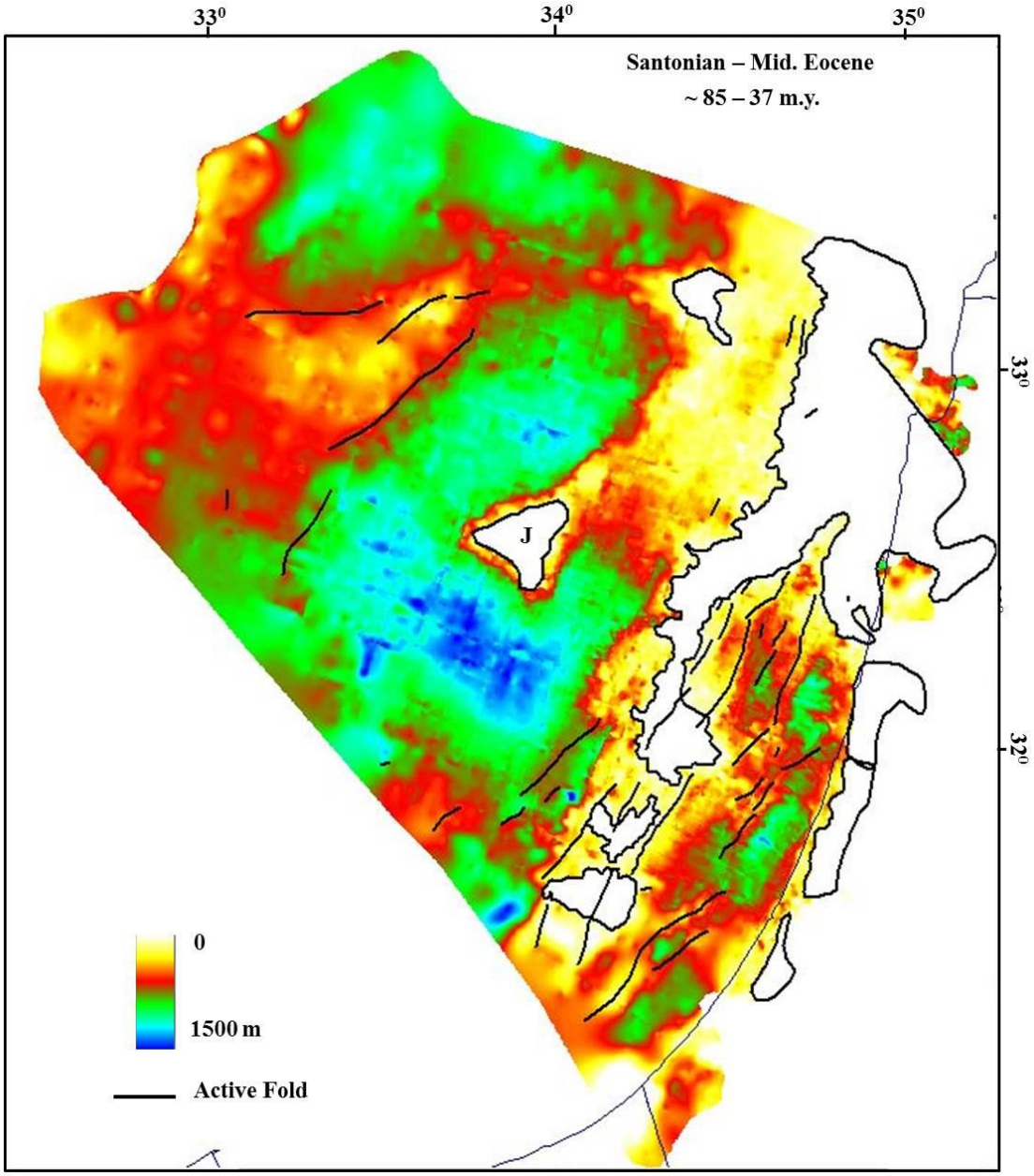

Appendix 1: Isopach of Santonian-Middle Eocene and the active folds. J – Jonah high. The lack of Santonian and Eocene section (white polygons) is interpreted as eroded in the shelf area and as non-deposition over the Jonah high.

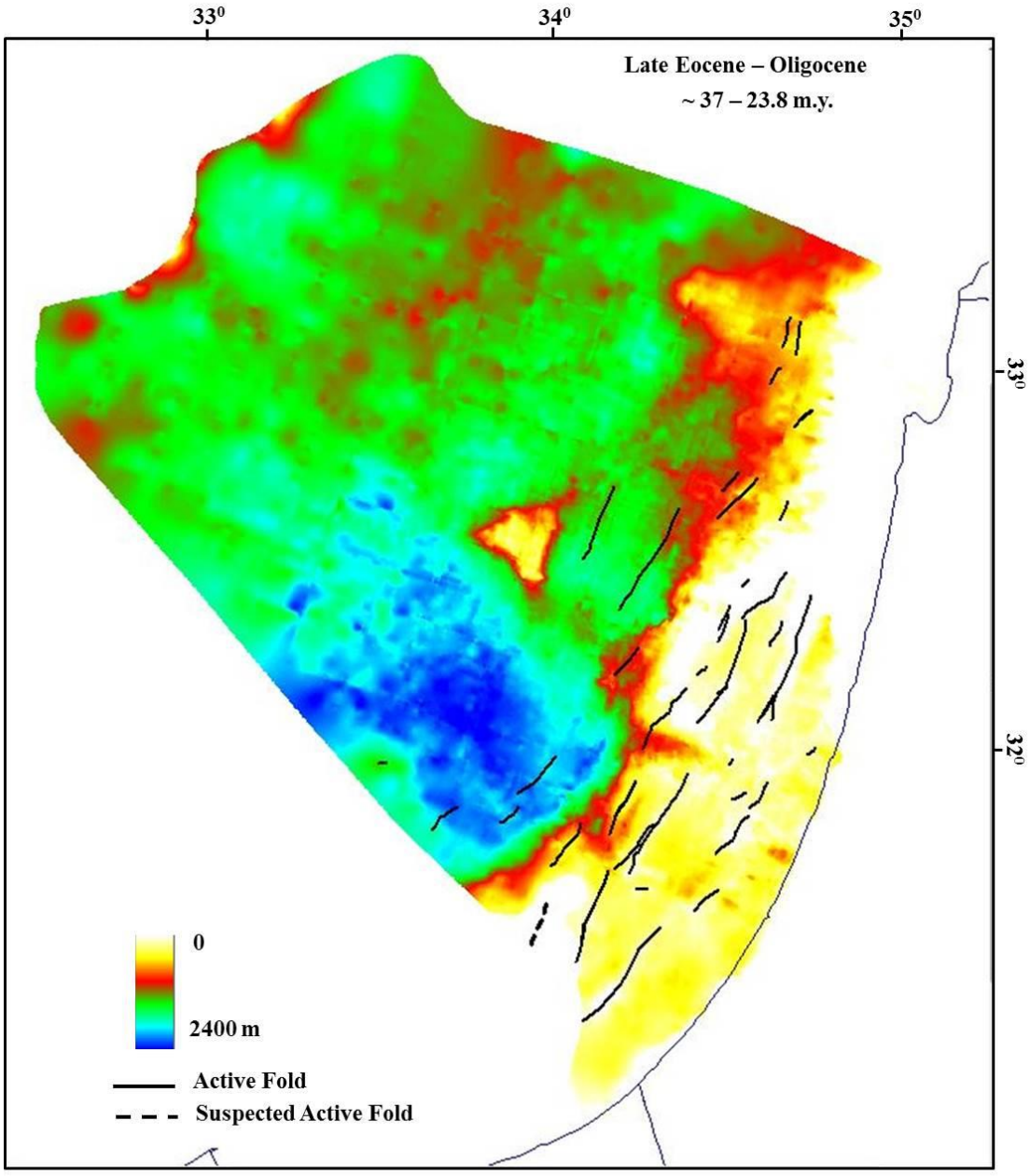

Appendix 2: Isopach of Late Eocene – Oligocene and the active folds.

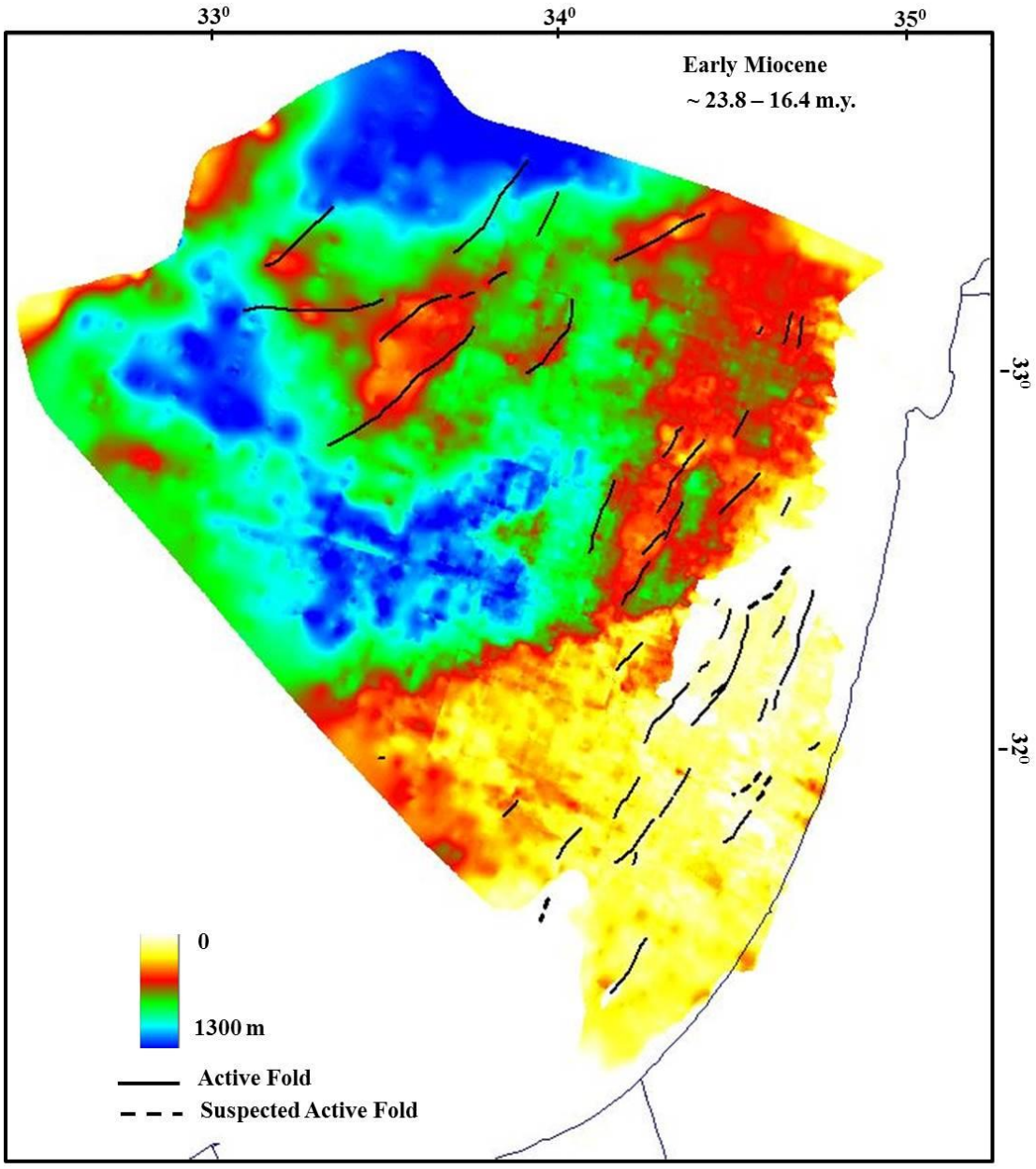

Appendix 3: Isopach of Early Miocene and the active folds.

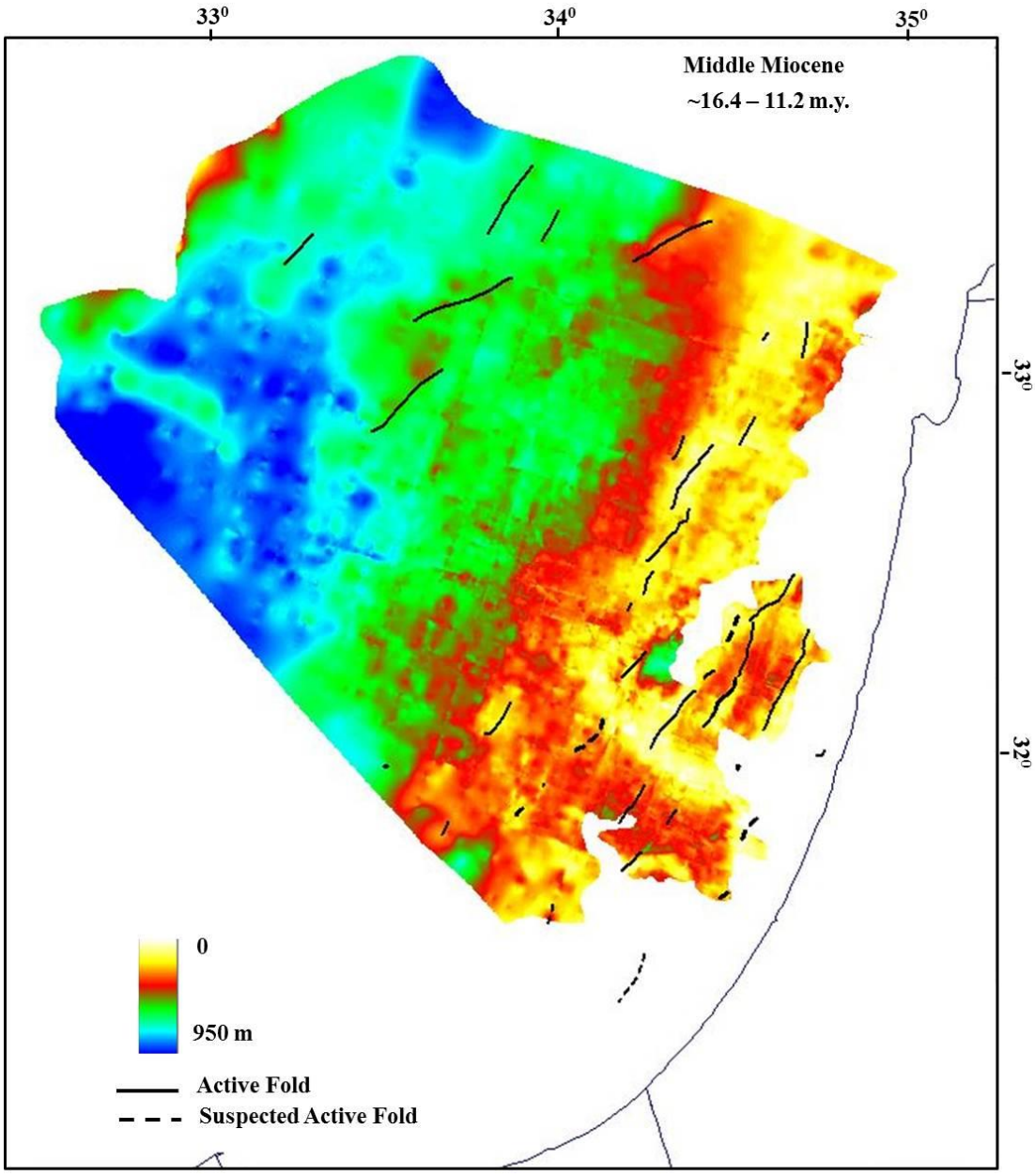

Appendix 4: Isopach of Middle Miocene and the active folds.

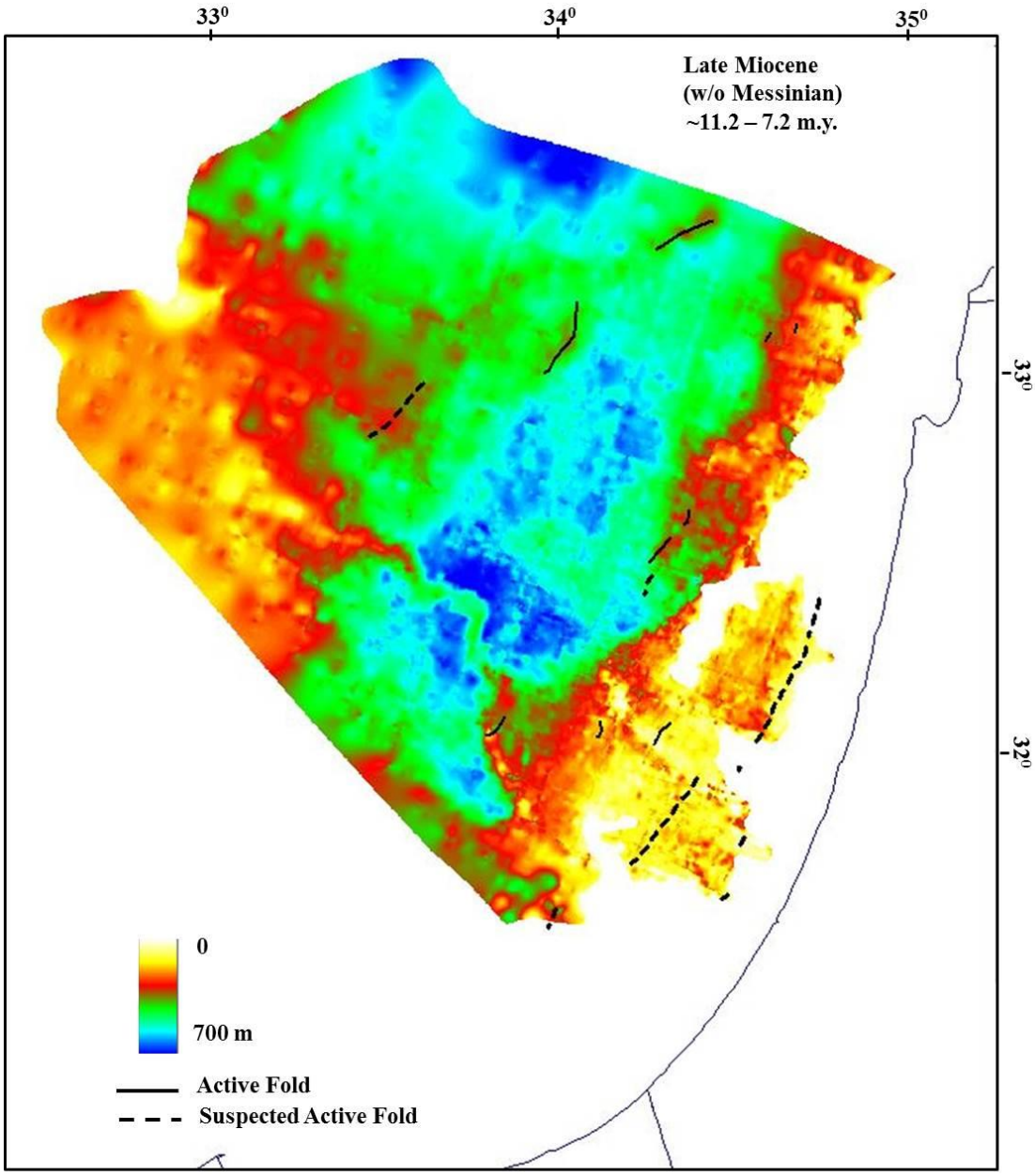

Appendix 5: Isopach of Late Miocene (not including the Messinian) and the active folds.

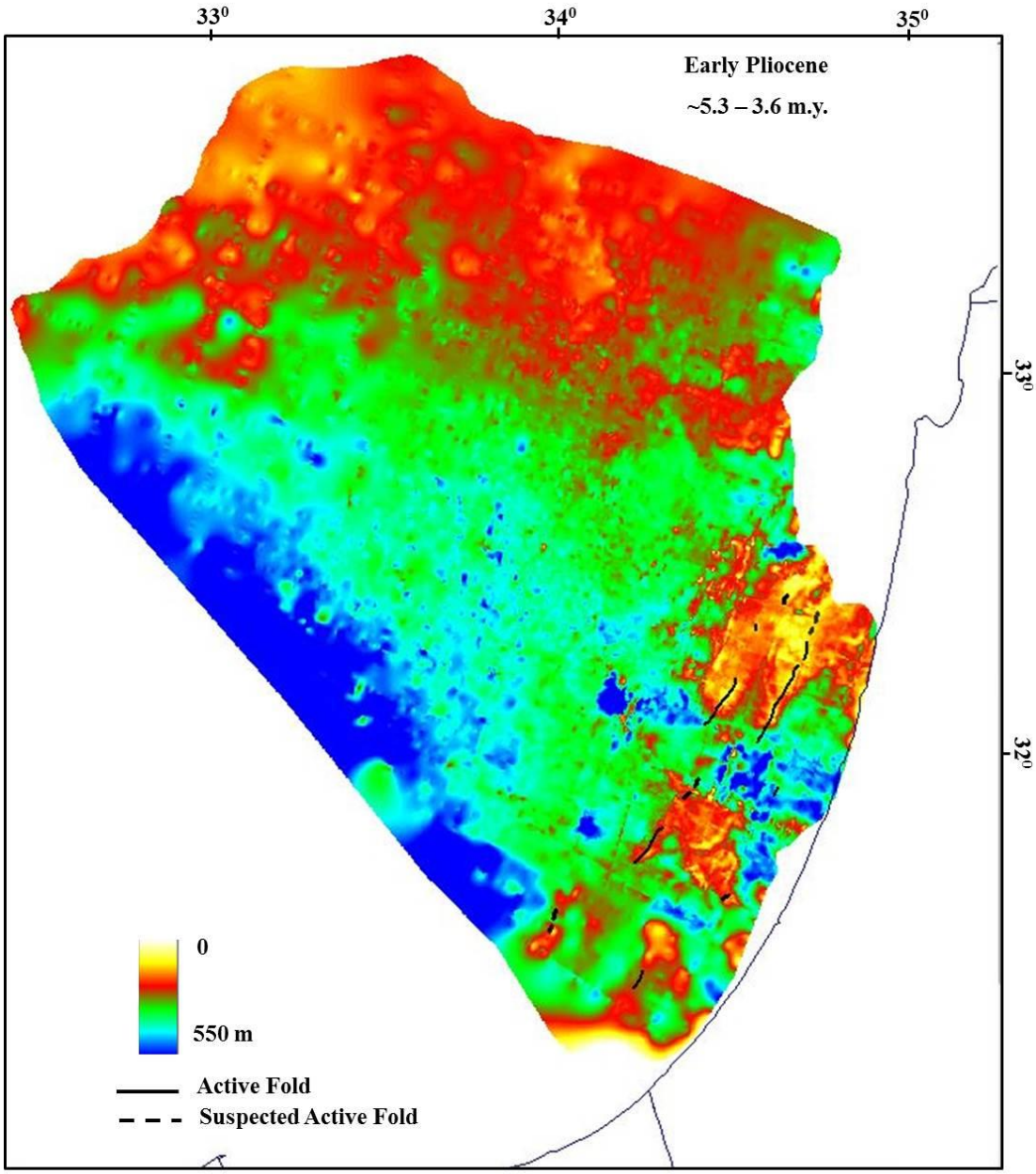

Appendix 6: Isopach of Early Pliocene and the active folds.

בנוסף למבני הקמטים הנפוצים באגן קיימים מבנים נוספים, יחודיים ושונים בצורתם ובגודלם ממבני הקמטים, בינהם מבנה לויתן ומבנה יונה המתוארים בעבודה הנוכחית. מבנה לויתן שלו צורת משולש רחב שונה במימדיו ממרבית הקמטים באגן. תוצאות העבודה תומכות במחקרים קודמים ומרמזות על כך שהוא הורסט קדום שנוצר בשלבי הביקוע שיצר את הטטיס. מונוקלינות שהתפתחו בשוליו מצביעות על כך שהוא הופעל מחדש במהלך פאזות ההתקצרות של האגן.

להבדיל ממבנה לויתן, מבנה יונה פוענח בעבודה הנוכחית כהורסט קדום שלא הופעל מחדש. זהו מבנה חריג לא רק מבחינת הגיאומטריה שלו ומימדיו, אלא גם בשל קיומה של אנומליה מגנטית משמעותית ואנומליה גרבימטרית משנית בקרבתו. תוצאות שיחזור התפתחות המבנה המוצגות בעבודה הנוכחית מצביעות על כך שמבנה יונה הנו הורסט עתיק תחום בגראבנים, שנוצר ככל הנראה במהלך הביקוע שייצר את הטטיס. אולם, בניגוד למבני מתיחה אחרים שהופעלו מחדש במהלך פאזות הקימוט של הקשת הסורית, מבנה יונה לא פעל והיווה הר-תת ימי הגבוה טופוגרפית מסביבתו במשך למעלה מ- 120 מ"ש, עד לקבורתו הסופית במהלך המיוקן התחתון. מבנה יונה, בדומה למבנה ארטוסטנס המפריד בין אגן הלבנט לאגן ההרודוטוס במערב, מייצג שארית של קרום יבשתי מדוקק במרכז אגן הלבנט.

ניתוח הפעילות הטקטונית באגן עם תצפיות משוליו החשופים מצביעים על אזור קימוט ומעוות לחיצתי ברוחב כולל של כ- 300 ק"מ, שפעל במשך למעלה מ 80 מ"ש ומשתרע מערבה מחופי ישראל. אזור רחב זה מצטרף לשורה ארוכה של אזורי לחיצה מגילים דומים הנצפים לאורך השוליים הצפוניים של הלוח האפריקאי ממרוקו ועד לסוריה. מוצע כאן שהגבול הצפון מזרחי של הלוח האפריקאי שעוצב בביקוע היווה תנאי שפה מחינת הגיאומטריה והריאולוגיה לפעילות הטקטונית שיצרה קמטים בכיוון צפון צפון-מזרח דרום דרום-מערב במשך כ- 80 מ"ש. התנועה המעגלית של לוח ערב ואפריקה צפונה לעבר אאורסיה, שהובילה לסגירת הטטיס במהלך המזוזואיקון העליון ועד הניאוגן, לוותה בעיוות הקרום הדק של צפון לוח אפריקה. הפסקת הקימוט במרכז ובמערב אגן הלבנט במהלך ההאאוקן העליון והאוליגוקן מבטאת את ספיגת המעוות לאורך רצועת השבירה שגרמה להתרוממות בלוק מדרגת הביניים בשיעור של כ- 2 ק"מ ביחס לאגן העמוק. באופן דומה, דעיכת הקימוט ברחבי האגן מאז המיוקן העליון והפסקתה בפליוקן העליון, מפוענחת כתוצאה של היווצרות גבולות לוחות חדשים – מדרום לקפריסין ולאורך בקע ים המלח, אשר ספגו את עיקר המעוות בקרבתם.

שילוב תוצאות הדימות בעומק עם פענוח רגיונלי של אופקים סייסמיים אפשר להבחין בין מבני הורסט לקמטים, ובפרט לבחון את היחסים הגיאומטריים בין המחזירים הסייסמיים למבנים השונים. הפעילות הטקטונית תועדה בעזרת אנליזת שינויי עובי של השכבות בסמוך ובתוך המבנים. הממצאים העולים מניתוח המבנים מובילים לתובנות חדשות באשר למבנה האגן ולהתפתחותו. תובנות אלו נתמכות גם בעזרת מידול נתוני הכבידה והמגנטיות.

פענוח עשרה אופקים, המוצג בעבודה הנוכחית, מתאר את התפתחות המבנים ואת הסטוריית המילוי של האגן מאז שלב הפוסט ריפט במשך 160 מ"ש. מבנה האגן כפי שמתואר במפות הסטרוקטורליות בנוי משלושה בלוקים המופרדים ב- 2 מדרגות סטרוקטורליות. בלוק מישור החוף (ממוקם מזרחית לקו החוף הנוכחי) מופרד ממדרגת הביניים בשיעור של כ- 2-1 ק"מ. בלוק מדרגת הביניים מופרד מבלוק האגן העמוק בשיעור של כ- 2 ק"מ לאורך רצועת דפורמציה ברוחב של כ- 10 ק"מ. בנוסף האגן מכיל מגוון מבנים מסדר שני המהווים את מוקד העבודה הנוכחית, הנפוצים מבין מבנים אלו הנם קמטים צרים וארוכים. תוצאות פענוח ומפוי של 72 קמטים ברחבי האגן, מצביעות על כך שמרביתם בעלי גיאומטריה אסימטרית, אורך ציריהם משתנה מ- 1 ק"מ עד 50 ק"מ וכיוונם צפון-צפון מזרח – דרום-דרום-מערב (אזימוט ממוצע של 36^0). לאורך קמטים בודדים בלבד מזוהה העתק בעומק. זיהוי פאזות פעילות לאורך הקמטים מבוצע ע"י ניתוח גיאומטריית המחזירים הסייסמיים בקרבת הקמטים תוך בחינה של שינויי עובי בשכבות המקומטות. שילוב תוצאות ניתוח זה עם סט מפות איזופך של האופקים השונים מאפשר תיעוד התפתחות הקמטים בזמן ובמרחב, על פני האגן כולו.

תוצאות הניתוח מראות שהקמטים באגן הלבנט החלו להתפתח בסנטון, בעיקר באזור מדף היבשת ובמדרון הנוכחיים, כאשר קמטים בודדים בלבד התפתחו באגן העמוק. במהלך האאוקן העליון ובאוליגוקן הקימוט באגן העמוק פסק ולעומת זאת בחלקו המזרחי של האגן - במדרגת הביניים התרחש קימוט אינטנסיבי. הקימוט באגן העמוק התחדש במהלך המיוקן התחתון ונמשך אל תוך המיוקן התיכון. מאז המיוקן העליון הקימוט ברחבי האגן דעך, ובפליוקן התחתון הוא הצטמצם לחלקו המזרחי של האגן - במדף היבשת הנוכחי. הדימיון הסטרוקטורלי והכרונולוגי בין קמטי הקשת הסורית ביבשה והמקבילה שלהם באגן העמוק, מצביע על אזור דפורמציה נרחב המשתרע למעלה מ- 200 ק"מ מערבה מחופי ישראל שהחל להתפתח בעצימות בסנטון ומתועד כאן כמתמשך במספר אפיזודות ובתתי-אזורים שונים באגן, עד הפליוקן התחתון.

תקציר

אגן הלבנט הלבנט הממוקם במזרח הים התיכון נוצר מביקוע והיפרדות הלוח האפרו-ערבי מגונדוונה שהתרחשו בסוף הפליאוזואיקון ועד המזוזואיקון התיכון. מיקומו הנוכחי של האגן בסמוך לשני גבולות לוחות - לוח אאורסיה עם לוח אפריקה בצפון ולוח ערב עם לוח אפריקה במזרח וצבירת המשקעים הרציפה לאורך יותר מ 250 מ"ש, מציבה אותו כאגן יחודי על פני כדוה"א. בעשור האחרון האגן מהווה כר נרחב לחיפושי הידרוקרבונים הן במדף היבשת והן באגן העמוק. חיפושים אלו שהובילו לתגליות מאגרי גז משמעותיות לוו בסקרים גיאופיסיים רבים ובקידוחים שחשפו מבנים גיאולוגים מטיפוסים שונים בכל חלקי האגן. העבודה הנוכחית מנצלת את מאגר המידע הגולמי הרב שנאסף ליצירת תמונה שלמה של התפתחות האגן מאז היורא העליון ועד היום. הניתוח המוצג מתמקד במקור המבנים באגן, בפריסתם המרחבית, בתקופות התפתחותם, בקשר שלהם להיסטוריה הטקטונית המקומית והאזורית ובקשר האפשרי לפעילות של מבנים אחרים בחלקו המזרחי החשוף של האגן. יתרה מכך, רציפות המשקעים באגן וזמן ההרבדה הממושך מהווים בסיס לניתוח מפורט של פעילות טקטונית, שבשילוב עם מידע מהיבשה, מאפשר קבלת תמונה שלמה בזמן ובמרחב של המערכות הטקטוניות האזוריות.

בסיס הנתונים לעבודה כלל כ- 27,000 ק"מ של קוי רפלקציה סיסמית דו-מימדים במימד הזמן, נתונים גרבימטריים ומגנטיים שנאספו לאורך יותר מ 18,000 תחנות וכן יותר מ- 30 קידוחים. בנוסף לכך, נתונים גולמיים של חמישה קווי רפלקציה סייסמית עברו עיבוד נתונים במימד העומק. התהליך כלל עיבוד pre-stack במהלכו נוקו הנתונים מרעש, החזרות משניות והגברת היחס אות לרעש. בהמשך בוצעה אנליזת מהירות מפורטת והנתונים עברו דימות (imaging) במימד העומק (Kirchhoff's pre-stack depth migration) שבמהלכו התקבלו הן חתך עומק והן מודל מהירויות אינטרוואליות. בעזרת המהירויות האינטרוואליות, שחושבו לאורך הקווים הסייסמיים, נבנו מפות מהירויות על פני כל המרחב עבור כל אופק. מפות אלו משמשות להמרת המפות הסטרוקטורליות מזמן לעומק. ככלל, תהליך עיבוד הנתונים בעומק תיקן עיוותים גיאומטריים, שיפר את הדימות הפנימי של המבנים בפרט ושל תת-הקרקע בכלל עד לעומק של יותר מ 15 ק"מ. יתרה מכך, מפות המהירות שחושבו מייצגות את השינויים הליתולוגיים בחתך הסדימנטרי. כך למשל, שינוי חריף במהירויות נצפה בחתך האוופוריטי של המסיניאן (כ- 4200 מ\ש לעומת כ- 2500 מ\ש עבור החתך שמעליו ומתחתיו) וכן לאורך מבנים עמוקים (כ- 6000 מ\ש לעומת 4500 מ\ש).

משרד התשתיות הלאומיות
האנרגיה והמים
המכון הגיאולוגי

תהליכים טקטונו-סדימנטריים באגן הלבנט העמוק

יעל שגיא

עבודה זו הוגשה כחיבור לקבלת תואר "דוקטור לפילוסופיה" לסנאט אוניברסיטת תל-אביב

העבודה נעשתה בהדרכתם של:
פרופ' זהר גבירצמן, המכון הגיאולוגי, ירושלים
פרופ' משה רשף, החוג למדעי כדור הארץ, אוניברסיטת תל-אביב

דוח מס' GSI/24/2016 ירושלים, סיון תשע"ו, יולי 2016